

DEVELOPMENT OF SHEAR WAVE VELOCITY PROFILES IN THE DEEP
SEDIMENTS OF THE MISSISSIPPI EMBAYMENT USING SURFACE WAVE AND
SPECTRAL RATIO METHODS

A Thesis presented to the Faculty of the Graduate School
University of Missouri-Columbia

In Partial Fulfillment
of the Requirements for the Degree

Master of Science

by
JONATHAN P. BAILEY

Dr. Brent L. Rosenblad, Thesis Supervisor

AUGUST 2008

The undersigned, appointed by the dean of the Graduate School, have examined the thesis entitled

DEVELOPMENT OF SHEAR WAVE VELOCITY PROFILES IN THE DEEP
SEDIMENTS OF THE MISSISSIPPI EMBAYMENT USING SURFACE WAVE AND
SPECTRAL RATIO METHODS

presented by Jonathan P. Bailey,

a candidate for the degree of Masters of Science,

and hereby certify that, in their opinion, it is worthy of acceptance.

Professor Brent L. Rosenblad

Professor John J. Bowders, P.E.

Professor Martin S. Appold

ACKNOWLEDGEMENTS

My advisor, Dr. Rosenblad, has been helpful throughout the thesis process. He has provided guidance and help whenever requested and has shown great patience. He has forced me to grow as a professional and a person that has been of great value and will be as I begin my professional career. Also he has been encouraging and always willing to put in the good word or letter of recommendation.

I would also like to thank Dr. Bowders, Dr. Loehr, and Dr. Likos. Dr. Bowders has an unquenchable enthusiasm for geotechnical engineering. This enthusiasm led to my interest in geotechnical engineering. He has not only passed this enthusiasm on to me but also taught me the value of hard work, teamwork, and technical writing. I thank Dr. Loehr for forcing me to think critically and apply knowledge to situations larger than the classroom setting. Dr. Likos for his guidance while I was an undergraduate student, deciding if graduate school was right for me, as well as the knowledge he has imparted to me within the classroom setting. All three professors were always willing to go above and beyond to lend guidance, as well as provide contacts or letters of recommendation.

I greatly appreciate Dr. Appold for taking the time to participate on my thesis committee and give me his valuable input.

Dr. Van Arsdale at the University of Memphis, along with his graduate students, should also be thanked for information provided.

I would also like to thank colleagues for taking the time to help with my study. Ryan Goetz and Jianhua Li were major participants in the fieldwork and without their assistance this study would not have been possible. Also Jianhua Li helped a great deal with data processing and general questions that arose. I would also like to thank Rick

Coffman, Nathan Rose, Nathan Textor, and Ryan Goetz for sporadic help and knowledge provided. They have been good friends and always willing to help.

The funding for the work in this thesis was supported primarily by the United States Geological Survey (USGS) as part of the National Earthquake Hazard Reduction Program (NEHRP) Award No. 06-HQGR0050. Also some of the data was collected as part of a separate grant (No. CMS -0086605) from the National Science Foundation as part of the Network for Earthquake Engineering Simulation (NEES) program.

Finally, I would like to thank my friends and family who have been great support and kept me going throughout the process. I would like to give a special thank you to Annette Krisko and Marc Krisko, my mother and step father, who helped throughout the process with formatting assistance and proof reading. I would also like to thank Roger and Barbara Bailey, my father and step mother, for their continued support and encouragement. Without their help, it would not have been possible to complete graduate school. Finally I would like to thank Meghan Holtschlag for her unbelievable understanding, support, and assistance. I sincerely appreciate each source of support.

TABLE OF CONTENTS

ACKNOWLEDGEMENTS.....	ii
LIST OF FIGURES	viii
LIST OF TABLES.....	xv
ABSTRACT.....	xviii
INTRODUCTION	1
1.1 Overview.....	1
1.2 Motivation.....	2
1.3 Objectives	3
1.4 Organization of Thesis.....	3
GEOLOGY OF THE UPPER MISSISSIPPI EMBAYMENT.....	5
2.1 Overview.....	5
2.2 Upper Mississippi Embayment Sediments	7
2.3 New Madrid Seismic Zone	9
2.4 Summary.....	11
PREVIOUS STUDIES	12
3.1 Introduction.....	12
3.2 Reference V_s Profile of Romero and Rix.....	13
3.3 Recent V_s Studies.....	14
3.4 Studies Estimating Average V_s Over Full Depth.....	21
3.5 V_s -Lithology Relationships.....	24
3.6 Summary	26
METHODS.....	27

4.1	Introduction.....	27
4.2	Overview of SASW Method.....	27
4.3	SASW Measurements in the Upper Mississippi Embayment.....	30
4.3.1	Field Equipment.....	30
4.3.2	Source-Receiver Locations.....	33
4.3.3	Data Collection.....	33
4.3.4	Data Processing.....	36
4.3.5	Data Inversion.....	40
4.4	Overview of H/V Method.....	44
4.5	H/V Measurements in Mississippi Embayment.....	46
4.5.1	Field Equipment.....	47
4.5.2	Data Collection.....	47
4.5.3	Data Processing.....	48
4.5.4	Sample Results.....	49
4.6	Summary.....	50
	SITE LOCATIONS AND LOCAL LITHOLOGY.....	52
5.1	Introduction.....	52
5.2	SITE 1: MORT.....	55
5.3	SITE 2: YARBRO (“JOE’S POND”).....	59
5.4	SITE 3: GNAR.....	62
5.5	SITE 4: LEPANTO.....	65
5.6	SITE 5: SHELBY FARMS.....	68
5.7	SITE 6: TNMT.....	71

5.8	SITE 7: GLAT	74
5.9	SITE 8: BRGM	78
5.10	SITE 9: PENM	81
5.11	SITE 10: EPRM	84
5.12	SITE 11: MSAR	87
5.13	Summary	90
RESULTS AND ANALYSIS		91
6.1	Introduction	91
6.2	SASW Results	91
6.2.1	V_s Profiles Using Generic Layering	91
6.2.2	General Characteristics of V_s Profiles	104
6.2.3	Modified V_s Profiles	105
6.3	Discussion of SASW Results	109
6.3.1	Comparison to Mississippi Embayment Reference Profiles	109
6.3.2	V_s -Soil Lithology	112
6.3.3	Average Velocities	115
6.4	H/V Spectra Results	116
6.5	Discussion of H/V Results	121
6.5.1	Comparison to Other Studies	121
6.5.2	Validity of H/V Estimate of Average V_s	124
6.6	Summary	125
CONCLUSIONS		127
7.1	Summary	127

7.2	Conclusions.....	127
7.3	Recommendations.....	129
	APPENDIX.....	130
	APPENDIX A.....	131
	APPENDIX B.....	133
	APPENDIX C.....	135
	APPENDIX D.....	137
	APPENDIX E.....	139
	APPENDIX F.....	141
	APPENDIX G.....	143
	APPENDIX H.....	145
	APPENDIX I.....	147
	APPENDIX J.....	149
	APPENDIX K.....	151
	REFERENCES.....	153

LIST OF FIGURES

Figure	Page
Figure 2.1 Idealized Cross Section of Mississippi Embayment Profile near Memphis, Tennessee (Hashash and Park, 2001).	5
Figure 2.2 Upper Mississippi Embayment Showing Holocene Age Deposits (Dark Gray) and the Pleistocene Age Deposits (Light Gray) (Romero and Rix, 2001).	6
Figure 2.3 Geologic Column for the New Madrid Seismic Zone (Van Arsdale and TenBrink, 2000).....	8
Figure. 2.4 New Madrid Seismic Zone within the Upper Mississippi Embayment (Mento et al., 1986).....	11
Figure 3.1 Summary of the Number and Penetration Depth of V_s Studies in the Mississippi Embayment Versus Profile Depth (Numbers Taken from Romero and Rix, 2001).....	12
Figure 3.2 Mississippi Embayment Reference Profile (a) Top 70 Meters of the Upland and Lowland Regions (b) Total Sediment Deposit Depth (Romero and Rix, 2001).....	14
Figure 3.3 Results of Refraction/Reflection Study by Williams et al. (2003). The Dark Bar Represents the Highest V_s Measured at Each Site with the Light Bar Representing the Lowest V_s for Each Site. The Number Above the Column is the Depth in Meters to the Top of the Highest Velocity Deposit.	16
Figure 3.4 Generalized Seismic Velocity Profile for Memphis as Described by Williams et al. (2003)	17
Figure 3.5 Shear Wave Velocity Profiles in the Upper Mississippi Embayment from Geophysical Logging at Well MLGW 236.....	18
Figure 3.7 H/V Data from a Selected Subset of Sites Having Different Sediment Thickness (Bodin et al., 2001).....	21
Figure 3.8 Results of H/V Testing Performed in the Upper Mississippi Embayment from Bodin et al. (2001).	22

Figure 3.9	Comparison of Shear Wave Velocities obtained from Microtremor Observations (Bodin et al., 2001).	24
Figure 3.10	Histograms of V_s Associated with each Lithologic Layer with Mean and Standard Deviation (Gomberg et al., 2003).	26
Figure 4. 1	Approximate Distribution of Vertical Particle Motion with Depth for Two Rayleigh Waves with Different Wavelengths (from Rix and Stokoe, 1989).	28
Figure 4. 2	SASW Testing Configuration (for Swept Sine Excitation) (from Rix and Stokoe, 1989).	30
Figure 4. 3	Photograph of Instrumented Sledgehammer Used to Excite High Frequency Energy.	32
Figure 4. 4	Photograph of Low Frequency Mobile Shaker “Liquidator” developed as part of the Network for Earthquake Engineering Simulation (NEES) Program.	32
Figure 4. 5	Photograph of Total Station Used to Measure Sensor Locations.	34
Figure 4. 6	Photograph of 1-Hz geophone Placed in the Ground and Leveled.	35
Figure 4. 7	Photograph of 1-Hz Geophone Buried and Insulated to Maintain Low Operating Temperature.	35
Figure 4. 8	Photograph of Undergraduate Research Assistant, Ryan Goetz, Taking GPS Reading at Site 2.	36
Figure 4. 9	Cross Power Spectrum and Coherence Plot from 300-meter Spacing at Site 1.	38
Figure 4. 10	Cross Power Spectrum and Coherence Plot from 300 meter Spacing at Site 1 after Masking (gray) is Applied.	39
Figure 4. 11	Dispersion Curve from Unwrapped Phase Plots.	40
Figure 4. 12	Comparison of a Theoretical and Experimental Dispersion Curve After Completion of Inversion Procedure.	43
Figure 4. 13	Shear Wave Velocity Profile Determined from SASW Measurements at Site 1.	44
Figure 4. 14	Schematic Showing the Site Response and Transfer Function for a Single Layer over Bedrock (Seht and Wohlenberg, 1999).	45
Figure 4. 15	Photograph of the 3-Component Geophone Being Placed at Site 5.	47
Figure 4. 16	Data Acquisition and Monitoring of Ambient Noise Measurements at Site 3.	48

Figure 4. 17	H/V Data from Site 1 after Input into the Program J-SESAME.....	49
Figure 4. 18	H/V Showing Windows of Data Used (Shaded) in Analysis after Filter is applied to Remove Transients.....	49
Figure 4. 19	Frequency Peaks Obtained from H/V Data Measured at Site 1.....	50
Figure 5.1	Site Location in the Mississippi Embayment (Map Modified from Romero & Rix, 2001)	54
Figure 5.2	Google Earth Image of Site 1 (MORT).	55
Figure 5.3	Photograph from the Furthest Receiver Location Looking Back Towards the Source.	56
Figure 5.4	Photographs of Geophone and Surficial Soil at Site 1.....	56
Figure 5.5	Estimated Soil Lithology at Site 1 (MORT).	58
Figure 5.6	Google Earth Image of Site 2 (Yarbro).	59
Figure 5.7	Photographs from the End of Array Looking Back Towards the Source. 60	
Figure 5.8	Estimated Soil Lithology at Site 2 (YARBRO).	61
Figure 5.9	Google Earth Image of Site 3 (GNAR).	62
Figure 5.10	Photograph of Distance from Array Line to Seismic Station.	63
Figure 5.11	Estimated Soil Lithology at Site 3 (GNAR).	64
Figure 5.12	Google Earth Image of Site 4 (Lepanto).	65
Figure 5.13	Photograph Looking Down the Array Towards the Source at Site 4.	66
Figure 5.14	Estimated Soil Lithology at Site 4 (LEPANTO).	67
Figure 5.15	Google Earth Image of Site 5 (Shelby Farms).	68
Figure 5.16	Photograph Looking Back Towards the Source.	69
Figure 5.17	Estimated Soil Lithology at Site 5 (SHELBY FARMS).	70
Figure 5.18	Google Earth Image of Site 6 (TNMT).	71
Figure 5.19	Photograph Looking Down the Array Towards the Source.....	72
Figure 5.20	Estimated Soil Lithology at Site 6 (TNMT).	73

Figure 5.21	Google Earth Image of Site 7 (GLAT).	74
Figure 5.22	Photograph of Site Looking Away from the Source.	75
Figure 5.23	Photograph of Site Looking Towards the Source.	75
Figure 5.24	Estimated Soil Lithology at Site 7 (GLAT).	77
Figure 5.25	Google Earth Image of Site 8 (BRGM).	78
Figure 5.26	Photograph of at Site 8 Looking Away from the Source.	79
Figure 5.27	Photograph at Site 8 Looking Towards the Source.	79
Figure 5.28	Estimated Soil Lithology at Site 8 (BRGM).	80
Figure 5.29	Google Earth Image of Site 9 (PENM).	81
Figure 5.30	Photograph of Site Layout Looking Away from the Source Location.	82
Figure 5.31	Photograph of Site Layout Looking Towards the Source Location.	82
Figure 5.32	Estimated Soil Lithology at Site 9 (PENM).	83
Figure 5.33	Google Earth Image of Site 10 (EPRM).	84
Figure 5.34	Photograph of Site Layout and Soil Conditions Looking Away from the Source.	85
Figure 5.35	Photograph of Site Layout and Soil Conditions Looking Towards the Source.	85
Figure 5.36	Estimated Soil Lithology at Site 10 (EPRM).	86
Figure 5.37	Google Earth Image of Site 11 (MSAR).	87
Figure 5.38	Photograph of Site Layout and Soil Conditions Looking Down the Array Towards the Source.	88
Figure 5.39	Estimated Soil Lithology at Site 11 (MSAR).	89
Figure 6.1	Results from SASW Measurements at Site 1 Showing (a) Experimental and Theoretical Dispersion Curves and (b) V_s Profile (with Sensitivity Bounds) and Estimated Soil Profile.	93
Figure 6.2	Results from SASW Measurements at Site 2 Showing (a) Experimental and Theoretical Dispersion Curves and (b) V_s Profile (with Sensitivity Bounds) and Estimated Soil Profile.	94

Figure 6.3	Results from SASW Measurements at Site 3 Showing (a) Experimental and Theoretical Dispersion Curves and (b) V_s Profile (with Sensitivity Bounds) and Estimated Soil Profile.....	95
Figure 6.4	Results from SASW Measurements at Site 4 Showing (a) Experimental and Theoretical Dispersion Curves and (b) V_s Profile (with Sensitivity Bounds) and Estimated Soil Profile.....	96
Figure 6.5	Results from SASW Measurements at Site 5 Showing (a) Experimental and Theoretical Dispersion Curves and (b) V_s Profile (with Sensitivity Bounds) and Estimated Soil Profile.....	97
Figure 6.6	Results from SASW Measurements at Site 6 Showing (a) Experimental and Theoretical Dispersion Curves and (b) V_s Profile (with Sensitivity Bounds) and Estimated Soil Profile.....	98
Figure 6.7	Results from SASW Measurements at Site 7 Showing (a) Experimental and Theoretical Dispersion Curves and (b) V_s Profile (with Sensitivity Bounds) and Estimated Soil Profile.....	99
Figure 6.8	Results from SASW Measurements at Site 8 Showing (a) Experimental and Theoretical Dispersion Curves and (b) V_s Profile (with Sensitivity Bounds) and Estimated Soil Profile.....	100
Figure 6.9	Results from SASW Measurements at Site 9 Showing (a) Experimental and Theoretical Dispersion Curves and (b) V_s Profile (with Sensitivity Bounds) and Estimated Soil Profile.....	101
Figure 6.10	Results from SASW Measurements at Site 10 Showing (a) Experimental and Theoretical Dispersion Curves and (b) V_s Profile (with Sensitivity Bounds) and Estimated Soil Profile.....	102
Figure 6.11	Results from SASW Measurements at Site 11 Showing (a) Experimental and Theoretical Dispersion Curves and (b) V_s Profile (with Sensitivity Bounds) and Estimated Soil Profile.....	103
Figure 6.12	Comparison of V_s Profiles at Site 10 from SASW Measurements and Reflection Measurements Performed within 1 Kilometer of Site 10 (Woolery and Street, 2002).....	105
Figure 6.13	Modified V_s Profiles (Black) Overlaying the Original V_s Profiles (Gray) at Sites 1-11 as (a)-(k), Respectively Developed using Thicker Layers Consistent with Estimated Formation Boundaries.....	107
Figure 6.14	(a) Average V_s Profile (Using Arithmetic Mean of 10 Lowland Sites) in the Top 70 Meters Compared to Reference Profiles from Romero and Rix, Herrmann and Akinci, and Dorman and Smalley (b) Coefficient of Variation from 10 Lowland Sites.....	111

Figure 6.15	(a) Average V_s Profile (Using Arithmetic Mean of 11 Sites) in the Top 220 Meters Compared to Reference Profiles from Romero and Rix, Herrmann and Akinci, and Dorman and Smalley (b) Coefficient of Variation from 11 Sites.	111
Figure 6.16	Shear Wave Velocity of the (a) Alluvium (b) Gravel (c) Jackson, Cockfield and Cook Mountain (Upper Claiborne) (d) Memphis Sand Soil Layer Compared with Median V_s Values \pm One Standard Deviation from Gomberg (2003).....	113
Figure 6.17	Comparison of V_s Values at Similar Depths of Four Soil Formations. ..	114
Figure 6.18	Peak Frequencies Obtained from H/V Measurements Performed at Site 1.....	117
Figure 6.19	Peak Frequencies Obtained from H/V Measurements Performed at Site 2.....	117
Figure 6.20	Peak Frequencies Obtained from H/V Measurements Performed at Site 3.....	117
Figure 6.21	Peak Frequencies Obtained from H/V Measurements Performed at Site 4.....	118
Figure 6.22	Peak Frequency Obtained from H/V Measurements Performed at Site 5.....	118
Figure 6.23	Peak Frequencies Obtained from H/V Measurements Performed at Site 6.....	118
Figure 6.24	Peak Frequencies Obtained from H/V Measurements Performed at Site 7.....	119
Figure 6.25	Peak Frequency Obtained from H/V Measurements Performed at Site 8.....	119
Figure 6.26	Peak Frequency Obtained from H/V Measurements Performed at Site 9.....	119
Figure 6.27	Peak Frequency Obtained from H/V Measurements Performed at Site 10.....	120
Figure 6.28	Peak Frequencies Obtained from H/V Measurements Performed at Site 11.....	120
Figure 6.29	Results Obtained from H/V Measurements at Eleven Test Sites Plotted with Results from Bodin et al. 2001 and Chen et al. 1996 (Modified from Bodin et al. 2001).....	122

Figure 6.30	Average V_s Values Below the Depth of the SASW Profiles Determined from H/V Measurements Compared to Deep V_s Reference Profiles.....	124
Figure 6.31	Travel Time Versus Frequency of Randomized Basin Models based on the V_s Profile Produced Within the Lower Rhine Embayment in the Cologne, Germany Area (Scherbaum, 2002).....	125
Figure A.1	H/V Showing Windows of Data Used (Shaded) in Analysis After Filter is Applied in the Program J-SESAME for Site 1.....	132
Figure B.1	H/V Showing Windows of Data Used (Shaded) in Analysis After Filter is Applied in the Program J-SESAME for Site 2.....	134
Figure C.1	H/V Showing Windows of Data Used (Shaded) in Analysis After Filter is Applied in the Program J-SESAME for Site 3.....	136
Figure D.1	H/V Showing Windows of Data Used (Shaded) in Analysis After Filter is Applied in the Program J-SESAME for Site 4.....	138
Figure E.1	H/V Showing Windows of Data Used (Shaded) in Analysis After Filter is Applied in the Program J-SESAME for Site 5.....	140
Figure F.1	H/V Showing Windows of Data Used (Shaded) in Analysis After Filter is Applied in the Program J-SESAME for Site 6.....	142
Figure G.1	H/V Showing Windows of Data Used (Shaded) in Analysis After Filter is Applied in the Program J-SESAME for Site 7.....	144
Figure H.1	H/V Showing Windows of Data Used (Shaded) in Analysis After Filter is Applied in the Program J-SESAME for Site 8.....	146
Figure I.1	H/V Showing Windows of Data Used (Shaded) in Analysis After Filter is Applied in the Program J-SESAME for Site 9.....	148
Figure J.1	H/V Showing Windows of Data Used (Shaded) in Analysis After Filter is Applied in the Program J-SESAME for Site 10.....	150
Figure K.1	H/V Showing Windows of Data Used (Shaded) in Analysis After Filter is Applied in the Program J-SESAME for Site 11.....	152

LIST OF TABLES

Table	Page
Table 4. 1 Receiver Pairs for 2006 Sites (S-R ₁ : Source to Receiver 1, R ₁ -R ₂ : Receiver 1 to Receiver 2).....	33
Table 4. 2 Receiver Pairs for 2007 Sites (S-R ₁ : Source to Receiver 1, R ₁ -R ₂ : Receiver 1 to Receiver 2).....	33
Table 5.1 Site Coordinates and Estimated Depth to Bedrock.....	54
Table 5.2 Estimated Profile at Site 1 (MORT) Provided by Roy Van Arsdale from the University of Memphis.	58
Table 5.3 Estimated Profile at Site 2 (YARBRO) Provided by Roy Van Arsdale from the University of Memphis.	61
Table 5.4 Estimated Profile at Site 3 (GNAR) Provided by Roy Van Arsdale from the University of Memphis.	64
Table 5. 5 Estimated Profile at Site 4 (LEPANTO) Provided by Roy Van Arsdale from the University of Memphis.	67
Table 5. 6 Estimated Profile at Site 5 (SHELBY FARMS) based on Profiles Presented by Gomberg (2003).	70
Table 5.7 Estimated Profile at Site 6 (TNMT) Provided by Roy Van Arsdale from the University of Memphis.	73
Table 5.8 Estimated Profile at Site 7 (GLAT) Provided by Roy Van Arsdale from the University of Memphis.	77
Table 5.9 Estimated Profile at Site 8 (BRGM) Provided by Roy Van Arsdale from the University of Memphis.	80
Table 5.10 Estimated Profile at Site 9 (PENM) Provided by Roy Van Arsdale from the University of Memphis.	83
Table 5.11 Estimated Profile at Site 10 (EPRM) Provided by Roy Van Arsdale from the University of Memphis.	86

Table 5.12	Estimated Profile at Site 11 (MSAR) Provided by Roy Van Arsdale from the University of Memphis.....	89
Table 6.1	Average Values of Lithologic Units with Standard Deviation.....	115
Table 6.2	Site Classifications Based on IBC Standards.....	116
Table 6.3	Average Vs Within the Top 200 Meters.....	116
Table 6.4	Average Vs at each Site Estimated from H/V Measurements.....	121
Table A.1	Profile Parameters Used to Develop Theoretical Dispersion Curve at Site 1.....	131
Table A.2	Profile Parameters Used to Develop Modified Theoretical Dispersion Curve at Site 1.....	131
Table B.1	Profile Parameters Used to Develop Theoretical Dispersion Curve at Site 2.....	133
Table B.2	Profile Parameters Used to Develop Modified Theoretical Dispersion Curve at Site 2.....	133
Table C.1	Profile Parameters Used to Develop Theoretical Dispersion Curve at Site 3.....	135
Table C.2	Profile Parameters Used to Develop Modified Theoretical Dispersion Curve at Site 3.....	135
Table D.1	Profile Parameters Used to Develop Theoretical Dispersion Curve at Site 4.....	137
Table D.2	Profile Parameters Used to Develop Modified Theoretical Dispersion Curve at Site 4.....	137
Table E.1	Profile Parameters Used to Develop Theoretical Dispersion Curve at Site 5.....	139
Table E.2	Profile Parameters Used to Develop Modified Theoretical Dispersion Curve at Site 5.....	139
Table F.1	Profile Parameters Used to Develop Theoretical Dispersion Curve at Site 6.....	141
Table F.2	Profile Parameters Used to Develop Modified Theoretical Dispersion Curve at Site 6.....	141
Table G.1	Profile Parameters Used to Develop Theoretical Dispersion Curve at Site 7.....	143

Table G.2	Profile Parameters Used to Develop Modified Theoretical Dispersion Curve at Site 7.....	143
Table H.1	Profile Parameters Used to Develop Theoretical Dispersion Curve at Site 8.....	145
Table H.2	Profile Parameters Used to Develop Modified Theoretical Dispersion Curve at Site 8.....	145
Table I.1	Profile Parameters Used to Develop Theoretical Dispersion Curve at Site 9.....	147
Table I.2	Profile Parameters Used to Develop Modified Theoretical Dispersion Curve at Site 9.....	147
Table J.1	Profile Parameters Used to Develop Theoretical Dispersion Curve at Site 10.....	149
Table J.2	Profile Parameters Used to Develop Modified Theoretical Dispersion Curve at Site 10.....	149
Table K.1	Profile Parameters Used to Develop Theoretical Dispersion Curve at Site 11.....	151
Table K.2	Profile Parameters Used to Develop Modified Theoretical Dispersion Curve at Site 11.....	151

DEVELOPMENT OF SHEAR WAVE VELOCITY PROFILES IN THE DEEP
SEDIMENTS OF THE MISSISSIPPI EMBAYMENT USING SURFACE WAVE AND
SPECTRAL RATIO METHODS

Jonathan P. Bailey

Dr. Brent L. Rosenblad, Thesis Supervisor

ABSTRACT

The deep soils of the Mississippi Embayment in the central United States will have a significant influence on earthquake ground motions generated by the New Madrid Seismic Zone. The seismic properties of these soils, which extend to depths of over 1000 meters in some areas, are poorly characterized at depths below 60 to 100 meters. This study presents shear wave velocity (V_s) profiles determined from Spectral-Analysis-of-Surface-Waves (SASW) measurements performed at eleven sites in Arkansas, Tennessee, and Missouri. These measurements were performed using the low-frequency field vibrator developed as part of the NSF Network for Earthquake Engineering Simulation (NEES) program. Shear wave velocity profiles were developed to depths of approximately 220 meters at eleven sites located throughout the Mississippi Embayment. In addition to the SASW measurements, ambient noise measurements of horizontal and vertical ground motions were performed to estimate the average V_s over the full profile depth using the H/V spectral ratio method. The V_s profiles derived from the SASW measurements compared well with V_s reference profiles that have been developed for the Mississippi Embayment and used in recent site response studies of the region. The observed variability of the profiles was found to be in general agreement with past assumptions used for the deep soil and correlated with changes in soil lithology. Relationships between the soil formations and V_s were consistent with past studies and

provided information to greater depths. Lastly the H/V spectral ratio measurements were successfully applied at each of the eleven sites, but appeared to overestimate the average V_s .

CHAPTER 1

INTRODUCTION

1.1 Overview

The upper Mississippi Embayment region of the central United States spans the states of Missouri, Kentucky, Arkansas, and Tennessee, and overlies the New Madrid Seismic Zone (NMSZ). Sediments in this region extend to depths of up to 1000 meters in some locations. The presence of these deep deposits will influence the amplitude and frequency content of future earthquake ground motion. In order to better predict the ground motions and design structures that will perform safely in a large seismic event, a reliable model of the deep sediment dynamic properties, particularly the shear wave velocity (V_s) profile is needed.

Large-strain dynamic properties (stiffness and damping) of soil are typically determined from direct laboratory measurements (such as resonant column) or from empirical relationships using basic soil parameters. Small-strain stiffness values, however, are determined in-situ by measuring small-strain shear wave velocities (V_s). The shear wave velocity profile is a vital input into ground motion calculations, and is also a common parameter used for assessing liquefaction susceptibility. In-situ borehole methods such as crosshole and downhole are often used to measure V_s values. However, these methods become prohibitively expensive as the profile depth increases. Non-intrusive surface wave methods have been demonstrated to be an effective means to determine in-situ V_s values for site response studies (Bay, 2003; Brown et al. 2000; Brown et al., 2002). Surface wave methods are favorable due to the lower cost as

compared to borehole methods such as crosshole, downhole, and suspension logging testing, especially when used for deep characterization studies.

The penetration depth of surface wave measurements depends on the ability to excite low-frequency surface waves. Conventional sources such as impact sources restrict the maximum penetration depth of V_s profiles to approximately 30 to 50-meters. Even with the use of conventional Vibroseis equipment the depth of penetration is still limited to typically 75 meters or less. Recently, a unique low-frequency vibrator has been developed at the University of Texas at Austin as part of the Network for Earthquake Engineering Simulation (NEES) project. The low frequency limit of this equipment extends over two octaves below the range of a conventional Vibroseis and should provide V_s profiles that penetrate three or four times as deep as those produced with conventional Vibroseis equipment.

1.2 Motivation

This study is driven by the current lack of deep V_s measurements throughout the upper Mississippi Embayment and the impact these deep deposits will have on ground motion. The vast majority of V_s studies in the Mississippi Embayment have been confined to the top 60 meters with most site classification studies focused on determining the V_s values in the top 30 meters of the soil deposit. However, studies by Park and Hashash (2005) have demonstrated the important effect deep sediments will have on the amplitude and frequency content of ground motions. In addition, Cramer (2004) has shown the importance of variability in the V_s profile in the top 300 meters on site amplification. The current reference V_s profile that has been used in site response studies

is based on deep soil information derived from limited data and assumed values of variability for deeper deposits (Romero and Rix, 2001).

1.3 Objectives

Three objectives are to be met by this study. The first objective is to non-intrusively characterize the V_s structure of the upper Mississippi Embayment sediments to a depth of 200 to 250 meters at eleven sites. This data will fill an existing gap in knowledge of the small-strain V_s structure of the Mississippi Embayment sediments and provide valuable data for comparison to the reference profile that has been used in several past studies. The second objective is to examine the correlation between V_s and soil lithology in the upper Mississippi Embayment. The final objective is to investigate the application of the H/V spectral ratio method (Nakamura's method) as a means to estimate the average V_s properties at greater depths.

1.4 Organization of Thesis

Chapter 2 is a brief overview of the geology of the upper Mississippi Embayment as well as a description of the New Madrid Seismic Zone. Chapter 3 is a literature review of previous V_s studies performed in the Mississippi Embayment. Past studies include seismic reflection and refraction data, downhole testing, seismic cone penetration tests, a limited number of shallow surface wave tests, and V_s data back calculated from sonic logs performed at two deep boreholes. A discussion of the equipment, data collection, data analyses, and interpretation used in this study is presented in Chapter 4. This includes the Spectral Analysis of Surface Waves (SASW) method and H/V spectral ratio method used in this work. In Chapter 5 a general description of each site, including site coordinates, and the estimated soil lithology inferred from nearby well logs at each site is

presented. The results obtained from the SASW method and H/V Spectral Ratio method are presented and discussed in Chapter 6. Also, comparisons to other published studies are made in Chapter 6. Chapter 7 is a summary of the findings, conclusions drawn from this work, and recommendations for future studies.

CHAPTER 2

GEOLOGY OF THE UPPER MISSISSIPPI EMBAYMENT

2.1 Overview

The Mississippi Embayment stretches from the Gulf of Mexico to Southern Illinois near Cairo and is located between the Ozark Uplift and the Nashville Dome. The Mississippi Embayment is a southward plunging syncline with an axis that closely traces the course of the Mississippi River (Mento et al., 1986). The synclinal nature as well as depth of sediments near Memphis are illustrated in Figure 2.1.

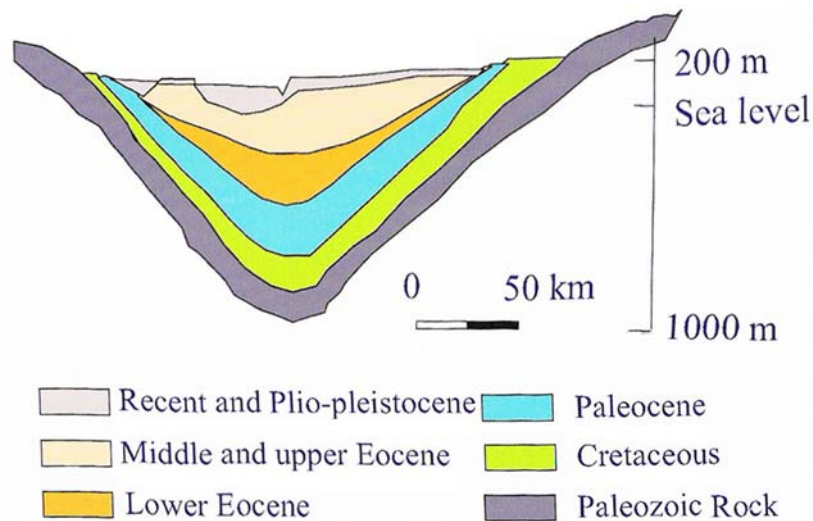


Figure 2.1 Idealized Cross Section of Mississippi Embayment Profile near Memphis, Tennessee (Hashash and Park, 2001).

Crustal movement and compaction of deposits caused subsidence and created a basin for the deposition of alluvial and eroded sediments. The basement rock is the Knox Dolomite from the Paleozoic era (Cushing et al., 1964). The stratigraphy above the Paleozoic rock consists of various deposits of sands, silts, and clays that range in total thickness from 477 meters at New Madrid Missouri, near the northern extent of this

study, to 987 meters in Memphis, Tennessee, near the southern extent of the study (Van Arsdale and TenBrink, 2000).

The upper Mississippi Embayment is the focus of this study. The spatial extent of the upper Mississippi Embayment is illustrated in Figure 2.2. The surface deposits of the embayment are broken into two classifications. Holocene deposits are found throughout the alluvial plains particularly in the Mississippi River floodplain and the floodplains of smaller rivers, as shown in Figure 2.2. Older Pleistocene deposits are located further inland in the upland region. The bluffs, which run along the eastern edge of the Mississippi River, are a geologic boundary that separates the upland Pleistocene deposits from the low-lying Holocene deposits (Romero and Rix, 2001)

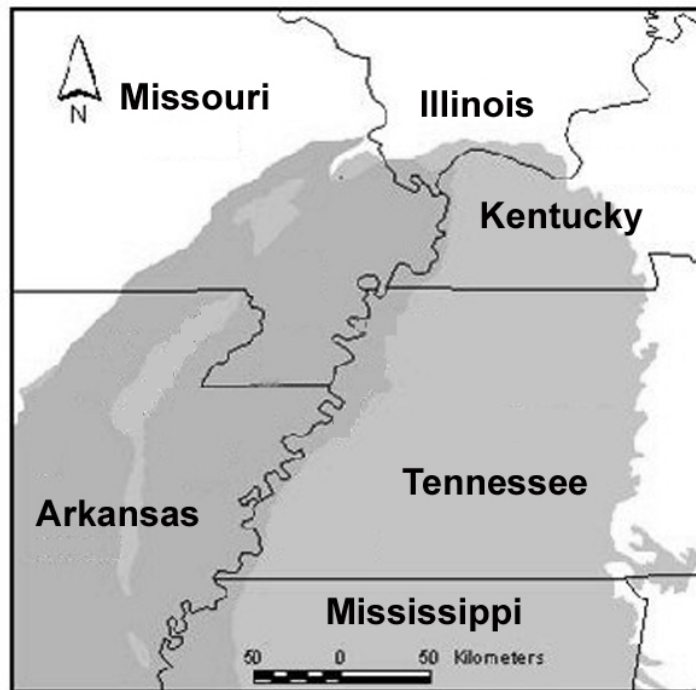


Figure 2.2 Upper Mississippi Embayment Showing Holocene Age Deposits (Dark Gray) and the Pleistocene Age Deposits (Light Gray) (Romero and Rix, 2001).

2.2 Upper Mississippi Embayment Sediments

The general stratigraphy for the New Madrid seismic zone, as developed by Van Arsdale and TenBrink (2000), is presented in Figure 2.3. The profile shown extends to bedrock. The profile depth for the surface wave portion of this study generally did not extend beyond the base of the Eocene Claiborne group.

The Eocene Claiborne Group marks a marine transgression, or period when the sea rose, leaving sedimentary deposits, and is divided into the Memphis Sand, the Cook Mountain Formation, and the Cockfield Formation. The Memphis Sand is fluvial/deltaic sand that ranges from approximately 225-meters thick below Shelby County, Tennessee thinning to about 110-meters thick below New Madrid, Missouri. The Memphis Sand has subordinate lenses or beds of clay and silt that can be confused with the Cook Mountain Formation (Van Arsdale and TenBrink, 2000). The Memphis Sand is the major aquifer providing water to Memphis. The top of the Memphis Sand layer as well as the bottom boundary, or start of the Wilcox Group, are defined as hydrologic boundaries rather than stratigraphic boundaries. The layer is part of the middle Claiborne aquifer as well as the lower Claiborne-upper Wilcox aquifer system (Parks and Carmichael, 1990). Above the Memphis Sand, the Cook Mountain Formation is a clay and silt fluvial /deltaic unit with minor sand lenses and lignite beds. The Cockfield Formation, located over the Cook Mountain Formation, is a fluvial/deltaic silt and clay interbedded with sand and lignite beds. These two formations have a combined thickness of about 65 meters under Shelby County and 30 meters under sites in southern Missouri (Van Arsdale and TenBrink, 2000).

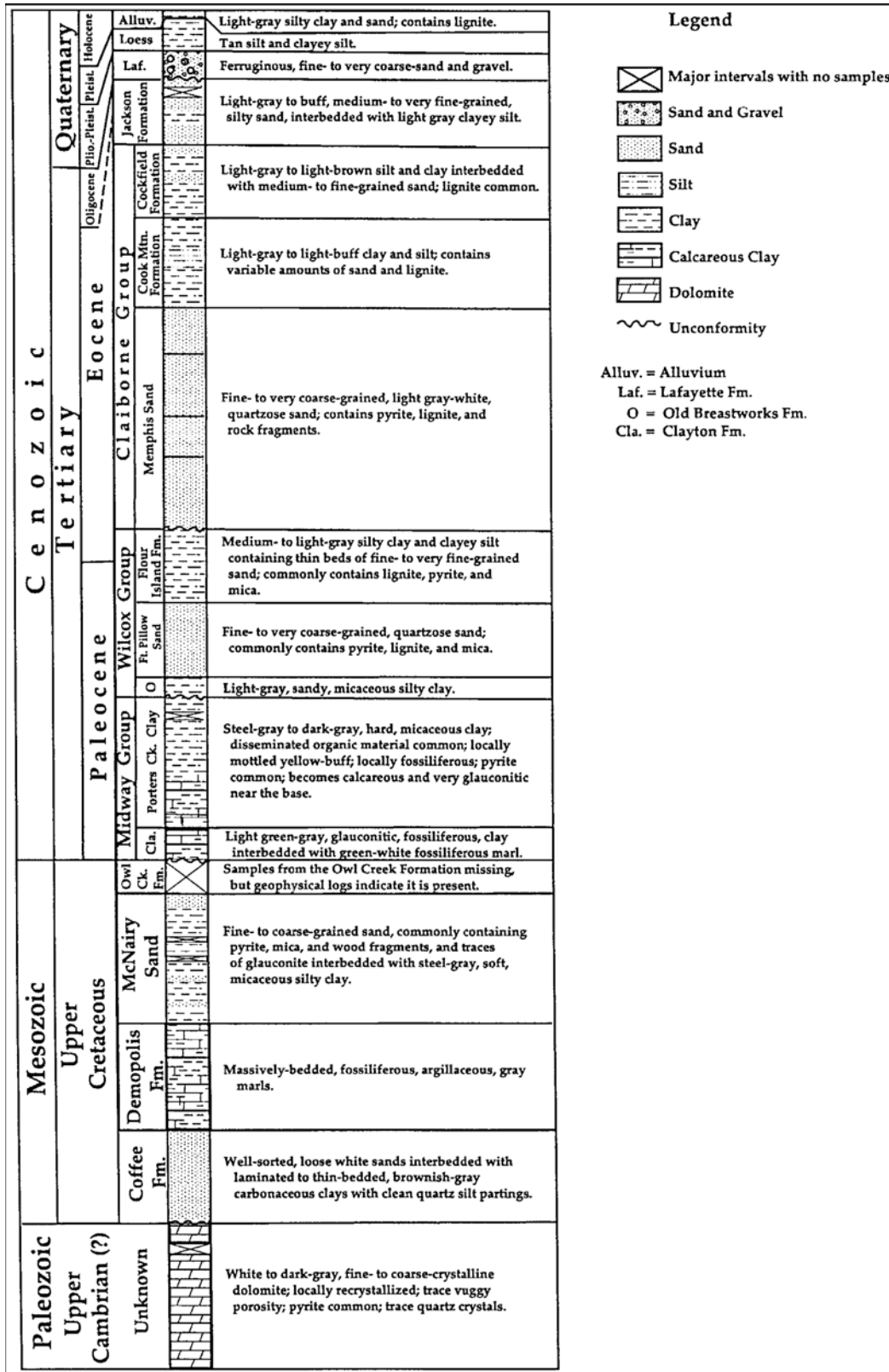


Figure 2.3 Geologic Column for the New Madrid Seismic Zone (Van Arsdale and TenBrink, 2000)

The Jackson Formation is fluvial/deltaic silty sand interbedded with clayey silt and lignite. The Jackson Formation becomes thicker in the northern portions of the embayment, increasing from about 15 meters under Shelby County in Memphis, Tennessee to approximately 40 meters beneath New Madrid, Missouri. The Jackson formation has a variable thickness throughout the embayment because its upper contact is an unconformity overlain by Quaternary Mississippi River alluvium within the valley and by the Pliocene-Pleistocene Lafayette Formation (Upland Gravel) on the bluffs east of the Mississippi River (Van Arsdale and TenBrink, 2000). The Mississippi River sediments, which consist of basal sandy gravel overlain by sands and capped by silts and clays, have a thickness of approximately 50 meters (Saucier, 1994).

The near-surface lithology is different between the west and east sides of the Mississippi River. On the eastern side of the bluffs the near-surface stratigraphy consists of the Upland Gravel and the overlying Pleistocene loess whereas on the western side of the Mississippi River bluffs the surface stratigraphy consists of Mississippi River Pleistocene (traces) and Holocene alluvium (Van Arsdale and TenBrink, 2000).

2.3 New Madrid Seismic Zone

The New Madrid seismic zone is located in the northern reaches of the Mississippi Embayment and is the source of the three largest earthquakes in the continental United States, having estimated moment magnitudes, **M**, of 7 to 8, as well as several large aftershocks. These large earthquakes struck the central United States in the winter of 1811-1812, inducing severe liquefaction and ground failures (Tuttle et al., 2002).

The shaded area in the Mississippi Embayment in Figure 2.4 is the New Madrid fault zone determined from seismicity. This area, which is inferred to be the source of the intense earthquakes that have occurred, is broken into three main zones. The first zone stretches from near Marked Tree, Arkansas, to an intersection with the second zone about 20 km northwest of Dyersburg, Tennessee. The first zone is approximately 100-km long and has components of right-lateral, strike-slip fault movement. The second zone begins north of Dyersburg and runs northwest for about 50-km to west of New Madrid, Missouri. Within this zone northeast compression is found with strike-slip and thrust components of stress being indicated. The third zone runs from west of New Madrid for approximately 50-km in a northeast direction to near the Illinois border. This zone exhibits east-west compression with strike-slip faulting (Mento et al., 1986). Within the New Madrid seismic zone a recurrence interval of: 70 to 140 years for magnitudes greater than 6.0, and an interval of 550 to 1100 years is estimated for magnitudes greater than 7.0 (Johnston and Nava, 1985).

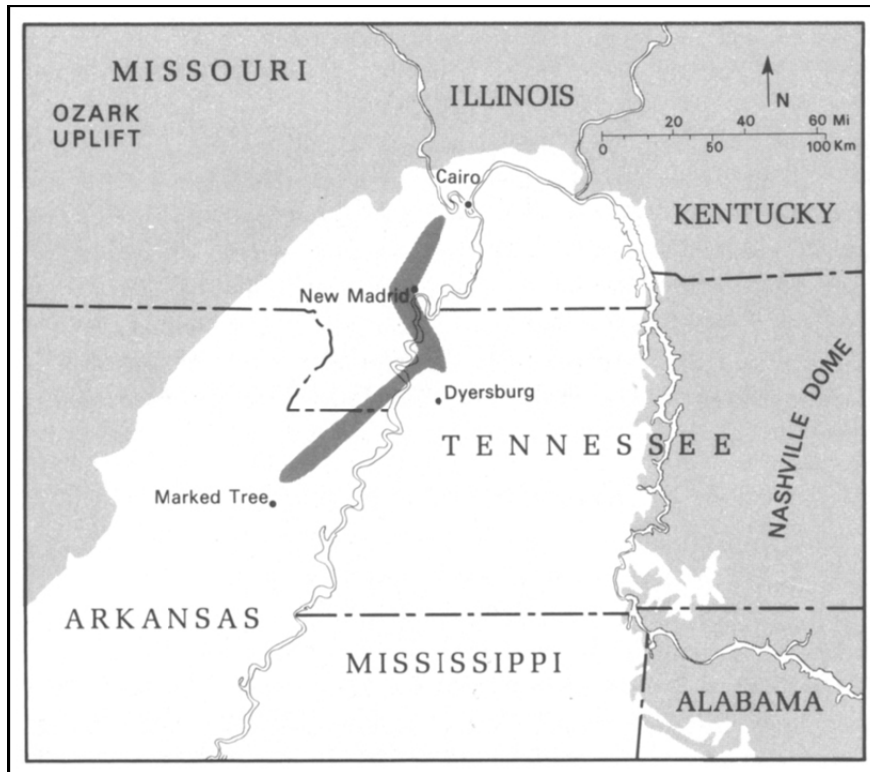


Figure. 2.4 New Madrid Seismic Zone within the Upper Mississippi Embayment (Mento et al., 1986).

2.4 Summary

The upper Mississippi Embayment is located in the seismically active New Madrid seismic zone. The Mississippi Embayment is synclinal in nature with sediments that range from depths of approximately 500 meters near New Madrid, Missouri to approximately 1000 meters near Memphis, Tennessee. To the west of the Mississippi River the deposits are of Holocene-age with deposits to the east of Pleistocene-age. The Eocene Claiborne, Jackson Formation, and near surface silts, sands, and gravels make up approximately the top 300 meters of the soil profile.

CHAPTER 3

PREVIOUS STUDIES

3.1 Introduction

The response of the Mississippi Embayment during a seismic event is strongly influenced by the thick sediment layer overlying the Paleozoic rock basement. Given that the highly populous city of Memphis and numerous critical transportation elements are located in this seismically active region, it is important to characterize better the properties of these deep sediments. The sediments of the upper Mississippi Embayment have been studied using seismic reflection and refraction, downhole testing, seismic cone penetration, suspension logging, surface wave testing, borehole reviews, and microtremor measurements. Figure 3.1 presents a summary of the number of previous studies and the depth of the investigation taken from a recent study (Romero and Rix, 2001). Important to note is the fact that most of these studies have focused on the top 60-meters with very few studies extending to greater depths. Although additional studies have been performed since 2001, the deeper deposits are still generally poorly characterized in this region. Some of these previous studies are discussed below.

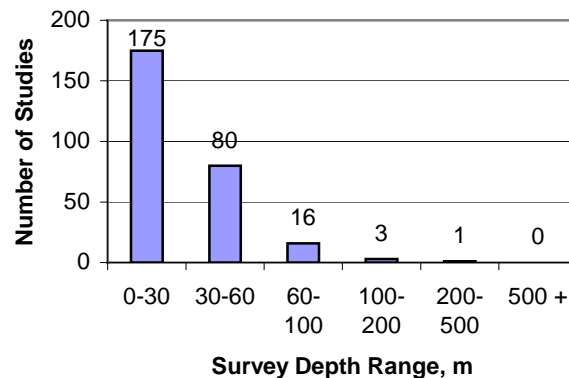


Figure 3.1 Summary of the Number and Penetration Depth of V_s Studies in the Mississippi Embayment Versus Profile Depth (Numbers Taken from Romero and Rix, 2001).

3.2 Reference V_s Profile of Romero and Rix

Romero and Rix (2001), compiled data of V_s profiles in the greater Memphis area from five main sources. These sources were Casey (1999), Liu et al. (1997), Schnedier and Mayne (1998), and Williams (2000). A total of ninety-three profiles were used. From this information Romero and Rix formulated general reference profiles of the Mississippi Embayment sediments. Figure 3.2a presents the profiles developed for the top 70 meters of soil. Separate profiles were developed for the lowland and upland regions. The lowland or Holocene age deposits show lower V_s and the upland or Pleistocene deposits exhibit higher V_s . Specific velocities are discussed later in the chapter.

Also developed by Romero and Rix (2001), is a general soil profile to the full depth of the Mississippi Embayment sediments, which is presented in Figure 3.2b. This profile exhibits an increase in V_s at 70 meters. A study of V_s variability was performed at three sites near Memphis Tennessee. At the three sites a total of twenty-two of the ninety-three measurements were performed. From the variability study, Romero and Rix found a value of the coefficient of variability of 0.15 represented the uncertainty of V_s profiles within their study area. It should be noted that the reference profile differs from a typical power law relationship that is often proportional to the quarter-power of effective stress.

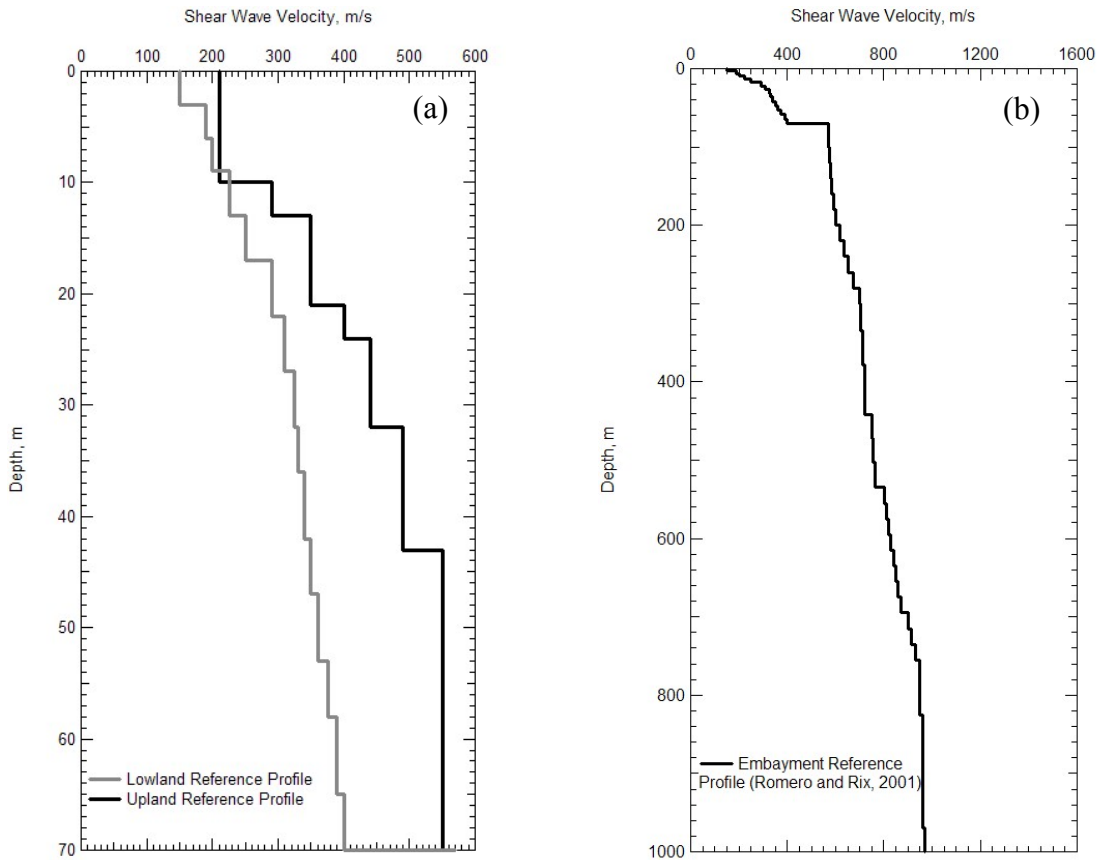


Figure 3.2 Mississippi Embayment Reference Profile (a) Top 70 Meters of the Upland and Lowland Regions (b) Total Sediment Deposit Depth (Romero and Rix, 2001)

3.3 Recent V_s Studies

Since the report published by Romero and Rix in 2001 some additional V_s studies have been performed in the upper Mississippi Embayment. In a study by Williams et al. (2003), refraction and reflection tests were performed at 65 locations to a depth of approximately 40 meters in the Memphis, Tennessee area. Of the 65 sites, 19 of the sites are located on the modern Mississippi River floodplain (Holocene-age deposits). The other 46 sites were further east on Pleistocene-age deposits in urban areas of Memphis. Figure 3.3 presents a summary of the results for the sites tested. The darker bar is the highest V_s measured at each site with the lighter V_s bar representing the lowest V_s for each

site. The number above the column is the depth in meters to the top of the highest velocity deposit. Of the 65 measurements only 10 extended beyond 60 meters.

From Williams's study, the Holocene-age deposits were found to have an average V_s of 206 m/s. This average is consistent with the range from other studies such as Liu et al. (1997) of 120 to 286 m/s. The Holocene age deposits have a top layer of Mississippi River alluvium that is estimated for the study to be 43-meters thick. At the bottom of this layer, V_s increases from 300 m/s to a range of 450 to 675 m/s. For the sites on Pleistocene-age deposits an approximately 12-meter thick layer of loess is present. These deposits had an average V_s of 210 m/s. This average also fell within the range from Liu's study of 177 to 306 m/s. At the bottom of this loess layer the velocity jumps from 300 m/s to about 450 to 600 m/s. Although both the loess and Mississippi river alluvium exhibit similar values of V_s , the layer thicknesses are much different. The bottom of each layer is thought to be the start of the Lafayette or Jackson Formation.

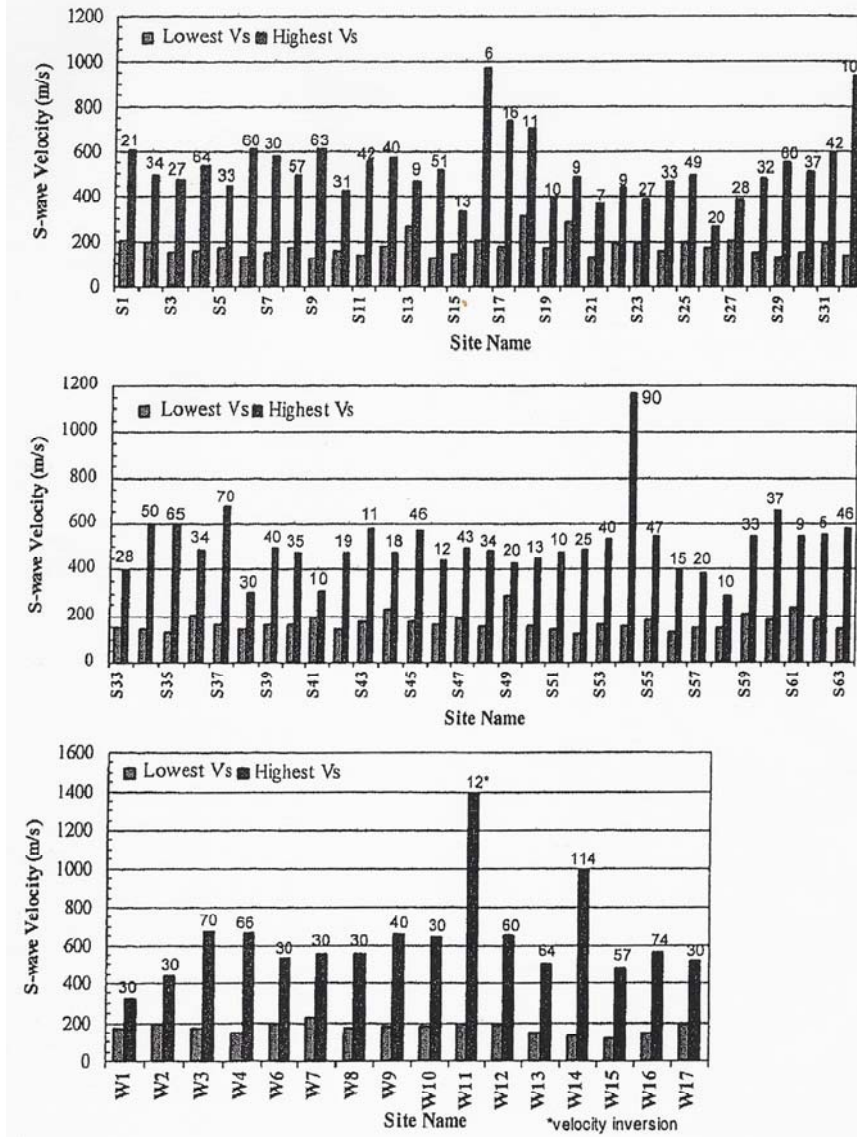


Figure 3.3 Results of Refraction/Reflection Study by Williams et al. (2003). The Dark Bar Represents the Highest V_s Measured at Each Site with the Light Bar Representing the Lowest V_s for Each Site. The Number Above the Column is the Depth in Meters to the Top of the Highest Velocity Deposit.

Also in Williams's study is an estimation of the compression wave and shear wave velocity profiles for Memphis. Figure 3.4 was developed from combining the results of Williams study, sonic logs shown in Crone and Russ (1979), and the thickness of sediments taken from interpretations of Luzietti et al. (1992). The V_s values are of importance to this study. Also the average V_s values at greater depth than the range of our study are given for changing lithology based on estimation from the sonic logs.

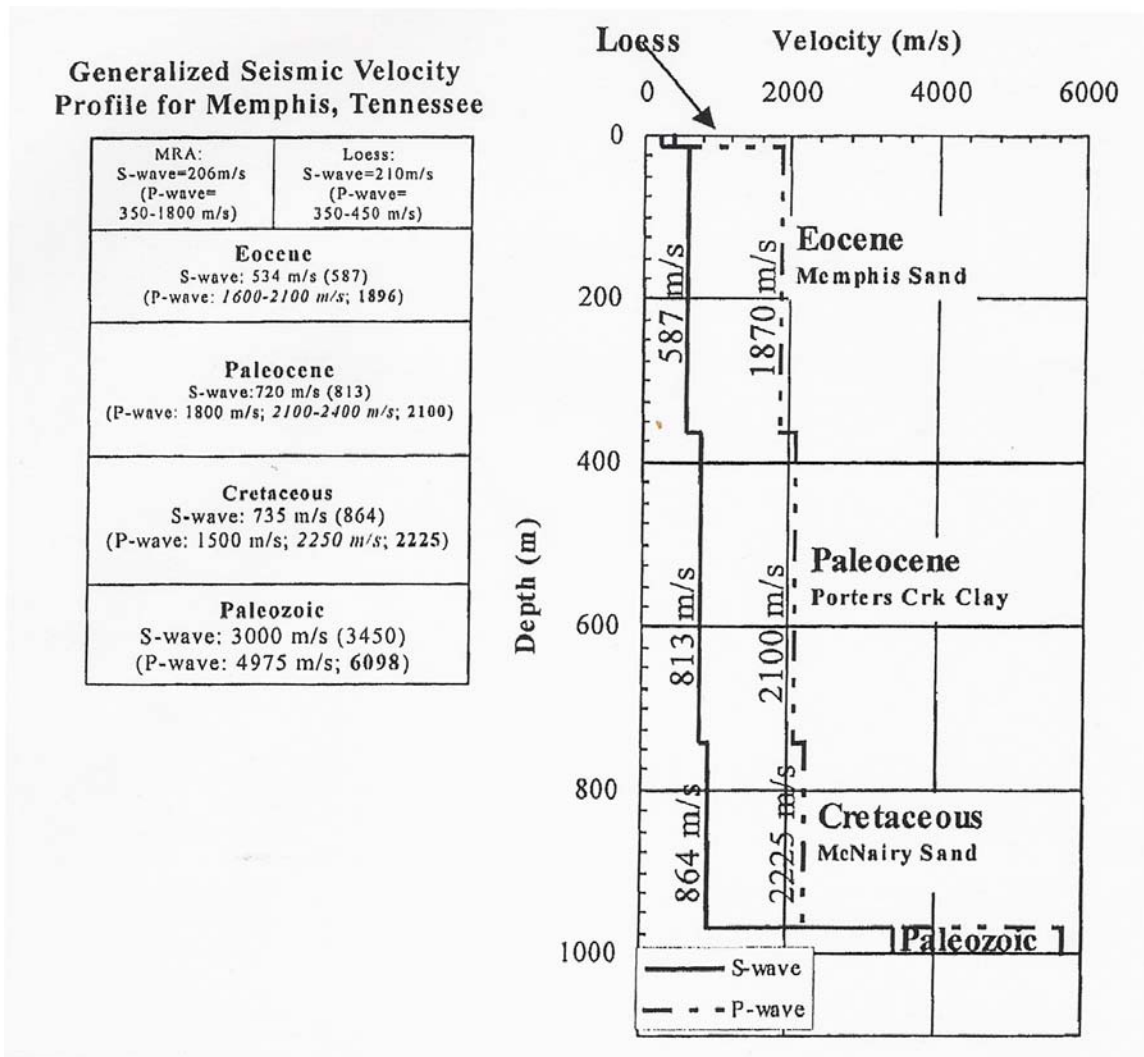


Figure 3.4 Generalized Seismic Velocity Profile for Memphis as Described by Williams et al. (2003)

In a workshop given by Rix (2004), two V_s profiles obtained from borehole reviews were presented. The first profile is in the Memphis, Tennessee area. The Memphis Light, Gas, and Water (MLGW) division approved the use of a well for scientific testing; this well was designated as MLGW #236. Shear wave logging was performed in May of 2002. This well allowed for direct measurement of shear wave velocity to a depth of 436 meters and was the first deep measurement taken in the upper Mississippi Embayment. The results of this testing are shown in Figure 3.5.

The second well presented in this paper is designated as Wilson 2-14. This well is an exploratory well near Keiser Arkansas that was drilled to a depth of 915-meters. Only P-wave measurements were performed in this well with no direct measurement of S-waves.

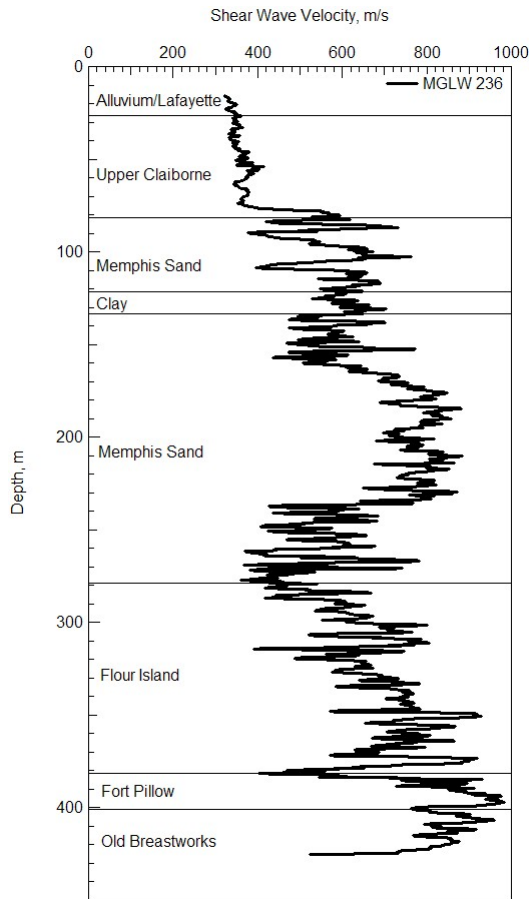


Figure 3.5 Shear Wave Velocity Profiles in the Upper Mississippi Embayment from Geophysical Logging at Well MGLW 236.

A downhole study was performed by Ge et al. (2007) at four sites in western Tennessee. Three methods were then used to determine the velocity structure; these methods were the approximate zero-offset method, layer-stripping method, and the waveform-matching method. From these methods the four V_s profiles shown in Figures 3.6 a, b, c, and d were developed. The dashed line is the zero-offset method, the thin solid line is the layer stripping method, and the bold line is the waveform-matching

method. Sites 1 and 2 exhibit lower shear wave velocities than sites 3 and 4. This is most likely do to the difference in sediments. Sites 3 and 4 are located further east of sites, 1 and 2, which is where Pleistocene age deposits are found. The four sites are in the vicinity of the Memphis, Tennessee area and have average velocities ranging from 250 m/s to 370 m/s, which correspond with the data from Liu (1997).

Woolery and Street (2002) performed seismic P-wave and horizontally-polarized shear waves (SH) reflection/refraction soundings at 15 sites within the Mississippi Embayment. In the near surface (70 meters and above), the V_s was found to range from approximately 200 m/s to 400 m/s. Deep deposits to a depth of approximately 350 meters had a V_s range of 540 to 800 m/s. The values are in agreement with the V_s values from the MLGW 236 well as well as the Williams et al. (2003) study.

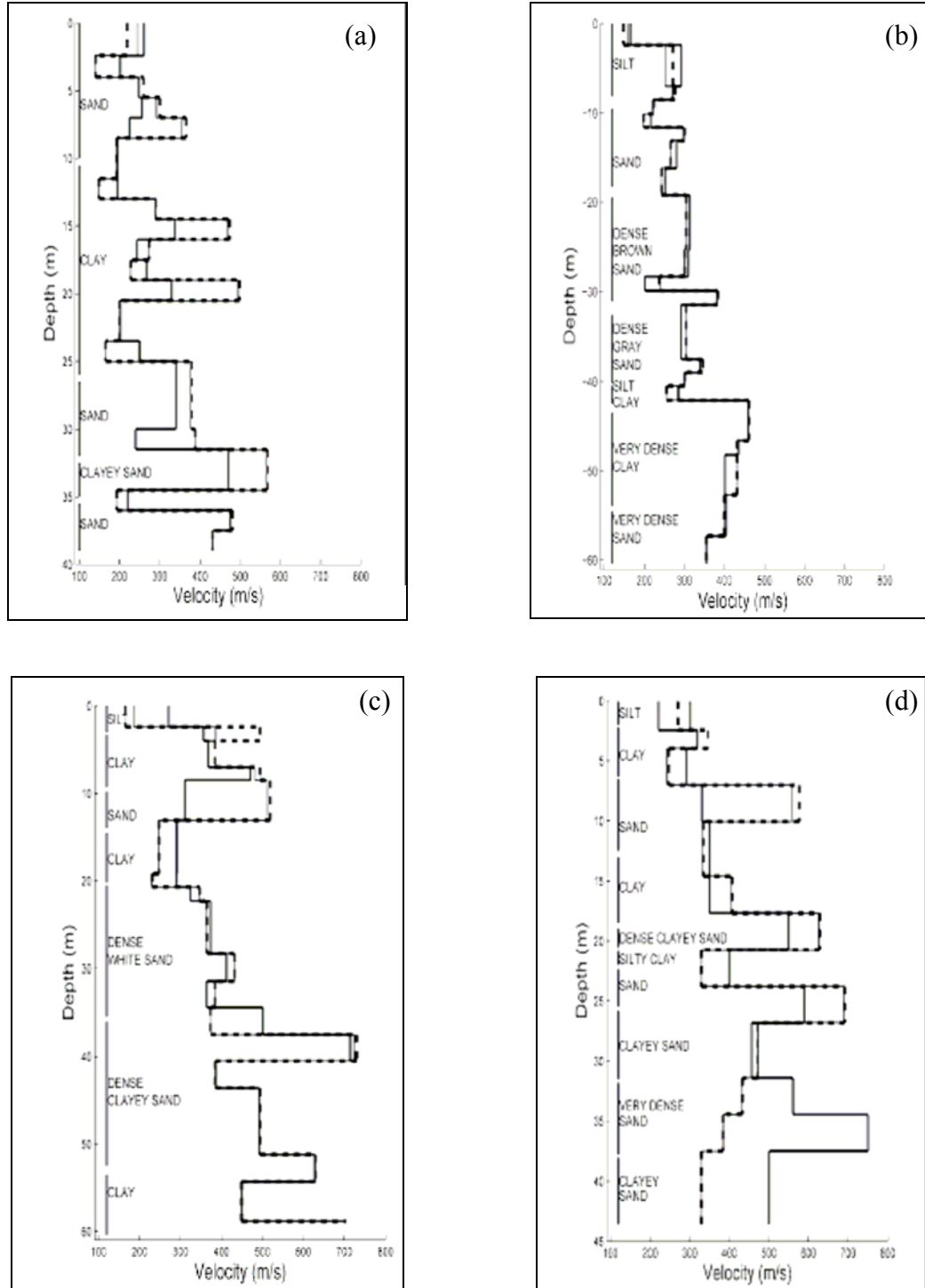


Figure 3.6 V_s Profiles at (a) Shelby Farms Velocity Profiles, Coordinates $(-89.84^\circ, 35.12^\circ)$ (b) Covington Velocity Profiles, Coordinates $(-89.63^\circ, 35.40^\circ)$ (c) Jackson Velocity Profiles, Coordinates $(-88.92^\circ, 35.64^\circ)$ (d) Brownsville Velocity Profiles, Coordinates $(-89.26^\circ, 35.54^\circ)$ with the Dashed Line Representing the Zero-Offset Method, Thin Solid Line Representing the Layer Striping Method, and the Bold Line Representing the Waveform-Matching Method (Ge et al., 2007)

3.4 Studies Estimating Average V_s Over Full Depth

Bodin et al. (2001) recorded ambient ground motions to estimate the fundamental vibration characteristics of more than 100 sites within and surrounding metropolitan Memphis, Tennessee. Using the Nakamura or H/V technique (Nakamura, 1989) and a quarter wavelength relationship, the fundamental resonance period, T_0 , was calculated at each site. In addition this study showed another lower peak, T_1 , which was interpreted as the first higher harmonic of T_0 .

Figure 3.7 shows a selected subset of sites with varying sediment thickness. The circles and lines represent the uncertainty and period of the maximum peak amplitude. Large circles represent T_0 with small circles representing T_1 . The gray lines represent the trend of decreasing period with decreasing sediment thickness (the dashed line at a period of about 1 indicates an electronic noise spike). It is seen that there is a strong correlation between peak periods and sediment thickness.

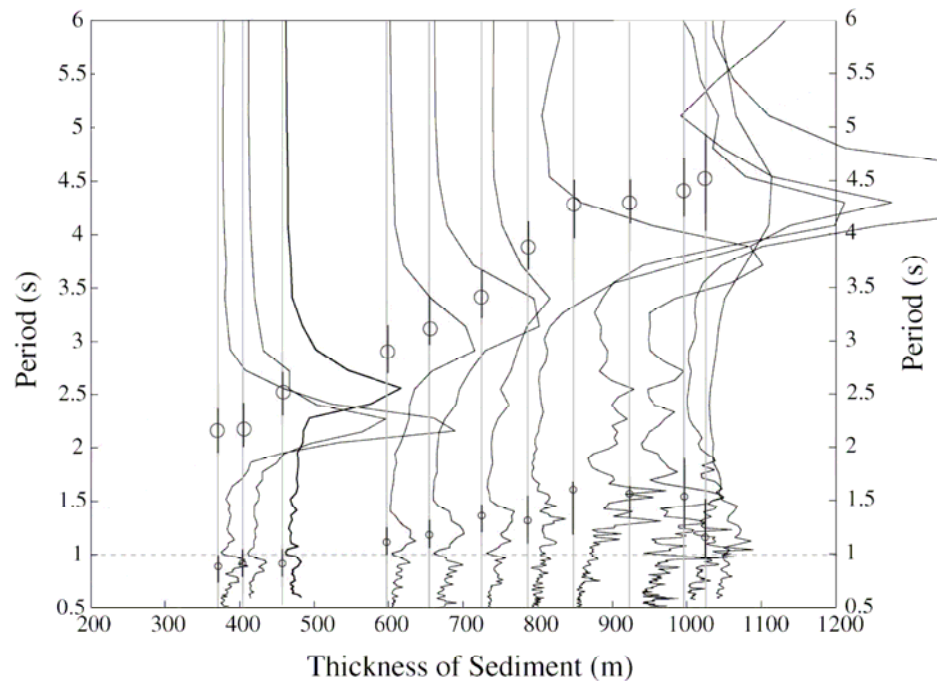


Figure 3.7 H/V Data from a Selected Subset of Sites Having Different Sediment Thickness (Bodin et al., 2001).

Figure 3.8 shows all the results from 112 sites where T_0 was measured and 55 sites where T_1 was measured. The fine solid lines represent the unweighted least squares fits of lines whereas the dashed fine curves represent unweighted least squares fits of second order polynomials. The heavy lines represent the ratios of the curves fit to the observations, T_0/T_1 , with the solid line being the ratio of linear fits and the dashed line the ratio of the polynomial fit. This data was used to support the hypothesis that T_1 is the harmonic of T_0 with the ratio of T_0/T_1 being near the theoretically expected value of 3. The correlation of T_0 with estimated thickness of sediments in the Mississippi Embayment was used to support the hypothesis that the dominant factor controlling average shear wave speed is the thickness of sediments at the site.

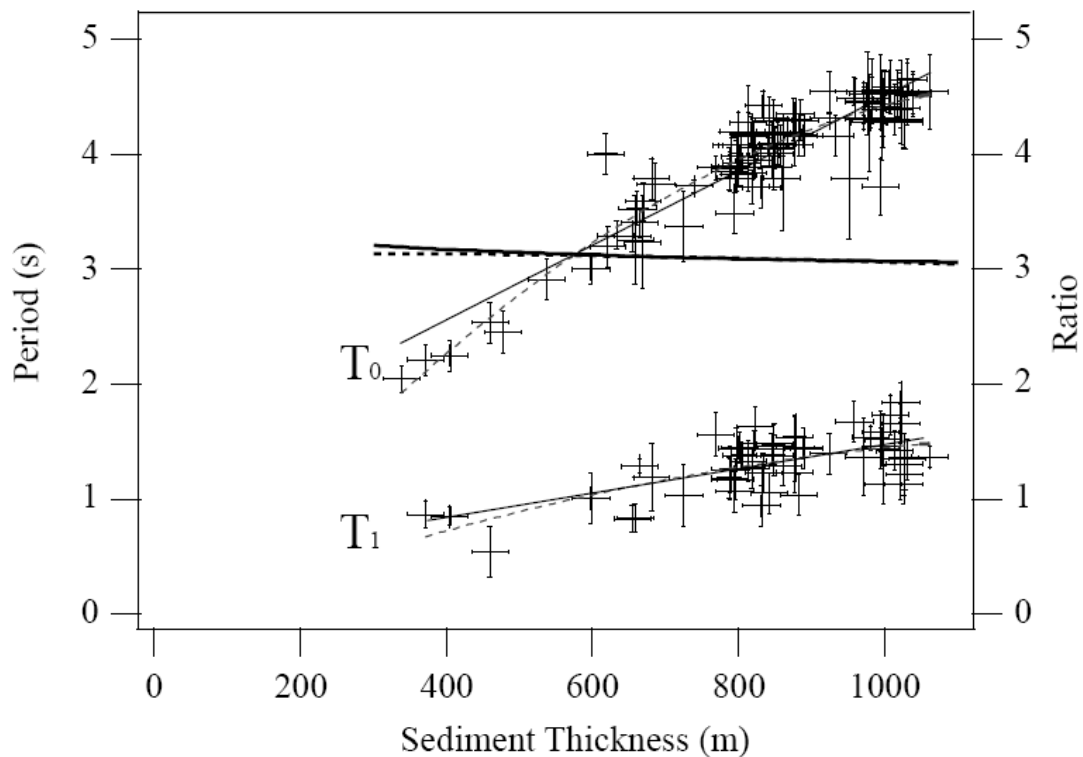


Figure 3.8 Results of H/V Testing Performed in the Upper Mississippi Embayment from Bodin et al. (2001).

A study by Chen et al. (1996) was performed to find the average V_s of the sediments within the upper Mississippi Embayment using S-to-P converted waves. Three

component digital seismograms recorded by 40 Portable Arrays for Numerical Data Acquisition (PANDA) stations throughout the New Madrid seismic zone were used. In this study the thickness of sediments beneath each PANDA station was determined by linear interpolation from well-log data with the average P-wave velocity for the sediments determined from seismic refraction data. With the knowledge of those two parameters the average V_s of the sediments beneath each PANDA station was determined based on the difference in arrival time of converted P and S waves from the bedrock. Figure 3.9 shows the combined results of the Bodin (2001) study as well as the Chen (1996) study. The solid circles represent Bodin's results with the solid line being an unweighted least-squares fit of the data to a straight line. The triangles are the results Chen obtained, with the dashed line showing the least-squares fit of the data to the estimates. Average V_s values for the full sediment depth range from approximately 600 to 900 m/s from the Bodin study and V_s values from Chen's study range from approximately 450 to 675 m/s. The results from Chen are approximately 25% lower, however, no explanation has been formulated to explain this discrepancy.

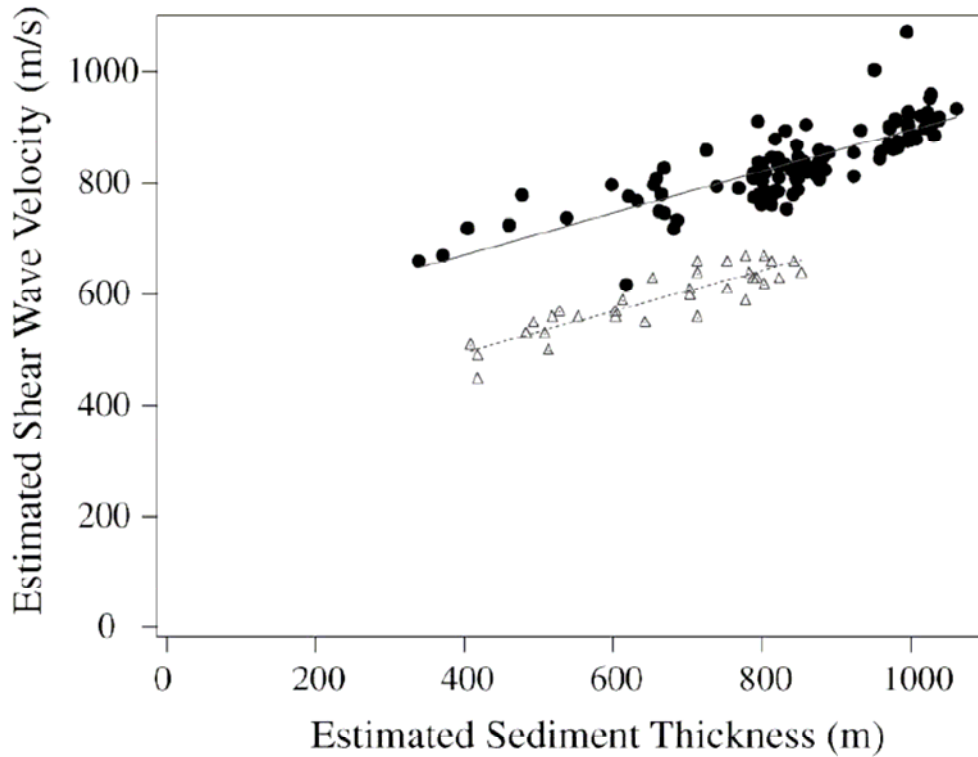


Figure 3.9 Comparison of Shear Wave Velocities obtained from Microtremor Observations (Bodin et al., 2001).

Herrmann and Akinci (1999) developed a deep soil model for mid-America to a depth of 1000 meters. They used a single empirical power law relation of:

$$V_s = 250 \bullet h^{0.18}, \quad (3.1)$$

where V_s is the shear wave velocity (in m/s) and h is the depth (in meters) of the sediment. The power law relation was constrained by shear-wave velocity measurement studies in the boot heel of Missouri, Memphis, Tennessee and western Kentucky (performed by Paul Mayne) and the requirement that the vertical travel time from rock/soil contact at New Madrid is at least 0.6 seconds.

3.5 V_s -Lithology Relationships

A goal of some past studies has been to relate V_s values to the soil lithology. In a study performed by Gomberg et al. (2003) the lithologic boundaries beneath Memphis, Tennessee were estimated using irregularly distributed geophysical well and soil boring

log data as constraints. Using 76 existing V_s profiles from refraction, a combination of refraction and reflection, and seismic piezocone (the same studies used by Romero and Rix, 2001) the estimated depth to each lithologic unit and velocity values were assigned. High-velocity layers were neglected when estimating the velocity of lithologic units. Also neglected was a designation between Mississippi River alluvium from that along other waterways. Histograms of V_s associated with each lithologic layer are presented in Figure 3.10. The velocity listed is the mean value with the horizontal line representing the standard deviation. Only a limited number of V_s values were obtained for the Memphis Sand.

The results from Gomberg et al. (2003) were compared with Romero and Rix (2001) and Williams et al. (2003). For the surficial alluvial deposits Gomberg estimated a value of 147-195 m/s with a mean value of 171 m/s, Romero and Rix estimated a value of 158-200 m/s, and Williams et al. estimated a value of 206 m/s, while using some profiles that were not used in the other two studies. The loess was estimated to have values of V_s from 155-229 m/s and mean values of 192 m/s, 176-274 m/s, and 210 m/s estimated by Gomberg et al., Romero and Rix, and Williams et al. respectively. The Lafayette Formation was estimated to have a range in V_s of 193-340 m/s from Gomberg et al. with a mean value of 268 m/s. Romero and Rix estimated the range to be 280-560 m/s. Williams et al. combined the Lafayette formation and upper Claiborne unit and found an average velocity of 455 m/s. Gomberg estimated the Jackson, Cockfield, and Cook Mountain or upper Claiborne (Eocene) to have a range of velocities from 308 m/s to 518 m/s with a mean value of 413 m/s. The Memphis Sand or lower Claiborne (Eocene) ranged from 296-to 664 m/s with a mean value of 530 m/s. The Memphis Sand

was estimated to have a V_s of 536-569 m/s by Romero and Rix and approximately 530 m/s by Williams et al. (2003). Given the uncertainties in determining soil lithology, the three studies show generally consistent results based on lithologic units. A table of values is presented in Section 3.2 of Chapter 6.

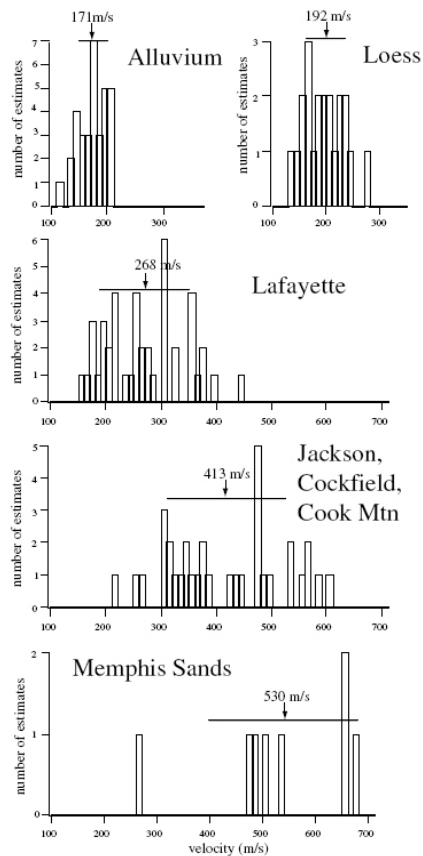


Figure 3.10 Histograms of V_s Associated with each Lithologic Layer with Mean and Standard Deviation (Gomberg et al., 2003).

3.6 Summary

Many studies have been conducted within the upper Mississippi Embayment. Within this chapter the widely used V_s reference profiles from Romero and Rix (2001) were discussed. Also studies that have been performed since the completion of Romero and Rix's study are discussed as well as studies estimating the average V_s over the full depth of the sediments within the Mississippi Embayment. Finally a comparison of findings relating the V_s to soil lithology was examined.

CHAPTER 4

METHODS

4.1 Introduction

In this study two field measurement methods were performed to determine V_s values. The first method was the Spectral-Analysis-of-Surface-Waves (SASW) method, which is a non-intrusive approach to determine V_s profiles. The second method was the H/V method, which is a common method used to estimate the fundamental frequency of a site. An overview of each method along with the implementation details for this study are presented.

4.2 Overview of SASW Method

The SASW method is one of several methods that use Rayleigh waves (R waves) to estimate V_s profiles. The primary advantage to the method is that it is non-intrusive, with the source and receivers placed directly on the ground surface. It is lower in cost as compared to conventional borehole methods, and allows for the characterization of soils that cannot be easily sampled. The method is based on the frequency-dependent penetration of surface wave energy. Surface waves with different wavelengths reach different layers of the system producing a variation of surface wave velocity with frequency, called dispersion, in a system with depth-dependent velocities (Stokoe et al., 1988). The receiver spacing and source characteristics are varied depending on the profile depth of interest. To measure near-surface layers, a short receiver spacing with a high-frequency source is used, whereas to sample deeper deposits a longer receiver spacing is required with a low-frequency source. The frequency-dependent penetration of surface waves is illustrated in Figure 4.1.

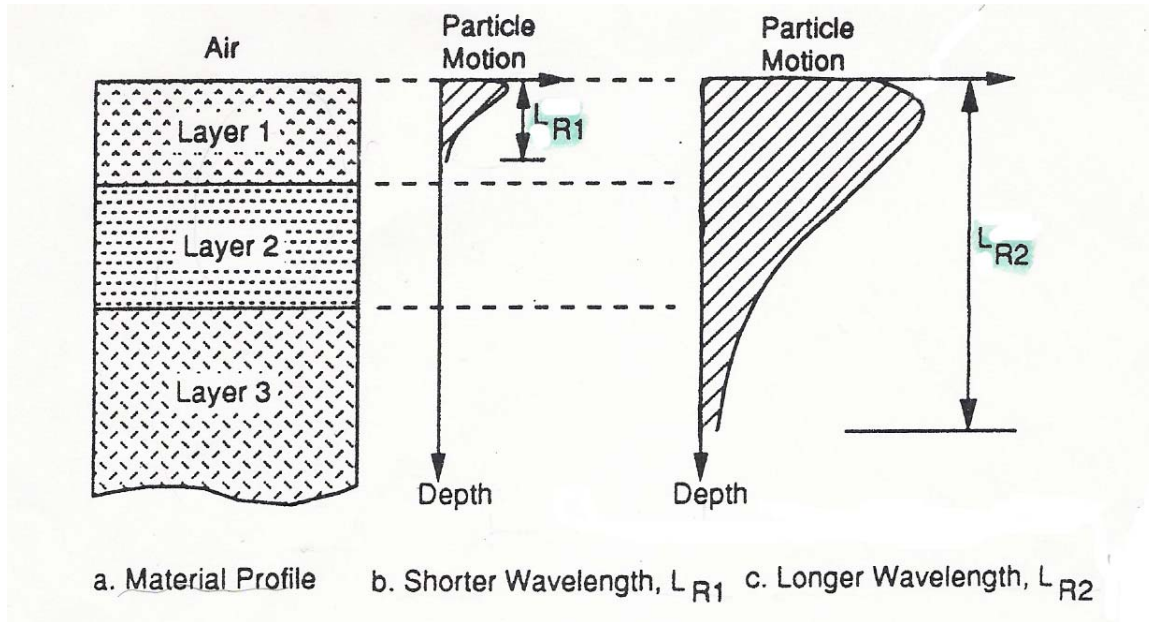


Figure 4.1 Approximate Distribution of Vertical Particle Motion with Depth for Two Rayleigh Waves with Different Wavelengths (from Rix and Stokoe, 1989).

The SASW measurement may be performed using an impulse, swept-sinusoidal or random-noise source at the ground surface. Vertically oriented receivers are placed on the surface, which record the vertical component of surface motions produced from R waves. The general setup is shown in Figure 4.2. In most cases an equal spacing is used for source-to-first-receiver and receiver-to-receiver. The receiver data is then digitized and recorded by a dynamic signal analyzer. A Fast Fourier Transform algorithm is used to calculate the wrapped phase difference ($\phi(f)$) between receiver pairs. The phase plot is manually unwrapped and the travel time, $t(f)$, between receivers is computed at each frequency by:

$$t(f) = \frac{\phi(f)}{360 \cdot f} \quad (4.1)$$

where ϕ is the unwrapped phase difference in degrees and (f) is the frequency in cycles per second. The distance between receivers (S_2-S_1) is known, so the wave velocity (V_R) is calculated using:

$$V_R = \frac{S_2 - S_1}{t(f)}. \quad (4.2)$$

The corresponding surface wavelength (λ_R) is determined using:

$$\lambda_R = \frac{V_R}{f}. \quad (4.3)$$

These calculations are performed for each frequency with the resulting data plotted as velocity versus frequency (or wavelength) termed an individual dispersion curve (Stokoe et al., 1994). This procedure is repeated for all receiver pairs producing multiple dispersion curves with overlapping sections between adjacent receiver pairs. The multiple dispersions curves are then combined to form a composite experimental (field) dispersion curve spanning the wavelengths (or frequency) of interest. The dispersion curve is an “apparent” velocity dispersion curve and may contain contributions from body wave and multiple surface wave modes. An inversion procedure is then used to determine the V_s profile that provides a matching theoretical dispersion curve to the experimental dispersion curve. The V_s profile that produces a theoretical dispersion curve most closely matching the experimental dispersion curve is presented as the V_s profile for the site. Details of each step in this procedure as well as sample data are presented below.

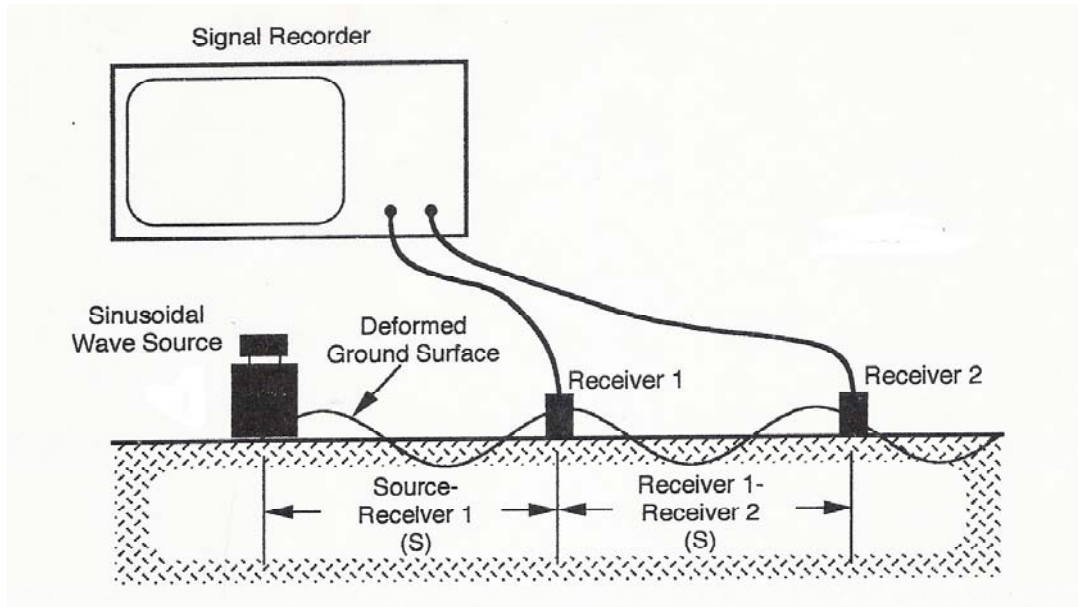


Figure 4.2 SASW Testing Configuration (for Swept Sine Excitation) (from Rix and Stokoe, 1989)

4.3 SASW Measurements in the Upper Mississippi Embayment

Measurements were performed at eleven sites in the upper Mississippi Embayment in the states of Missouri, Arkansas, and Tennessee. The sites are discussed in detail in Chapter 5. The following sections discuss field equipment, source and receiver locations, data collection, data processing, and data inversion used in this study.

4.3.1 Field Equipment

All receivers were 1-Hz geophones manufactured by Sercel Incorporated. These geophones have a flat response over a range of approximately 2 Hz to 100 Hz. Each geophone was calibrated in the lab at the University of Texas at Austin and pairs that were well matched in phase were used for low frequency measurements.

For high frequency, short-wavelength measurements (20-meters and less) an instrumented sledgehammer was used to excite the surface wave energy, as shown in Figure 4.3. The low frequency, long-wavelength measurements were performed using a unique mobile field shaker known as Liquidator, that is operated by The University of

Texas at Austin. The vibrator, shown in Figure 4.4, was developed as part of the Network for Earthquake Engineering Simulation (NEES) program funded by the National Science Foundation (NSF). This source is able to provide much higher output than a conventional Vibroseis source at frequencies below 4 Hz and can operate to frequencies of less than 1 Hz. The truck weighs 31,750 kilograms (70,000 pounds) and is 9.75 meters (32 feet) long by 2.45 meters (8 feet) wide. The truck has two vibration orientations, horizontally or vertically, but was set up to shake vertically for this study. The reaction mass is a 5,900 kilograms (13,000 pound) block of steel. The peak-to-peak stroke of the reaction mass is 0.4 meters (16 inches), with the truck being able to produce a peak force of 89 kilonewtons (20,000 pounds). Liquidator can operate at frequencies from 80 Hz to less than 0.5 Hz. The truck allows for surface wave velocity measurements at wavelengths of 3 to 4 times those excited by conventional Vibroseis equipment.



Figure 4.3 Photograph of Instrumented Sledgehammer Used to Excite High Frequency Energy.



Figure 4.4 Photograph of Low Frequency Mobile Shaker “Liquidator” developed as part of the Network for Earthquake Engineering Simulation (NEES) Program.

4.3.2 Source-Receiver Locations

Tables 4.1 and 4.2 present the source and receiver pair combinations used to create the composite experimental dispersion curves at each site. The tables are divided into the first five sites where measurements were performed in 2006 and the last six sites where measurements were performed in 2007.

Table 4.1 Receiver Pairs for 2006 Sites (S-R₁: Source to Receiver 1, R₁-R₂: Receiver 1 to Receiver 2).

SITE 1		SITE 2		SITE 3		SITE 4		SITE 5	
S-R ₁ (meters)	R ₁ -R ₂ (meters)	S-R ₁ (meters)	R ₁ -R ₂ (meters)	S-R ₁ (meters)	R ₁ -R ₂ (meters)	S-R ₁ (meters)	R ₁ -R ₂ (meters)	S-R ₁ (meters)	R ₁ -R ₂ (meters)
2	2	55	20	3	3	3	3	8	8
4	4	105	60	40	10	40	40	50	40
40	20	205	80	40	20	100	80	100	50
60	40	105	100	40	40	220	200	100	80
100	80	105	140	40	100	340	320	50	120
180	160	285	160	340	240			340	310
340	300	285	230	340	320				

Table 4.2 Receiver Pairs for 2007 Sites (S-R₁: Source to Receiver 1, R₁-R₂: Receiver 1 to Receiver 2).

SITE 6		SITE 7		SITE 8		SITE 9		SITE 10		SITE 11	
S-R ₁ (meters)	R ₁ -R ₂ (meters)	S-R ₁ (meters)	R ₁ -R ₂ (meters)	S-R ₁ (meters)	R ₁ -R ₂ (meters)	S-R ₁ (meters)	R ₁ -R ₂ (meters)	S-R ₁ (meters)	R ₁ -R ₂ (meters)	S-R ₁ (meters)	R ₁ -R ₂ (meters)
3.048	3.352	5.49	1.83	5.49	1.83	5.49	1.83	5.49	3.65	5.49	3.65
6.44-	6.44	5.49	3.65	5.49	3.65	10.98	10.97	10.98	10.97	16.46	9.2
30	30	16.46	9.2	10.98	10.97	60	56	60	56	60	56
60-	60	40	40	40	40	76	72	76	72	76	72
150	150	80	80	64	64	100	80	100	80	100	80
300	300	160	144	80	80	200	200	200	200	200	200
		208	192	208	192	250	250	250	250	250	250
		280	264	280	264	300	300	300	300	300	300

4.3.3 Data Collection

The receiver locations were surveyed in using a Nikon total station (Figure 4.5). Prior to testing, measurements with the total station were verified with tape measurements to a distance of 100 meters. After the locations were surveyed, the receivers were buried and leveled on site, as shown in Figure 4.6. Due to the high

temperatures in the field, excessive geophone temperatures that could impact the geophone performance were controlled by surrounding the geophones with cold packs and insulation, as shown in Figure 4.7. The temperature of each geophone was monitored throughout the testing using an infrared thermometer to assure that they were within their operational limits. The location of geophones as well as the source and seismic station were then recorded with a handheld GPS device, as shown in Figure 4.8.



Figure 4.5 Photograph of Total Station Used to Measure Sensor Locations.

The recording device used was a VXI-Technology, 48-channel dynamic signal analyzer for the sites measured in 2006, and a Data Physics dynamic signal analyzer for the sites measured in 2007. The source output of the dynamic signal analyzer was used to control the vibration frequency and amplitude of the source. The SASW measurements were performed in swept-sine mode. In general a frequency range from 0.7 Hz to 20 Hz was used. The number of averages at each frequency ranged from 5 to 20 and the integration time was typically 20 cycles.



Figure 4. 6 Photograph of 1-Hz geophone Placed in the Ground and Leveled.



Figure 4. 7 Photograph of 1-Hz Geophone Buried and Insulated to Maintain Low Operating Temperature.



Figure 4.8 Photograph of Undergraduate Research Assistant, Ryan Goetz, Taking GPS Reading at Site 2.

4.3.4 Data Processing

The stepped-sine measurements allowed for calculation of the cross-power spectra which provides the phase difference between each receiver pair. The analyzer transforms the signals into the frequency domain ($X(f)$ and $Y(f)$) and calculates the power spectra (G_{XX} and G_{YY}), cross spectrum (G_{XY}), wrapped phase ($\phi(f)$), and the coherence function (γ^2). Expressions for these quantities are:

$$G_{XX} = X^*(f)X(f), \quad (4.4)$$

$$G_{YY} = Y^*(f)Y(f), \quad (4.5)$$

$$G_{XY} = X^*(f)Y(f), \quad (4.6)$$

$$\phi(f) = \arctan \frac{\text{Im}(G_{XY})}{\text{Re}(G_{XY})}, \quad (4.7)$$

$$\text{and } \gamma^2 = \frac{G_{XY}G_{XY}^*}{G_{XX}G_{YY}}, \quad (4.8)$$

where (*) represents the complex conjugate of the quantity, Im signifies the imaginary part of the expression, and Re signifies the real part of the expression (Stokoe et al, 1994).

The phase of the cross spectrum and the coherence function are key spectral quantities in SASW testing. The coherence function indicates the quality of the measurements. A coherence value near one indicates a high signal-to-noise ratio with values going towards zero as the data quality decreases. The phase of the cross power spectrum represents the wrapped phase difference (lead or lag of 180°) between the two receivers. One set of the spectral functions is measured for each spacing.

Figure 4.9 shows the wrapped phase spectrum and coherence function recorded using a receiver spacing of 300 meters at Site 1. In the cross power spectrum a “saw tooth” pattern is observed. The coherence function shows coherence of near one at frequencies down to less than 1 Hz.

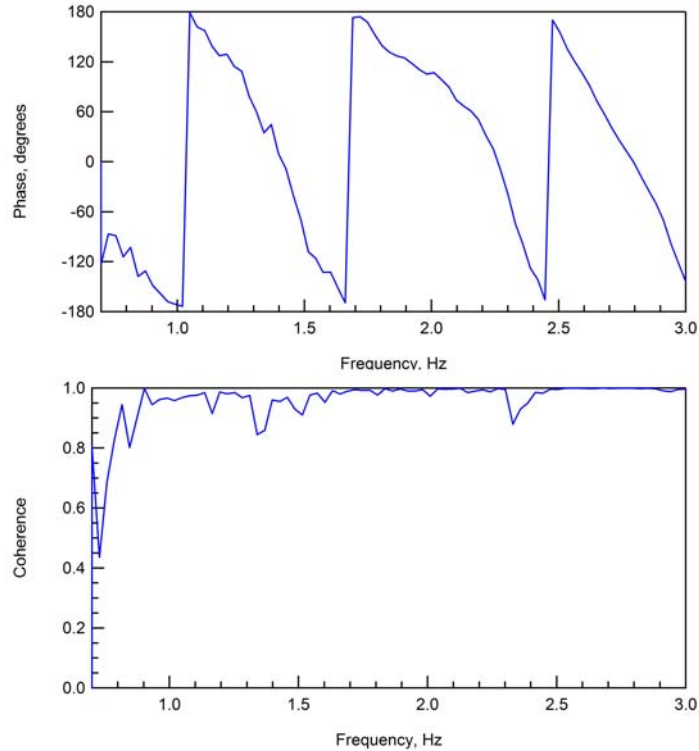


Figure 4.9 Cross Power Spectrum and Coherence Plot from 300-meter Spacing at Site 1.

The data collected in the form of phase plots and coherence functions were input into the program WinSASW2 developed by Prof. Sung Ho Joh at the University of Texas at Austin. A masking procedure was applied to the phase plot to eliminate poor quality data due to low signal quality or near-field effects. Near-field effects are dominant when the distance, S_1 (from the source to the first receiver), is small relative to the wavelength, λ_R . Under these conditions the wave cannot be approximated as a plane Rayleigh wave (Stokoe et al, 1994). To minimize near-field effects, the following criterion is imposed on the dispersion data:

$$\lambda_{R\max} < (2 \cdot S_1) \quad (4.9)$$

All lower frequency data not meeting this criterion are eliminated from the dispersion curve (Stokoe et at, 1994). Figure 4.10 presents the 300 meter spacing at Site 1 with masking applied.

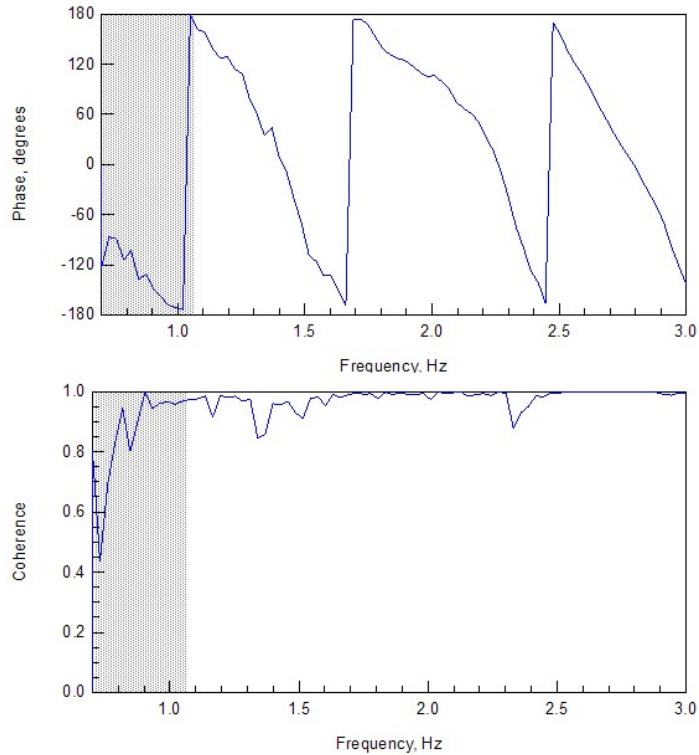


Figure 4. 10 Cross Power Spectrum and Coherence Plot from 300 meter Spacing at Site 1 after Masking (gray) is Applied.

Each jump in the “saw-tooth” pattern represents 360 degrees of phase. The masking along with the 360-degree jumps is used to manually unwrap the phase plots and calculate the individual dispersion curve using Equations 4.1 and 4.2. This process was repeated for all receiver spacings to create a composite experimental dispersion curve. The composite experimental dispersion curve is presented in Figure 4.11. The portion from the 300 meter spacing is highlighted. It should be noted that the dispersion data collected in the 2007 field study had a logarithmic distribution of frequency. WinSASW2 is not able to upload this data correctly, so the unwrapping procedure was performed using an EXCEL[®] spreadsheet.

It should also be noted that field data was collected using more sensors than were used in the SASW processing. This was done to allow for a comparison between different processing methods (SASW vs. multi-channel methods) as part of another

study. For a few, sites and phase plots (Sites 3, 8, and 10) the multi-channel analyses of the data were used to aid in interpreting the SASW phase unwrapping.

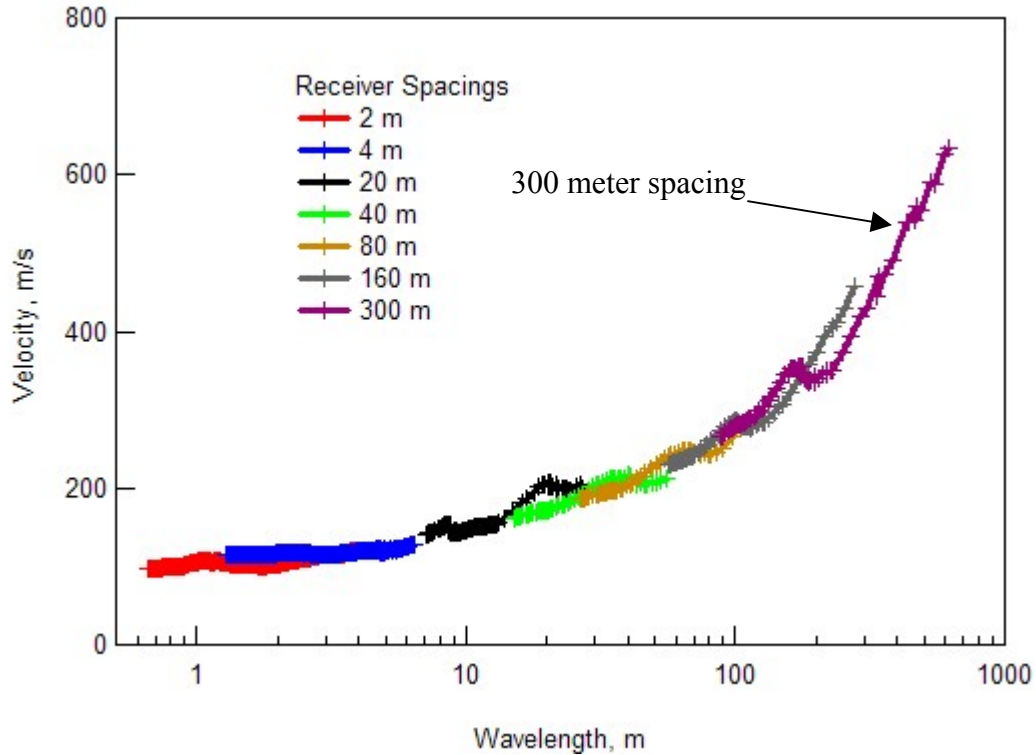


Figure 4.11 Dispersion Curve from Unwrapped Phase Plots

4.3.5 Data Inversion

This study utilized the surface wave inversion program WinSASW 2.3.1 created at the University of Texas at Austin, to develop V_s profiles from the measured dispersion curves. An automated array inversion technique described by Joh (1996) and implemented in WinSASW2 was used to develop the V_s profiles for the eleven site locations. The array inversion technique involves calculating individual theoretical dispersion curves for each receiver pair location used in the experimental measurements using a one-dimensional layered model. The mismatch between the experimental and theoretical dispersion curves is calculated and the model parameters are updated using the sensitivity matrix calculated from the forward equation. The forward equation calculated

in WinSASW2 uses the stiffness matrix approach (Kausel and Roesset 1981) and requires input of: layer thickness, V_s , Poisson's ratio (or compression wave velocity [V_p]), mass density, and material damping ratio.

The parameters used in this study were as follows. For soils above the water table (depth of 4 m or less), a Poisson's ratio value of 0.25 was assumed. Below the water table, V_p of 1,600 m/s was assumed for soils with V_s of 650 m/s or less. The V_p was increased to 1,800 m/s for soils with V_s greater than 650 m/s. These values are consistent (within 10%) with V_p measurements over a similar depth range obtained from well logs in the embayment (Cramer et al. 2004). Mass density values of 1,900 kg/m³ and material damping ratios of 2% were assumed for all soil layers. Mass density values are consistent (within 5%) with values used in other studies (Romero and Rix, 2001; Cramer, 2006) and damping values are consistent with those reported by Chen et al. (1994).

The inversion procedure implemented in WinSASW2 is a maximum likelihood approach that consists of two general steps. First, a starting V_s model is developed from the measured dispersion data. This procedure involves creating a layered profile with the same number of layers as there are points in the experimental dispersion curve. The thickness of each layer is determined based on the wavelength of the given dispersion data point and an assumed depth-to-wavelength factor, α . The V_s of the layers are determined one-by-one starting from the top layer and working down. The first layer is assumed to be a single layer system and the stiffness matrix for this system is assembled. The V_s is initially assumed to be the same as the phase velocity and is then varied to make the determinant of the stiffness matrix zero. This procedure is repeated for the second point using a two-layer system and continued on for all of the data points. From

this preliminary profile, a starting profile is determined using the profile layering information input into the program and averaging the velocity values in these profile layers. The forward model is then solved using this starting model and the RMS error calculated. The entire process is repeated for a range of α values (typically five values in the range of 0.4 to 0.8 were used) in order to find the best-fitting starting model.

Once the best starting model is found the inversion procedure is applied. The inversion engine consists of the calculation of the misfit between experimental and theoretical dispersion curves and updating the model parameters. The approach developed by Joh (1996) requires estimates of the standard deviations for the data values and the model values to provide stability to the inversion process. For this study, a value of 5% of the data and model values was used for the estimated standard deviation. Details of the inversion approach are provided in Joh (1996).

The generic profile layering used in this study was created using thicker layers at greater depths to account for the decreased sensitivity to layer thickness with depth. Layer thickness was increased from less than 1 m at the surface to over 50 m at a depth of 200 m. No *a priori* information on stratigraphy was used to develop the profile layering. The initial profile layering extended to a depth of 400 m (two-thirds of the maximum wavelength). Several iterations of the inversion procedure were performed until the best fit was achieved between the experimental and theoretical dispersion curves as indicated by the root-mean-square (RMS) error. Figure 4.12 presents the experimental and matching theoretical dispersion curves developed at Site 1. Figure 4.13 demonstrates the ability of the array inversion approach to fit the variations in the individual dispersion curves using a single one-dimensional profile.

Once a theoretical dispersion curve was matched with the experimental dispersion curve a depth resolution analysis was performed. For this study the depth of resolution of each profile was determined from a manual sensitivity study of the response of the theoretical dispersion curve to changes in the V_s of the deepest layer. This procedure involved changing the velocity of the deepest layer by 25% and observing the change in the phase velocity at the longest wavelength. If no appreciable change was observed in the dispersion curve, the lowest layer was removed and the half-space velocity was assigned to the value of the next higher layer. The procedure was repeated until a change of approximately 5% was observed in the theoretical dispersion curve at the longest wavelength. The sensitivity of each layer to the profile was indicated by increasing and decreasing the V_s value until a 10% change in RMS error was observed. An example of the V_s profile produced after the resolution and sensitivity analysis were performed is presented in Figure 4.13. The bars on each layer represent the layer sensitivity.

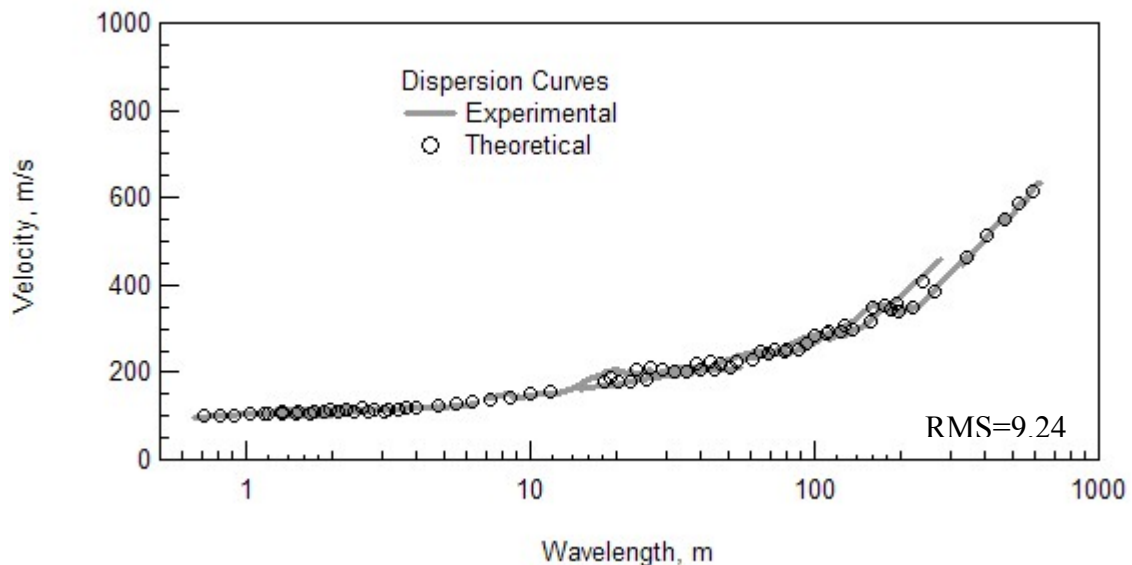


Figure 4.12 Comparison of a Theoretical and Experimental Dispersion Curve After Completion of Inversion Procedure.

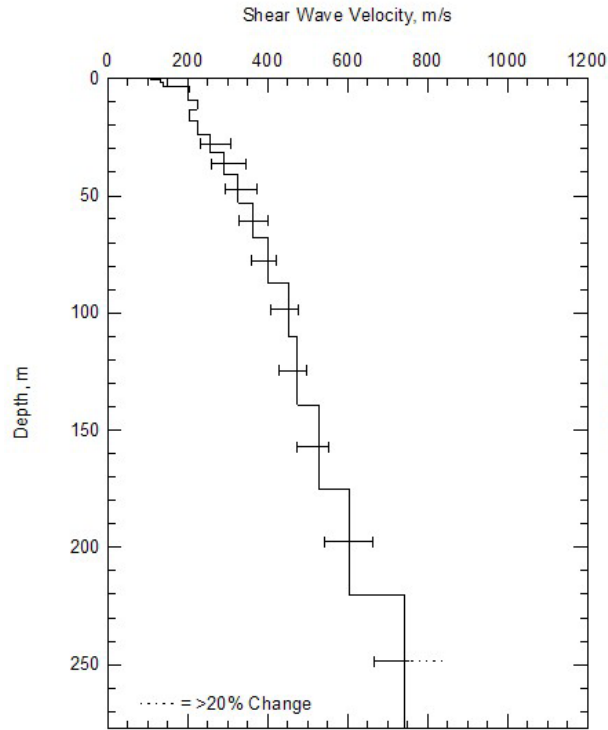


Figure 4.13 Shear Wave Velocity Profile Determined from SASW Measurements at Site 1.

4.4 Overview of H/V Method

The H/V method is a common method to estimate the fundamental frequency of a site. Using ambient noise measurements (microtremors) the ratio of the horizontal-component noise spectrum to that of the vertical component noise spectrum can be used to estimate the fundamental resonant frequency of the soft sediments. The term microtremor summarizes all ground vibrations not due to events of short duration, such as earthquakes or explosions (Steinwachs, 1974). Wind, rain, human noise, and coastal activity are all sources for these microtremors. This method of using the H/V spectrum to determine the fundamental frequency is also known as Nakamura's technique. If the depth to bedrock (or a large velocity contrast of ≈ 4 or greater) is known, the frequency can be used to estimate the average V_s in the soil above bedrock.

Figure 4.14 is a simple two-layer model, which shows the basic principle of the site effect given in terms of a transfer function. A soft sedimentary layer of thickness (m) and shear wave velocity (V_s) overlies a rock basement. For such a system the resonant frequencies occur for thickness that are uneven multiples of $\lambda/4$. Therefore the transfer function has a maximum at frequencies:

$$f_r = \frac{n \cdot v_s}{4m}, \text{ where } n=1,3,5, \text{ etc} \quad (4.10)$$

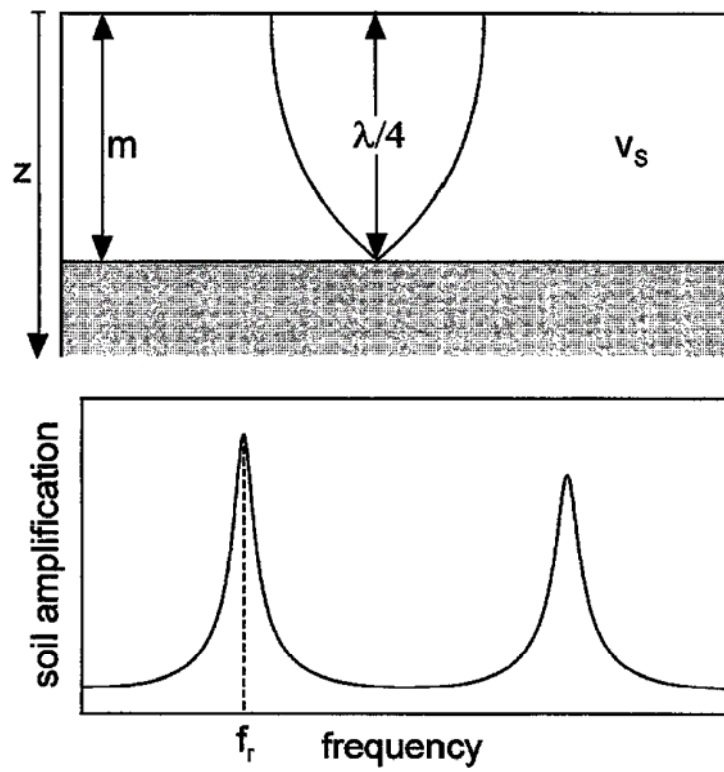


Figure 4.14 Schematic Showing the Site Response and Transfer Function for a Single Layer over Bedrock (Seht and Wohlenberg, 1999).

A noise spectrum is generally considered as the superposition of source influences (source effects) and subsoil influences (site effects). Nakamura's technique requires only one recording location where the horizontal and the vertical components are recorded and the spectral ratio (H/V spectrum) is calculated.

There are two interpretations of how Nakamura's technique works. The first explanation is that this process is said to eliminate the influence of the source effect since it is presumably made up of body waves having horizontal and vertical components. However according to Asten (2003) ambient noise is rarely dominated by body wave motion. The second explanation is that the ambient noise is predominately surface wave energy. For cases where the velocity contrast is about four or greater the vertical component of surface waves goes to near zero at a frequency that is close to the shear wave resonant frequency for the site. Therefore, the H/V spectra produces a sharp peak at a frequency that is close to the V_s resonant frequency for the site. Nakamura's technique is less expensive than other techniques because only one recording station is needed. Also the measurements can be performed quickly and can be used in areas where other measurements cannot be performed due to limited space or noise. The approach has been shown to provide reasonable results, however, a satisfactory theoretical explanation of the method has not yet been given (Seht and Wohlenberg, 1999).

4.5 H/V Measurements in Mississippi Embayment

Measurements were performed at each of eleven sites within the upper Mississippi Embayment. In the second year of testing, 2007, H/V measurements were performed at the same time as the SASW measurements, as is discussed further in Chapter 5. However, H/V measurements were not performed at the first five sites in 2006, so a return trip to the first five sites was made on November 1, 2007 to record H/V measurements.

4.5.1 Field Equipment

Measurements were performed using a Mark Product Inc. three-component seismometer with 1-Hz geophones (Model Number L-4-3D), at the same locations as the SASW measurements. The 3-component geophone was buried with one horizontal geophone having a northerly orientation, and leveled using the level bubble present on the top of the casing. Figure 4.15 is a photograph of the three-component geophone being placed at Site 5.



Figure 4. 15 Photograph of the 3-Component Geophone Being Placed at Site 5.

4.5.2 Data Collection

After the geophones were in place, ambient noise was recorded for thirty minutes at a sampling rate of 205 Hz at each site. The data was collected using the Data Physics Dynamic Signal Analyzer in the throughput mode. Figure 4.16 is a photograph of graduate students Jianhua Li and Jonathan Bailey monitoring data collection.



Figure 4. 16 Data Acquisition and Monitoring of Ambient Noise Measurements at Site 3.

4.5.3 Data Processing

The data collected was input into the J-SESAME program developed as part of a European project SESAME (Site EffectS assessment using AMbient Excitations) which provided a standardized software solution for the H/V spectral ratio technique.

Parameters were set to window out transients from the noise records automatically. The data was processed in blocks of 50 seconds, as recommended for the low-frequency nature of our measurements. The data from the vertical and two horizontally oriented geophones from Site 1, after input into the J-SESAME program, are shown in Figure 4.17. An example of windowed noise data from Site 1 is shown in Figure 4.18. The gray windows show the 50 second blocks of data that were used, while white windows represent the portion of data that was not used due to transients.

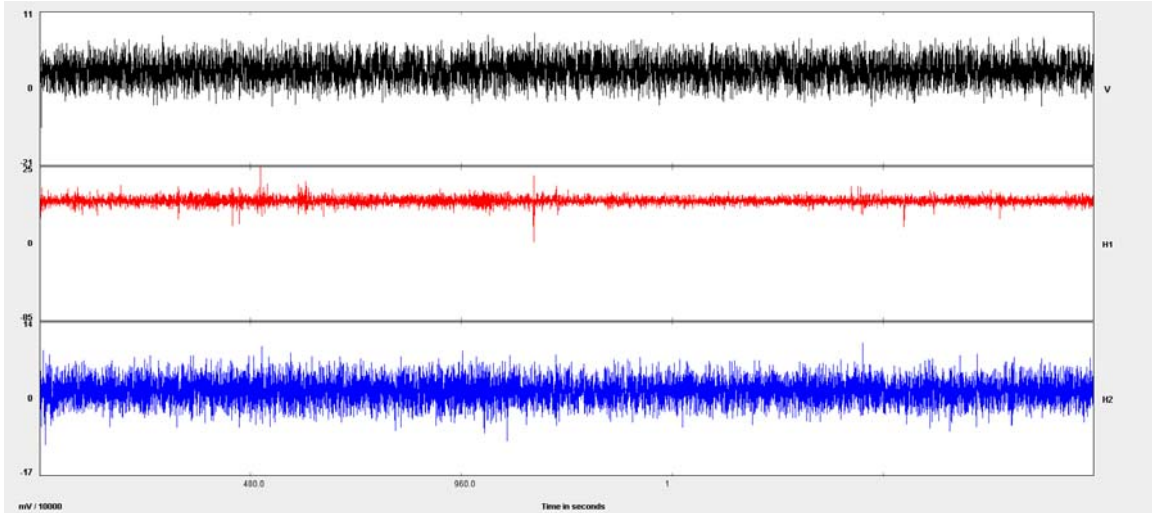


Figure 4.17 H/V Data from Site 1 after Input into the Program J-SESAME.

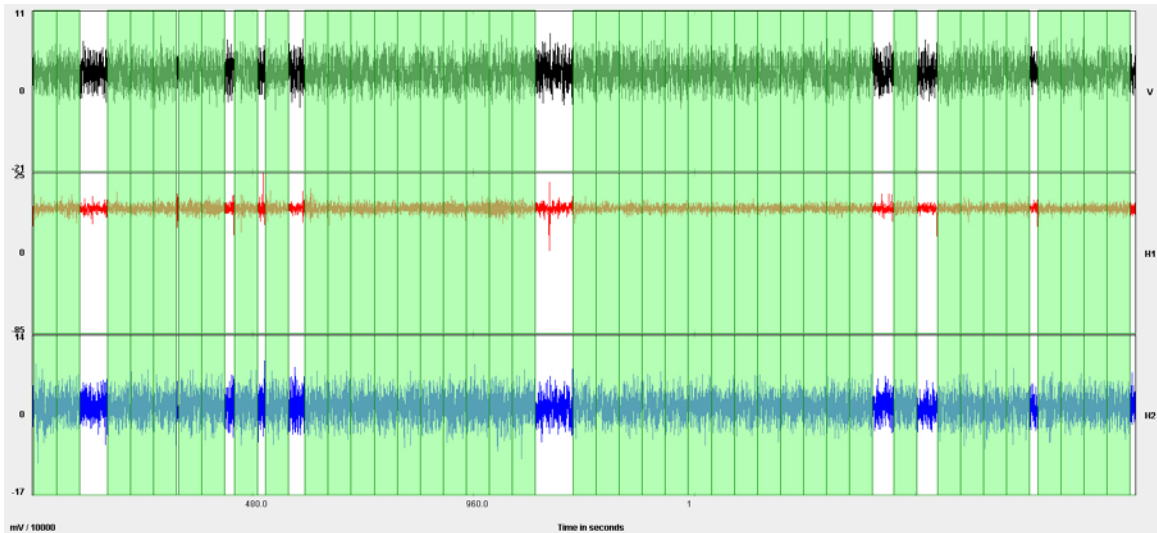


Figure 4.18 H/V Showing Windows of Data Used (Shaded) in Analysis after Filter is applied to Remove Transients.

4.5.4 Sample Results

The output file from J-SESAME is in the form of a text file, which was input into the program IGOR for plotting. The H/V ratio versus frequency plot for Site 1 is presented in Figure 4.19. Two clear peaks can be observed. Assuming a quarter wavelength relationship (Equation 4.10) along with the peak frequency and depth to bedrock, the average shear wave velocity of the sediment layer can be calculated. Further discussion of the H/V results is presented in Chapter 6.

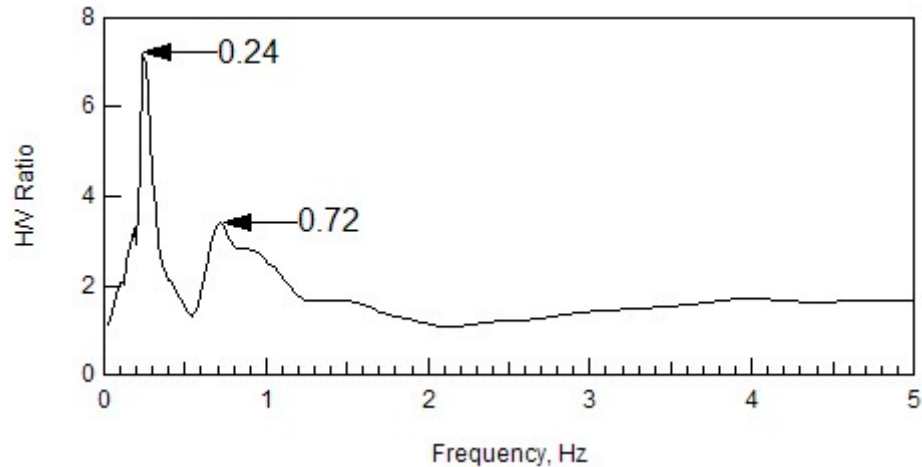


Figure 4.19 Frequency Peaks Obtained from H/V Data Measured at Site 1.

4.6 Summary

The SASW and H/V procedures used in this study were presented in this chapter. The vertical surface motion from Rayleigh wave propagation is measured in the SASW method. From the data, a phase and coherence plot is created which is masked and converted into a dispersion curve. A separate dispersion curve is created for each receiver pair at the site. The dispersion curves from the site are then combined to make an experimental dispersion curve spanning a wide range of wavelengths. An inversion analysis is performed to fit a theoretical dispersion curve to the experimental dispersion curve. The V_s profile estimate at the site is determined from the best-fit theoretical dispersion curve to the measured experimental dispersion curve.

Using ambient noise from microtremors the ratio of the horizontal-component noise spectrum to that of the vertical-component noise spectrum is found in order to predict the fundamental frequency for the site (H/V method). If the depth of bedrock is known, the average V_s can be estimated using a quarter wavelength approximation. A three-component geophone was used to perform these measurements, which were then recorded and analyzed using the computer program J-SESAME. The output file from J-

SESAME is plotted as the H/V ratio versus frequency. The plot shows the peak frequencies measured at each site, which is used along with sediment thickness to predict the average V_s of a site.

CHAPTER 5

SITE LOCATIONS AND LOCAL LITHOLOGY

5.1 Introduction

Eleven sites within the Mississippi Embayment were evaluated using both the SASW method as well as the H/V method. Figure 5.1 presents a map of the Mississippi Embayment region showing the locations of the eleven sites. Ten sites are located in the lowlands or Holocene-age deposits with one site (Site 7) located in the uplands or Pleistocene-age deposits. Table 5.1 presents the GPS coordinates at the center of the array of each site as well as the depth to bedrock.

Sites were chosen based on multiple criteria. First, the large field vibrator (“Liquidator”) had to be able to access the site and operate safely without affecting nearby structures. Secondly, the site needed to have a flat linear stretch of open land in excess of 600 meters in length to allow for deployment of the sensors. Also for sites that met the previous criteria, permission had to be obtained from the local landowner to access the site. When possible, sites were chosen adjacent to seismic stations operated by the Center for Earthquake Research and Information (CERI) at the University of Memphis. Also, sites near the location of previous research studies were considered. Lastly, it was desired to distribute the sites around the Mississippi Embayment to sample variable sediment conditions and depth to bedrock.

In this chapter, a brief overview of each site is presented. This includes the location of the site, a site description with photos, and the estimated local site lithology provided to us by Professor Roy Van Arsdale from the University of Memphis. Dr. Van Arsdale, along with help from Ph.D. students, provided information on the estimated

depths to the geologic tops of each unit for each of our site locations. According to Dr. Van Arsdale this was done using nearby wells and depth converted seismic reflection lines for each stratigraphic top over a large area to create a structure contour map for the upper Mississippi Embayment. The constructed surfaces were queried for each stratigraphic top at each of the site locations. The values returned were presented in the form of elevation of each formation top. Using the elevations at each site along with the elevations to the top of each formation, each soil profile was developed. The depth to the alluvial deposits and top of the upper Claiborne deposits at the eleven sites were based on geologic and geotechnical logs. In most cases, the nearest well site was within 0.5 to 1.5 km of the site location. The depth to the top of the mid Claiborne and lower Claiborne was based on more sparsely sampled well data that were typically located 4 to 8 km from our sites. Therefore, the depths to the formation tops presented in this study are interpolated values for our locations.

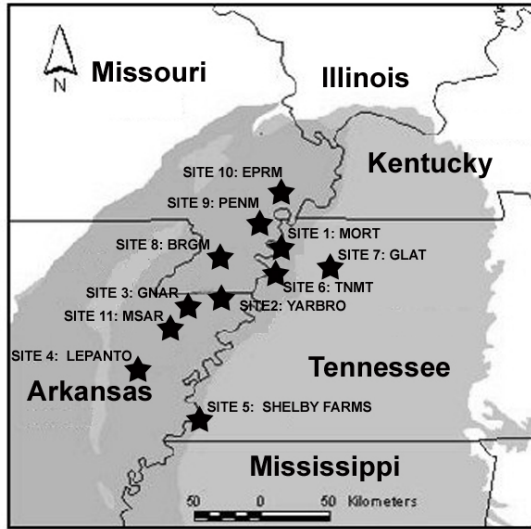


Figure 5.1 Site Location in the Mississippi Embayment (Map Modified from Romero & Rix, 2001)

Table 5.1 Site Coordinates and Estimated Depth to Bedrock (Δ denotes CERL Station)

Site	Name	GPS Coordinates at Array Center		Depth To Bedrock (Meters)
		Latitude	Longitude	
1	MORT ^Δ	Latitude	Longitude	703
		32°32'65.02" N	89°56'72.03" W	
2	YARBRO	Latitude	Longitude	820
		35°58'54.16" N	89°54'47.35" W	
3	GNAR ^Δ	Latitude	Longitude	783
		35°57'37.58" N	90°0'58.07" W	
4	LEPANTO	Latitude	Longitude	794
		35°36'51.62" N	90°24'42.47" W	
5	SHELBY FARMS	Latitude	Longitude	840
		35°8'9.56" N	89°50'46.36" W	
6	TNMT ^Δ	Latitude	Longitude	783
		36°9'41.05" N	89°34'43.27" W	
7	GLAT ^Δ	Latitude	Longitude	751
		36°15'45.16" N	89°17'16.31" W	
8	BRGM ^Δ	Latitude	Longitude	714
		36°15'45.16" N	89°17'16.31" W	
9	PENM ^Δ	Latitude	Longitude	586
		36°27'14.04" N	89°37'42.74" W	
10	EPRM ^Δ	Latitude	Longitude	451
		36°42'59.90" N	89°21'40.24" W	
11	MSAR ^Δ	Latitude	Longitude	847
		35°46'54.21" N	90°8'57.69" W	

5.2 SITE 1: MORT

The first SASW measurement was performed on May 17, 2006 at the CERI seismic station named MORT. On November 1, 2007 a return trip was made to conduct the H/V measurement at the site. Site 1 is located in western Tennessee west of State Route 78 approximately ten miles southeast of Site 9 in Mooring, Tennessee. Figure 5.2 presents a Google Earth image of Site 1 with the extent and orientation of the SASW array shown with a black line. The surface wave measurements were performed as described in Section 4.3 of Chapter 4. The location of the source is indicated on the site map. The location of the CERI seismic station, MORT, is also indicated in Figure 5.2. A maximum receiver spacing of 300 meters was used with a maximum source-to-far-receiver distance of 640 meters. Figure 5.3 presents a view looking from the end of the array towards the source, and Figure 5.4 is a close up view of the geophone being placed at the site.

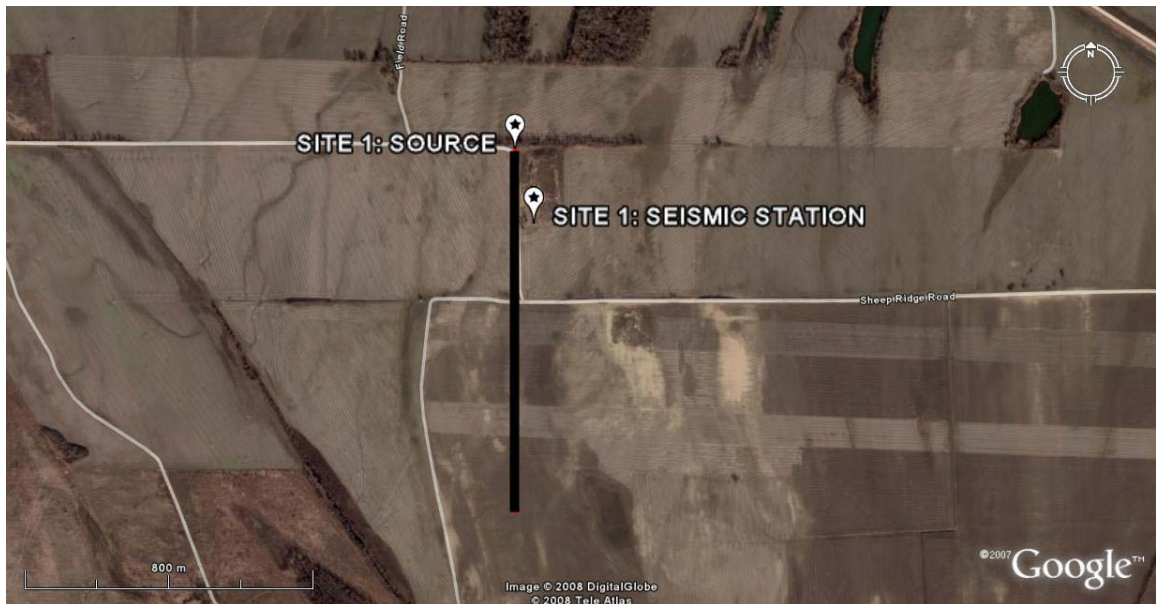


Figure 5.2 Google Earth Image of Site 1 (MORT).

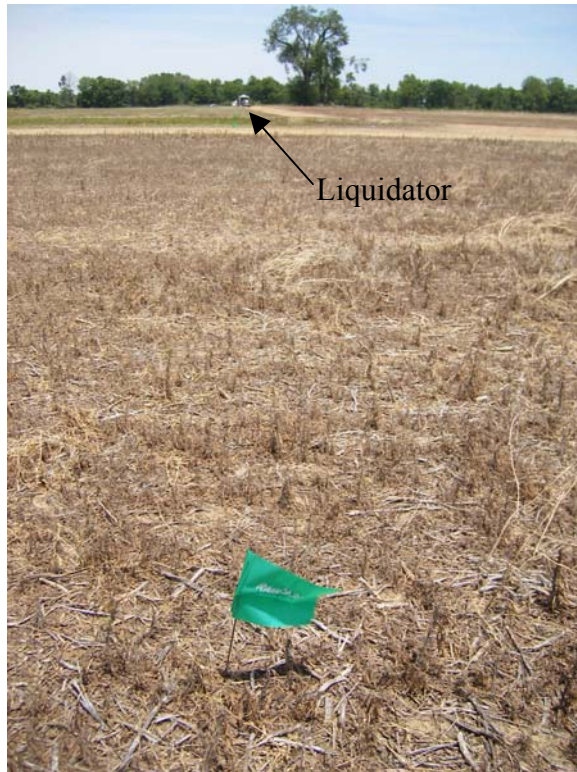


Figure 5.3 Photograph from the Furthest Receiver Location Looking Back Towards the Source.



Figure 5.4 Photographs of Geophone and Surficial Soil at Site 1.

Site 1 is located on Holocene-age, near-surface alluvial deposits on farmland approximately a mile from the Mississippi River. In Table 5.2 and Figure 5.5 the estimated site lithology down to the mid-Wilcox boundary (312 meters) is presented. Silt/clay, sand, and gravel compose the top three layers of the soil lithology followed by a thick upper Claiborne layer overlying the Memphis Sand. The depth to bedrock at Site 1 is estimated to be approximately 700 meters.

Table 5.2 Estimated Profile at Site 1 (MORT) Provided by Roy Van Arsdale from the University of Memphis.

Depth (meters)	Thickness (meters)	Deposit
0-8	8	Silt/Clay
8-19	11	Sand
19-41	22	Gravel
41-156	115	Upper Claiborne (Jackson, Cockfield and Cook Mountain Formations)
156-212	56	Mid Claiborne (Memphis Sand Formation)
212-312	100	Lower Claiborne/Upper Wilcox (Memphis Sand/Flour Island Formations)

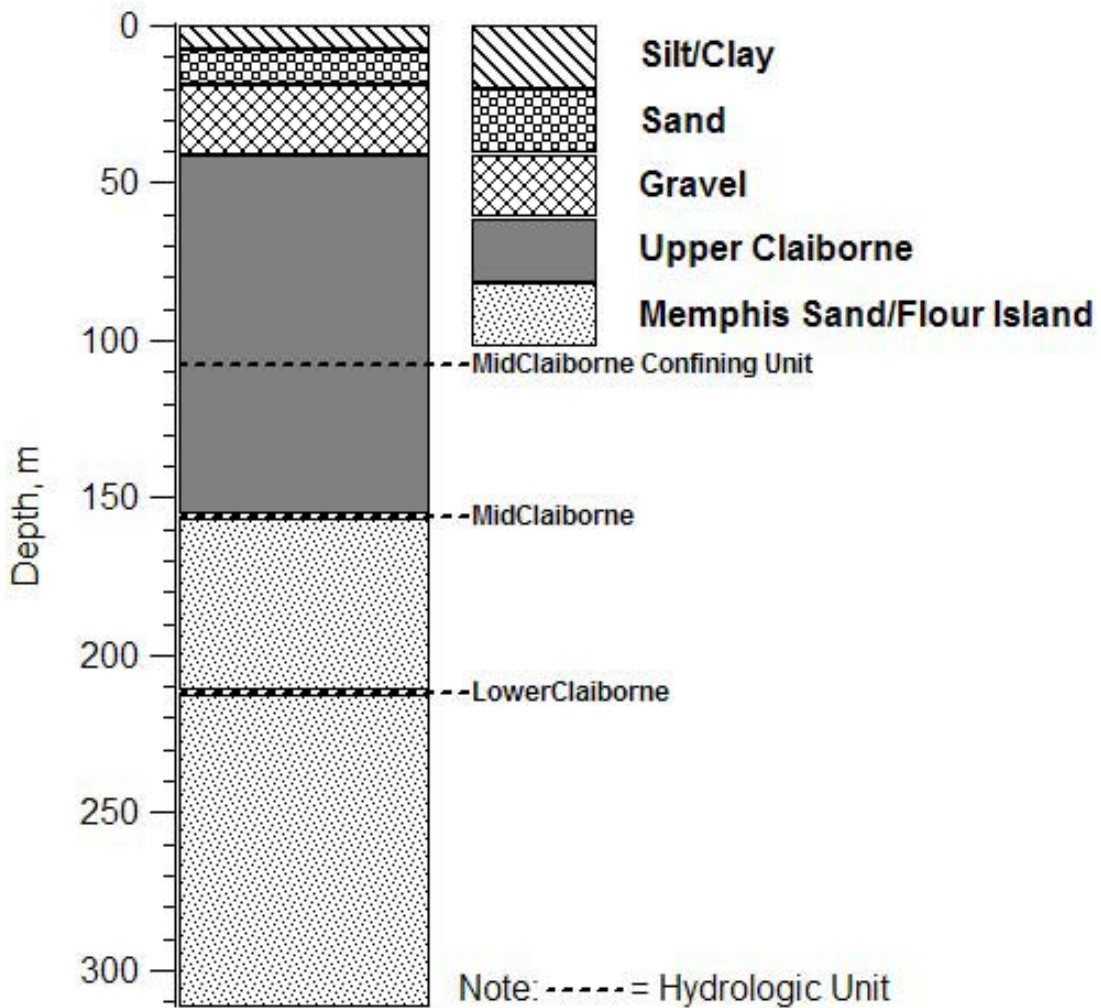


Figure 5.5 Estimated Soil Lithology at Site 1 (MORT).

5.3 SITE 2: YARBRO (“JOE’S POND”)

SASW measurements were performed on May 21, 2006 at Site 2. On November 1, 2007 a return trip was made to conduct the H/V measurement at the site. Site 2 is located in northeastern Arkansas to the west of Interstate 55 and north of State Route 150, approximately fifteen miles south of Site 8. The site was chosen because of past liquefaction studies that have been conducted near this site. Figure 5.6 presents a Google Earth image of Site 2 with the extent and orientation of the SASW array shown with a black line. The surface wave measurements were performed as described in Section 4.3 of Chapter 4. The location of the source is indicated on the site map. A maximum receiver spacing of 230 meters was used at Site 2 with a maximum total source-to-far-receiver distance of 515 meters. Space limitations at the site prevented the use of a longer array. Figure 5.7 presents a view looking from the end of the array towards the source.

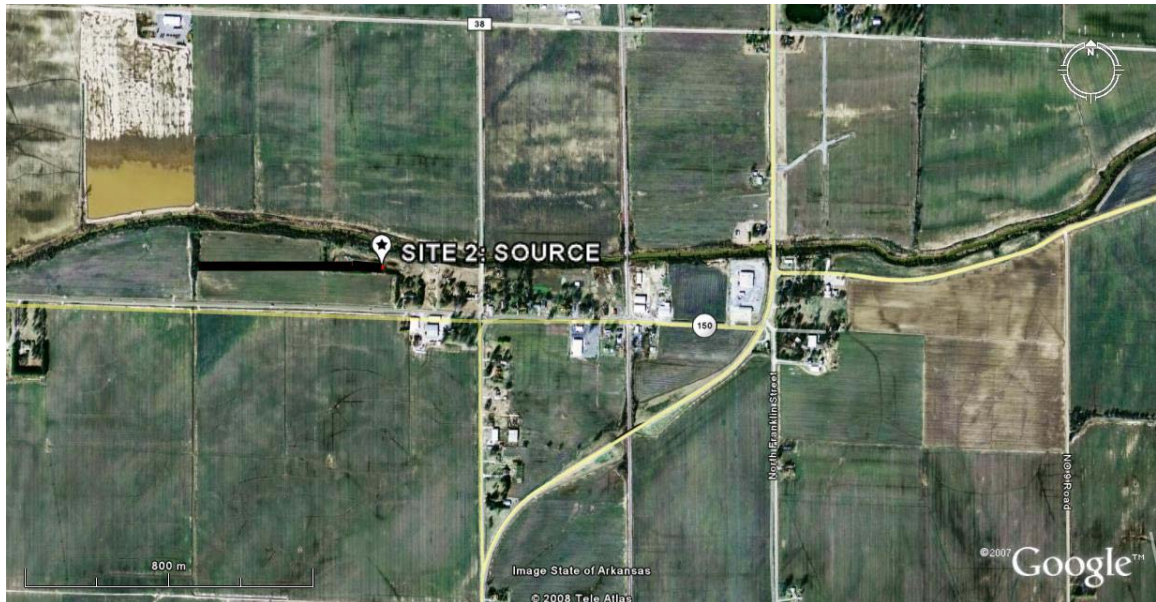


Figure 5.6 Google Earth Image of Site 2 (Yarbro).



Figure 5.7 Photographs from the End of Array Looking Back Towards the Source.

Site 2 is located on Holocene-age, near-surface alluvial deposits. In Table 5.3 and Figure 5.8 the estimated site lithology down to the mid-Wilcox boundary (288 meters) is presented. Sand, and gravel compose the top two layers of the soil lithology followed by an upper Claiborne layer overlying the Memphis Sand. At Site 2 a thick upper Claiborne Formation is seen. The depth to bedrock at Site 2 is estimated to be approximately 820 meters.

Table 5.3 Estimated Profile at Site 2 (YARBRO) Provided by Roy Van Arsdale from the University of Memphis.

Depth (meters)	Thickness (meters)	Deposit
0-0	0	Silt/Clay
0-21	21	Sand
21-39	18	Gravel
39-118	79	Upper Claiborne (Jackson, Cockfield and Cook Mountain Formations)
118-181	63	Mid Claiborne (Memphis Sand Formation)
181-288	107	Lower Claiborne/Upper Wilcox (Memphis Sand/Flour Island Formations)

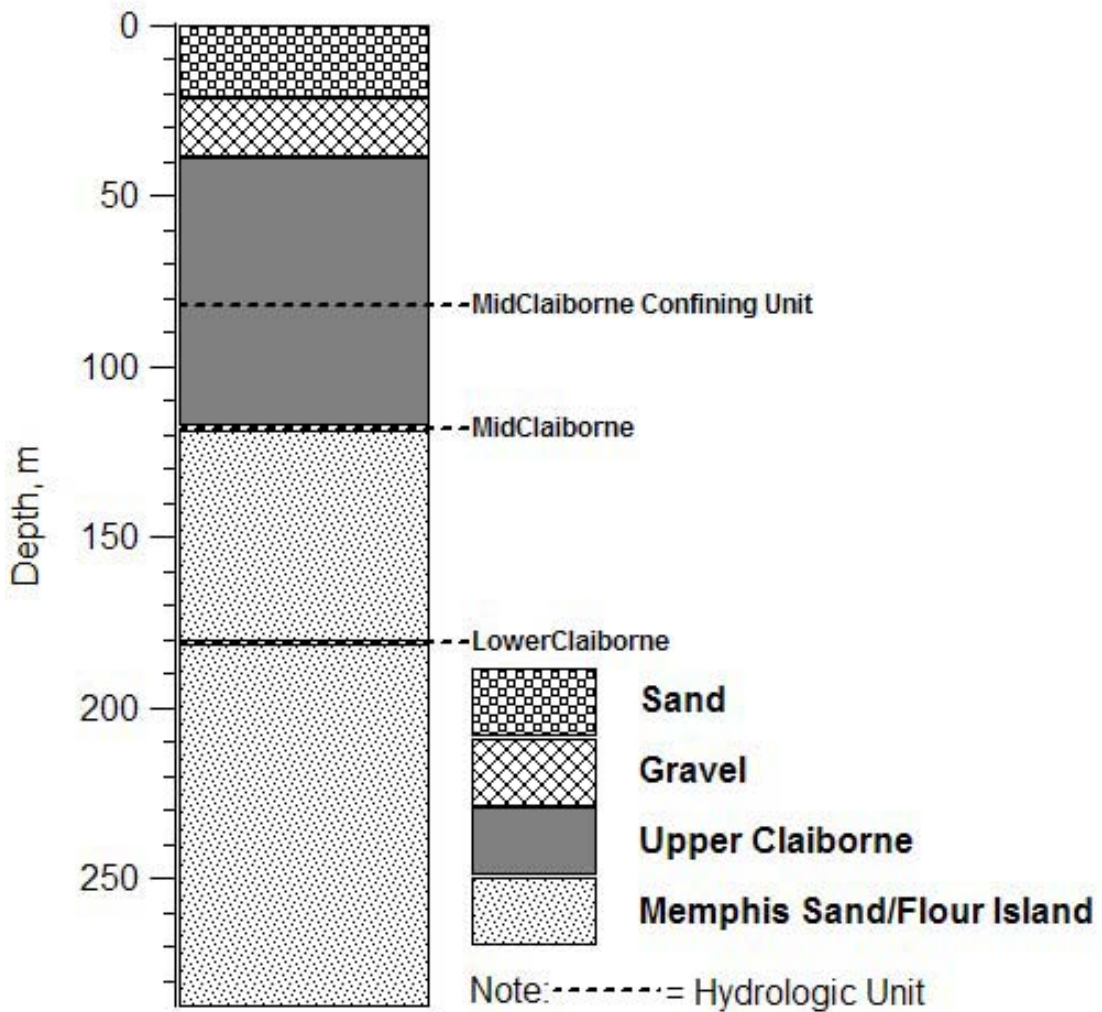


Figure 5.8 Estimated Soil Lithology at Site 2 (YARBRO).

5.4 SITE 3: GNAR

SASW measurements were performed on May 23, 2006 at the CERI seismic station named GNAR. On November 1, 2007 a return trip was made to conduct the H/V measurement at the site. Site 3 is located approximately six miles southwest of Site 2 in northeastern Arkansas. Figure 5.9 presents a Google Earth image of Site 3 with the extent and orientation of the SASW array shown with a black line. The surface wave measurements were performed as described in Section 4.3 of Chapter 4. The location of the source is indicated on the site map. The location of the CERI seismic station, GNAR, is also indicated in Figure 5.9. A maximum receiver spacing of 320 meters was used at Site 3 with a maximum total source-to-far-receiver distance of 660 meters. A photograph of Site 3 is presented in Figure 5.10, with the seismic station, GNAR, evident in the background.



Figure 5.9 Google Earth Image of Site 3 (GNAR).



Figure 5.10 Photograph of Distance from Array Line to Seismic Station.

Site 3 is located on Holocene-age, near-surface alluvial deposits. In Table 5.4 and Figure 5.11 the estimated site lithology down to the mid-Wilcox boundary (275 meters) is presented. Silt/clay, sand, and gravel compose the top three layers of the soil lithology followed by a thick upper Claiborne layer overlying the Memphis Sand. The depth to Memphis Sand is relatively shallow at Site 3. The depth to bedrock at Site 3 is estimated to be approximately 780 meters.

Table 5.4 Estimated Profile at Site 3 (GNAR) Provided by Roy Van Arsdale from the University of Memphis.

Depth (Meters)	Thickness (meters)	Deposit
0-8	8	Silt/Clay
8-22	14	Sand
22-42	20	Gravel
42-100	58	Upper Claiborne (Jackson, Cockfield and Cook Mountain Formations)
100-169	69	Mid Claiborne (Memphis Sand Formation)
169-275	106	Lower Claiborne/Upper Wilcox (Memphis Sand/Flour Island Formations)

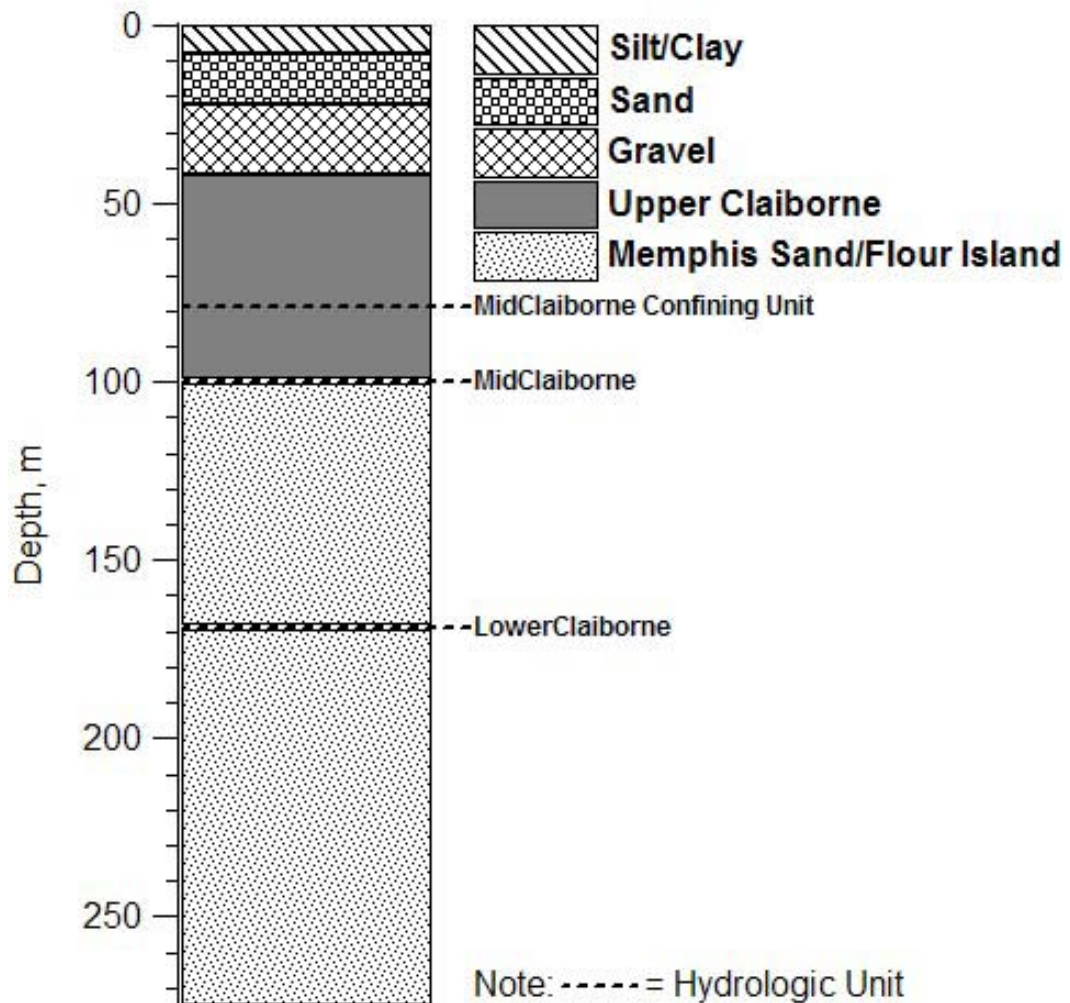


Figure 5.11 Estimated Soil Lithology at Site 3 (GNAR).

5.5 SITE 4: LEPANTO

SASW measurements were performed on May 25, 2006 at Site 4. On November 1, 2007 a return trip was made to conduct the H/V measurement at the site. Site 4 in northeastern Arkansas is located approximately nineteen miles southwest of Site 11. Site 4 is west of Interstate 55 and approximately five miles past the city of Lepanto on State Road 14. Figure 5.12 presents a Google Earth image of Site 4 with the extent and orientation of the SASW array shown with a black line. The surface wave measurements were performed as described in Section 4.3 of Chapter 4. The location of the source is indicated on the site map. A maximum receiver spacing of 320 meters was used at Site 4 with a maximum total source-to-far-receiver distance of 660 meters. Figure 5.13 presents a photograph looking down the array layout towards the source. Also shown in Figure 5.13 is the instrumentation van.

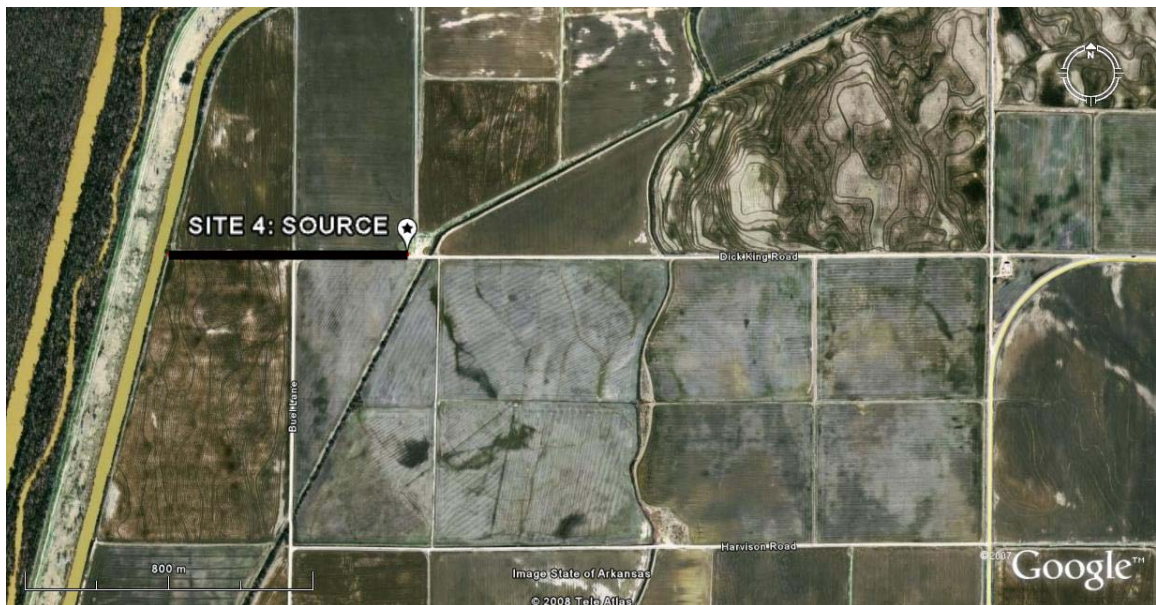


Figure 5.12 Google Earth Image of Site 4 (Lepanto).



Figure 5.13 Photograph Looking Down the Array Towards the Source at Site 4.

Site 4 is located on Holocene-age, near-surface alluvial deposits. In Table 5.5 and Figure 5.14 the estimated site lithology down to the mid-Wilcox boundary (297 meters) is presented. Silt/clay, sand, and gravel compose the top three layers of the soil lithology followed by a relatively thin upper Claiborne layer overlying the Memphis Sand. The depth to bedrock at Site 4 is estimated to be approximately 790 meters.

Table 5.5 Estimated Profile at Site 4 (LEPANTO) Provided by Roy Van Arsdale from the University of Memphis.

Depth (meters)	Thickness (meters)	Deposit
0-5	5	Silt/Clay
5-27	22	Sand
27-47	20	Gravel
47-94	47	Upper Claiborne (Jackson, Cockfield and Cook Mountain Formations)
94-167	73	Mid Claiborne (Memphis Sand Formation)
167-297	130	Lower Claiborne/Upper Wilcox (Memphis Sand/Flour Island Formations)

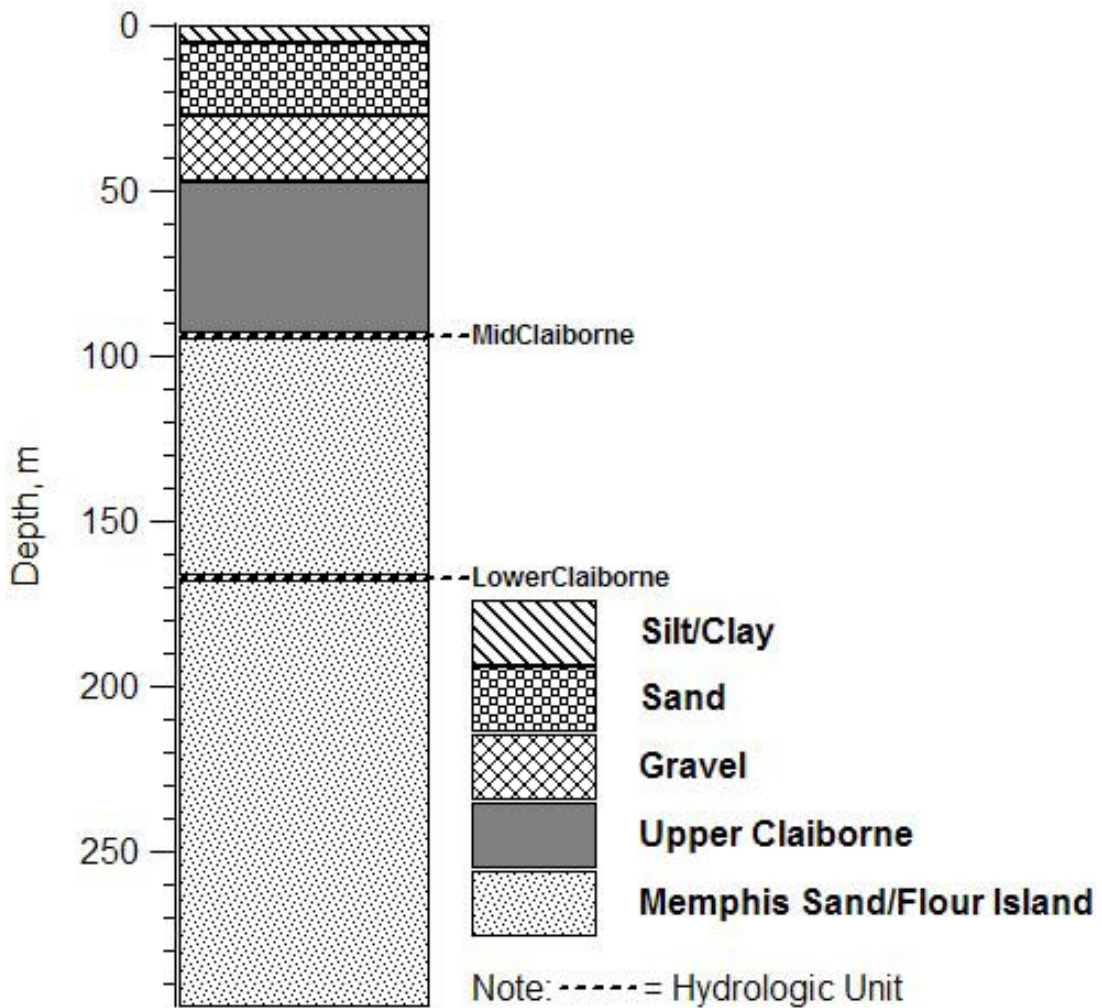


Figure 5.14 Estimated Soil Lithology at Site 4 (LEPANTO).

5.6 SITE 5: SHELBY FARMS

SASW measurements were performed on May 27, 2006 at Site 5. On November 1, 2007 a return trip was made to conduct the H/V measurement at the site. Site 5 is located west of Interstate 240 and to the north of Walnut Grove Road in Memphis, Tennessee. Site 5 is the furthest site to the south and is approximately 46 miles southeast of Site 4 in a public park named Shelby Farms. Site 5 was the only site located in an urban environment. Several shallow studies discussed in Chapter 3 have been conducted near Site 5. The deep borehole with suspension log measurements, shown in Figure 3.5, was located approximately 5 kilometers from Site 5. Figure 5.15 presents a Google Earth image of Site 5 with the extent and orientation of the SASW array shown with a black line. The surface wave measurements were performed as described in Section 4.3 of Chapter 4. The location of the source is indicated on the site map. A maximum receiver spacing of 310 meters was used at Site 5 with a maximum total source-to-far-receiver distance of 650 meters. Figure 5.16 presents a view looking down the array towards the source.



Figure 5.15 Google Earth Image of Site 5 (Shelby Farms).

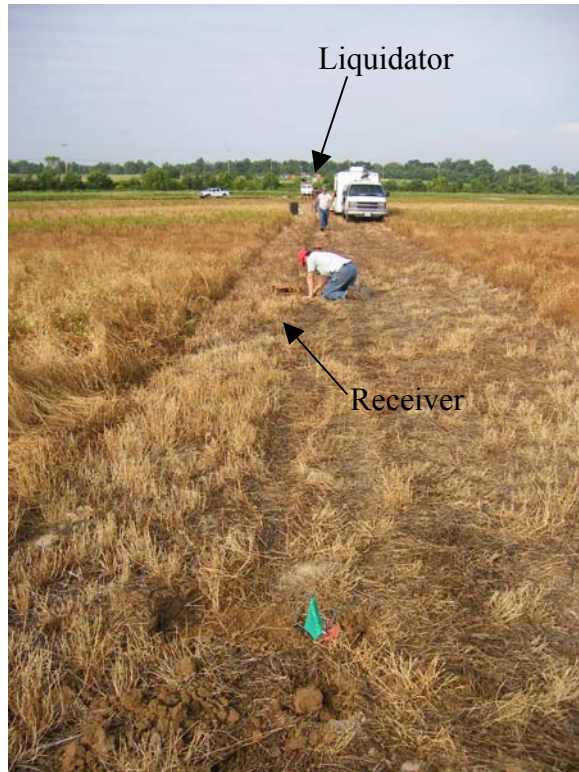


Figure 5.16 Photograph Looking Back Towards the Source.

Site 5 is located on Holocene-age, near-surface alluvial deposits in the floodplain of the Wolf River. In Table 5.6 and Figure 5.17 the estimated site lithology down to the mid-Wilcox boundary (210 meters) is presented. The lithology at this location was estimated from published profiles near this site (Gomberg, 2003). Silt/clay and gravel compose the top two layers of the soil lithology followed by a thin upper Claiborne layer overlying the Memphis Sand. At Site 5 due to the thin alluvial deposits as well as the thin upper Claiborne deposits, the top of the Memphis Sand is very shallow as compared to the other 10 sites. The depth to bedrock at Site 5 is estimated to be approximately 840 meters.

Table 5.6 Estimated Profile at Site 5 (SHELBY FARMS) based on Profiles Presented by Gomberg (2003).

Depth (meters)	Thickness (meters)	Deposit
0-10	10	Silt/Clay
10-18	8	Gravel
18-40	22	Upper Claiborne (Jackson, Cockfield and Cook Mountain Formations)
40-250	210	Memphis Sand (Mid Claiborne/Lower Claiborne)

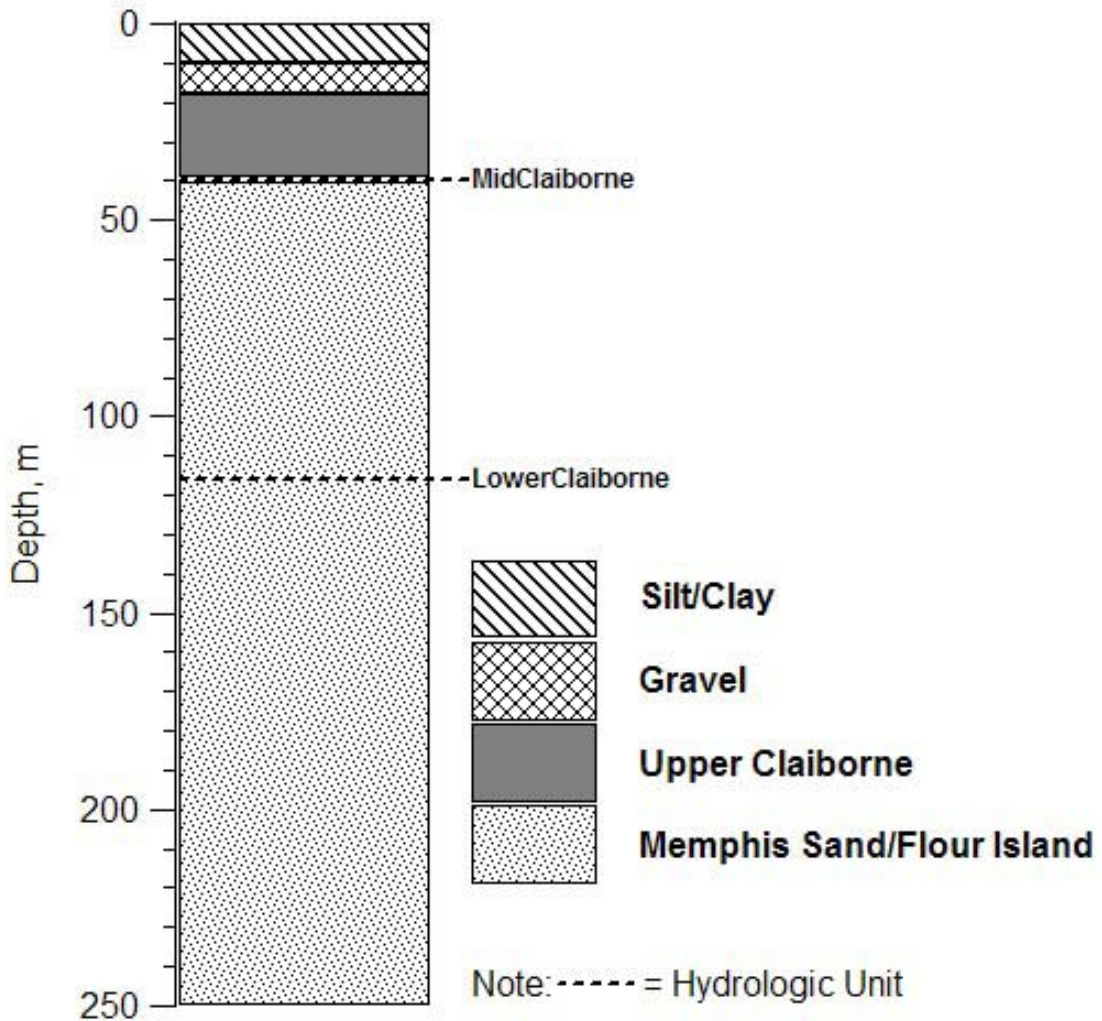


Figure 5.17 Estimated Soil Lithology at Site 5 (SHELBY FARMS).

5.7 SITE 6: TNMT

SASW and H/V measurements were performed on May 17, 2007 at the CERI seismic station named TNMT. Site 6 is located to the north of State Road 103 past the town of Tennemo on Woods Road in western Tennessee. Site 6 is located approximately eleven miles south of Site 1. Figure 5.18 presents a Google Earth image of Site 6 with the extent and orientation of the SASW array shown with a black line. The surface wave measurements were performed as described in Section 4.3 of Chapter 4. The location of the source is indicated on the site map. The location of the CERI seismic station, TNMT, is also indicated in Figure 5.19. A maximum receiver spacing of 300 meters was used at Site 6 with a maximum total source-to-far-receiver distance of 600 meters. Figure 5.19 presents a view looking down the array towards the source.



Figure 5.18 Google Earth Image of Site 6 (TNMT).

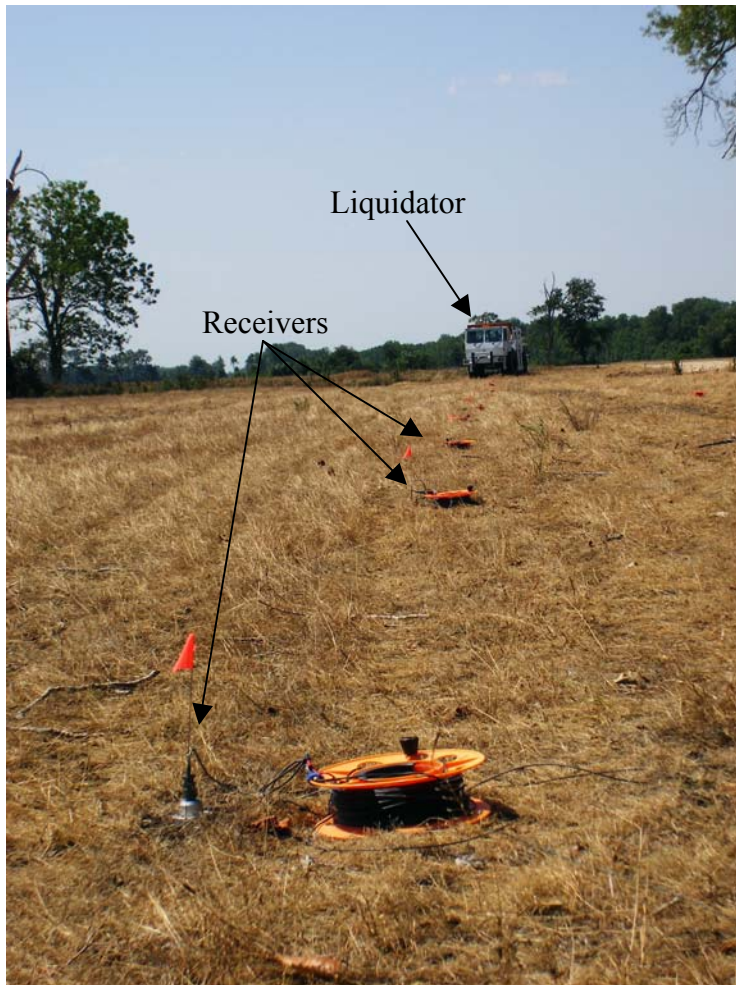


Figure 5.19 Photograph Looking Down the Array Towards the Source.

Site 6 is located on Holocene-age, near-surface alluvial deposits. In Table 5.7 and Figure 5.20 the estimated site lithology down to the mid-Wilcox boundary (322 meters) is presented. Silt/clay, sand, and gravel compose the top three layers of the soil lithology followed by a thick upper Claiborne layer overlying the Memphis Sand. The depth to bedrock at Site 6 is estimated to be approximately 780 meters.

Table 5.7 Estimated Profile at Site 6 (TNMT) Provided by Roy Van Arsdale from the University of Memphis.

Depth (meters)	Thickness (meters)	Deposit
0-9	9	Silt/Clay
9-20	11	Sand
20-49	29	Gravel
49-157	108	Upper Claiborne (Jackson, Cockfield and Cook Mountain Formations)
157-225	68	Mid Claiborne (Memphis Sand Formation)
225-322	97	Lower Claiborne/Upper Wilcox (Memphis Sand/Flour Island Formations)

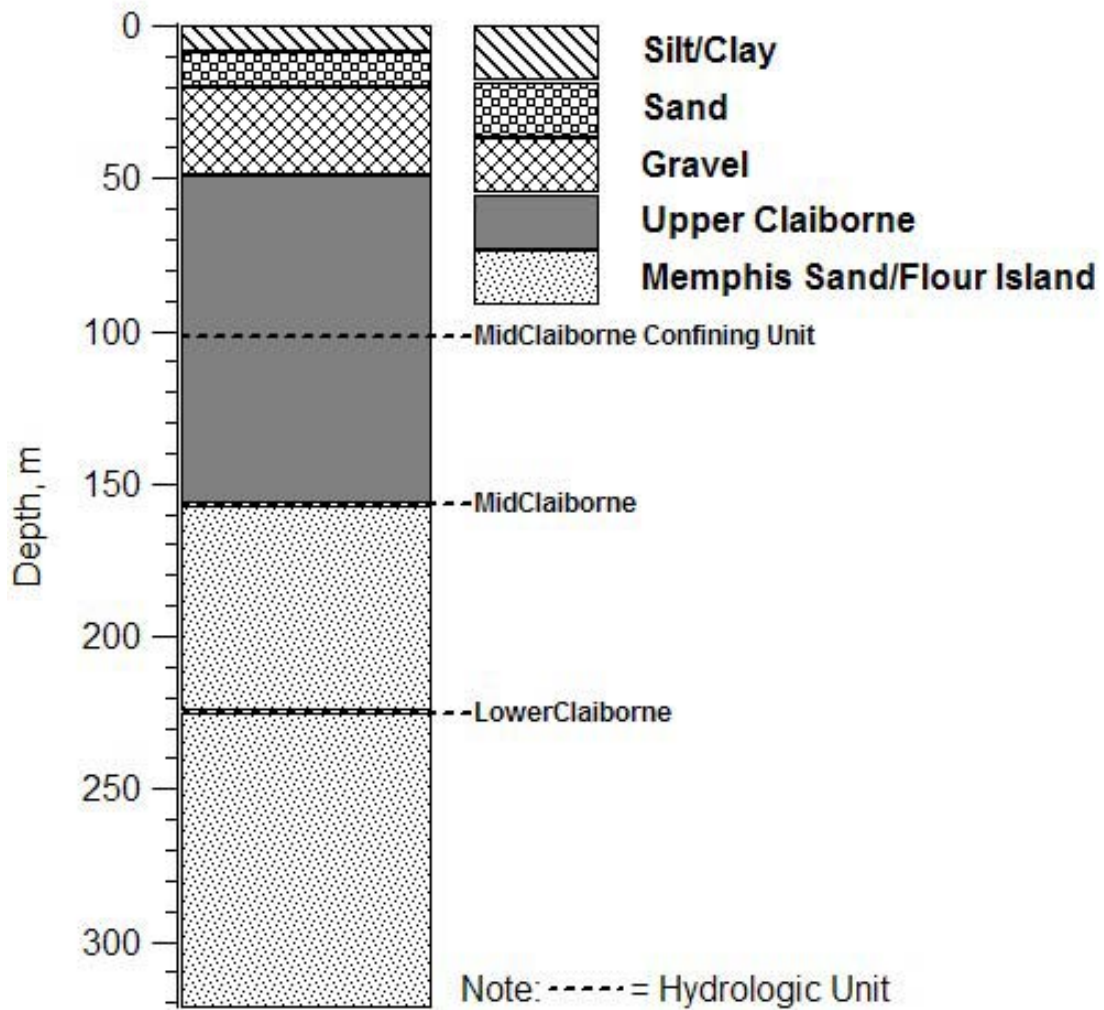


Figure 5.20 Estimated Soil Lithology at Site 6 (TNMT).

5.8 SITE 7: GLAT

SASW and H/V measurements were performed on May 18, 2007 at the CERI seismic station named GLAT. Site 7 is located to the west of Interstate 51 and north of Elbridge Obion Road in western Tennessee approximately seventeen miles southwest of Site 1. Figure 5.21 presents a Google Earth image of Site 7 with the extent and orientation of the SASW array shown with a black line. The surface wave measurements were performed as described in Section 4.3 of Chapter 4. The location of the source is indicated on the site map. The location of the CERI seismic station, GLAT, is also indicated in Figure 5.21. A maximum receiver spacing of 264 meters was used at Site 7 with a maximum total source-to-far-receiver distance of 544 meters. Figure 5.22 presents a photograph looking away from the source with Figure 5.23 being a view looking towards the source from one of the receiver locations.



Figure 5.21 Google Earth Image of Site 7 (GLAT).



Figure 5.22 Photograph of Site Looking Away from the Source.



Figure 5.23 Photograph of Site Looking Towards the Source.

Site 7 was the only one of the sites located in the uplands on Pleistocene-age deposits. This was due to the fact that the Pleistocene-age deposits have generally rougher terrain and insufficient room was available at many sites to set out long arrays. The surface soil at this site was very hard therefore geophones could not be buried on site. In Table 5.8 and Figure 5.24 the estimated site lithology down to the mid-Wilcox boundary (335 meters) is presented. Soil lithology information was not available above the mid Claiborne layer. The depth to bedrock at Site 7 is estimated to be approximately 750 meters.

Table 5.8 Estimated Profile at Site 7 (GLAT) Provided by Roy Van Arsdale from the University of Memphis.

Depth (meters)	Thickness (meters)	Deposit
?	?	Silt/Clay
?	?	Sand
?	?	Gravel
?	?	Upper Claiborne (Jackson, Cockfield and Cook Mountain Formations)
134-206	72	Mid Claiborne (Memphis Sand Formation)
206-335	129	Lower Claiborne/Upper Wilcox (Memphis Sand/Flour Island Formations)

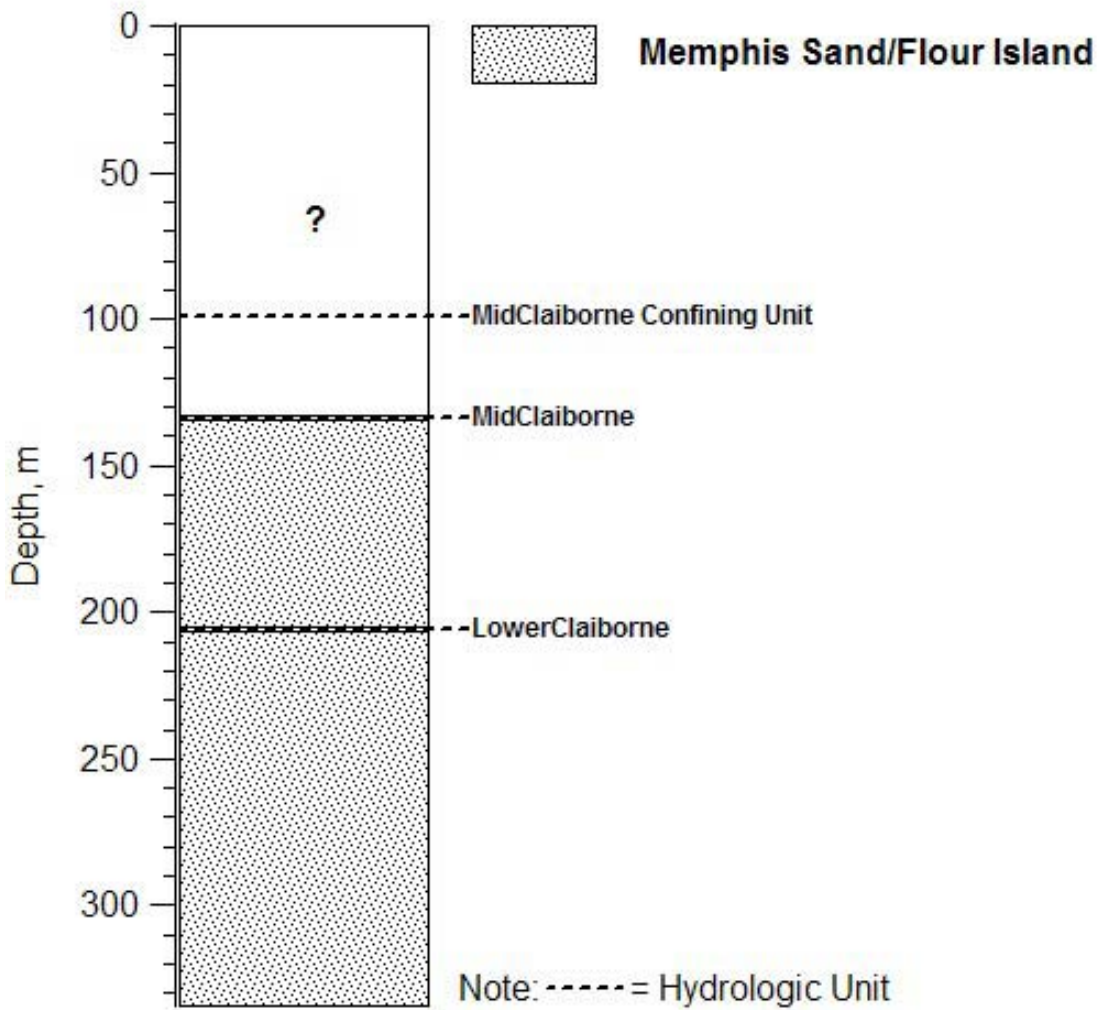


Figure 5.24 Estimated Soil Lithology at Site 7 (GLAT).

5.9 SITE 8: BRGM

SASW and H/V measurements were performed on May 19, 2007 at the CERI seismic station named BRGM. Site 8 is located west of Hayti, Missouri between County Roads 413 and 415 in the boot heel of Missouri about eighteen miles southeast of Site 1. Figure 5.25 presents a Google Earth image of Site 8 with the extent and orientation of the SASW array shown with a black line. The surface wave measurements were performed as described in Section 4.3 of Chapter 4. The location of the source is indicated on the site map. The location of the CERI seismic station, BRGM, is also indicated in Figure 5.25. A maximum receiver spacing of 264 meters was used at Site 8 with a maximum total source-to-far-receiver distance of 544 meters. Figure 5.26 presents a view looking away from the source with Figure 5.27 presenting a view looking towards the source.



Figure 5.25 Google Earth Image of Site 8 (BRGM).



Figure 5.26 Photograph of at Site 8 Looking Away from the Source.

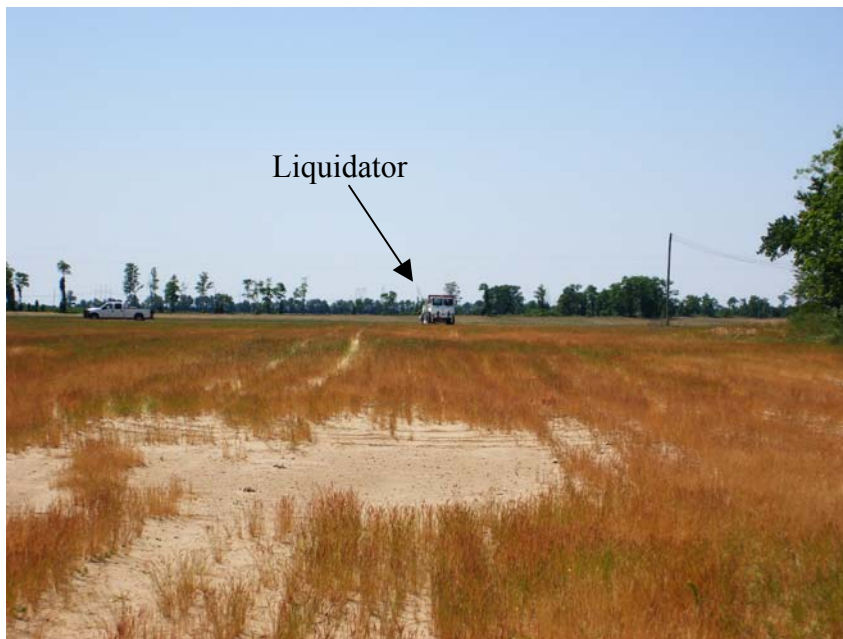


Figure 5.27 Photograph at Site 8 Looking Towards the Source.

Site 8 is located on Holocene-age, near-surface alluvial deposits. In Table 5.9 and Figure 5.28 the estimated site lithology down to the mid-Wilcox boundary (248 meters) is presented. Silt/clay, sand, and gravel compose the top three layers of the soil lithology followed by a relatively thin upper Claiborne layer overlying the Memphis Sand. The depth to bedrock at Site 8 is estimated to be approximately 715 meters.

Table 5.9 Estimated Profile at Site 8 (BRGM) Provided by Roy Van Arsdale from the University of Memphis.

Depth (meters)	Thickness (meters)	Deposit
0-7	7	Silt/Clay
7-21	14	Sand
21-56	35	Gravel
56-101	45	Upper Claiborne (Jackson, Cockfield and Cook Mountain Formations)
101-133	32	Mid Claiborne (Memphis Sand Formation)
133-248	115	Lower Claiborne/Upper Wilcox (Memphis Sand/Flour Island Formations)

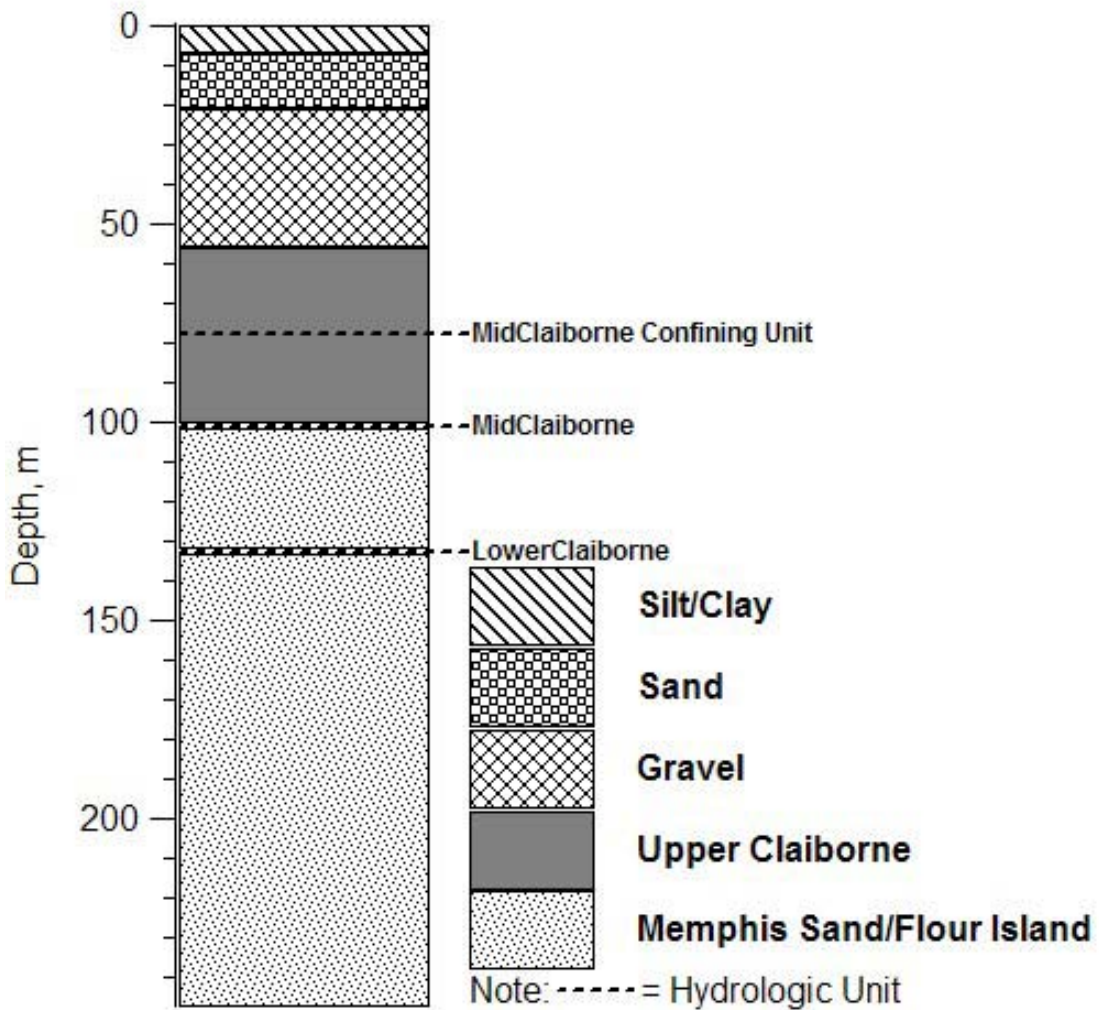


Figure 5.28 Estimated Soil Lithology at Site 8 (BRGM).

5.10 SITE 9: PENM

SASW and H/V measurements were performed on May 21, 2007 at the CERI seismic station named PENM. Site 9 is located on the east side of Interstate 55 north of County Highway 422 in the boot heel of Missouri approximately nine miles north of Site 1. Figure 5.29 presents a Google Earth image of Site 9 with the extent and orientation of the SASW array shown with a black line. The surface wave measurements were performed as described in Section 4.3 of Chapter 4. The location of the source is indicated on the site map. The location of the CERI seismic station, PENM, is also indicated in Figure 5.29. A maximum receiver spacing of 300 meters was used at Site 9 with a maximum total source-to-far-receiver distance of 600 meters. Figure 5.30 presents a view looking away from the source with Figure 5.31 presenting a view looking towards the source.

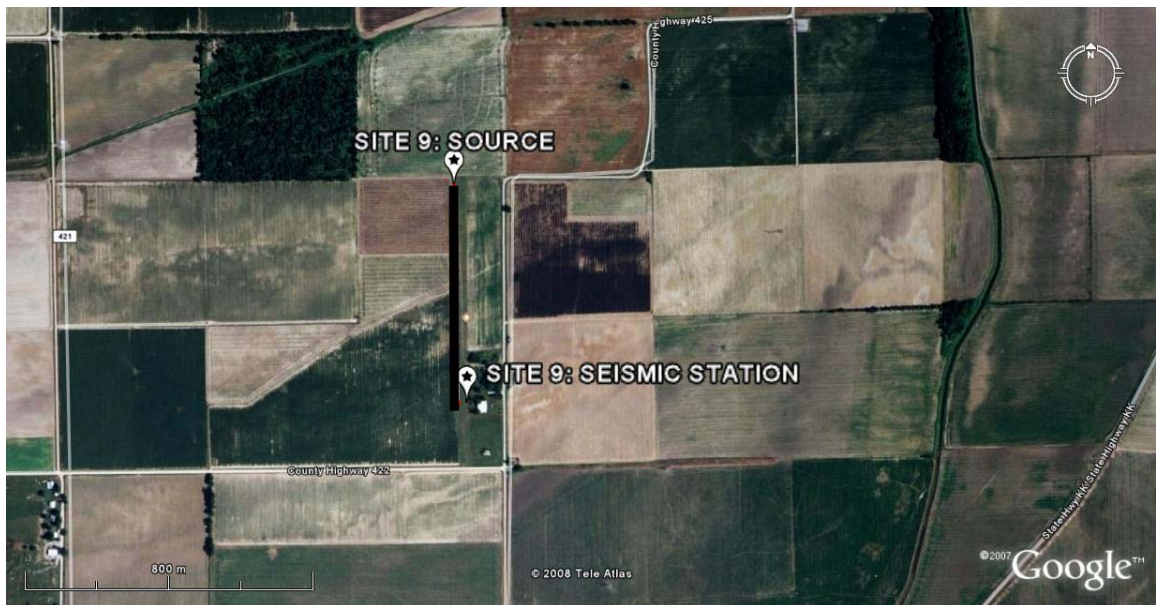


Figure 5.29 Google Earth Image of Site 9 (PENM).



Figure 5.30 Photograph of Site Layout Looking Away from the Source Location.



Figure 5.31 Photograph of Site Layout Looking Towards the Source Location.

Site 9 is located on Holocene-age, near-surface alluvial deposits. In Table 5.10 and Figure 5.32 the estimated site lithology down to the mid-Wilcox boundary (276 meters) is presented. Silt/clay, sand, and gravel compose the top three layers of the soil lithology followed by a thick upper Claiborne layer overlying the Memphis Sand. The depth to bedrock at Site 9 is estimated to be approximately 590 meters.

Table 5.10 Estimated Profile at Site 9 (PENM) Provided by Roy Van Arsdale from the University of Memphis.

Depth (meters)	Thickness (meters)	Deposit
0-17	17	Silt/Clay
17-21	4	Sand
21-56	35	Gravel
56-145	89	Upper Claiborne (Jackson, Cockfield and Cook Mountain Formations)
145-184	39	Mid Claiborne (Memphis Sand Formation)
184-276	92	Lower Claiborne/Upper Wilcox (Memphis Sand/Flour Island Formations)

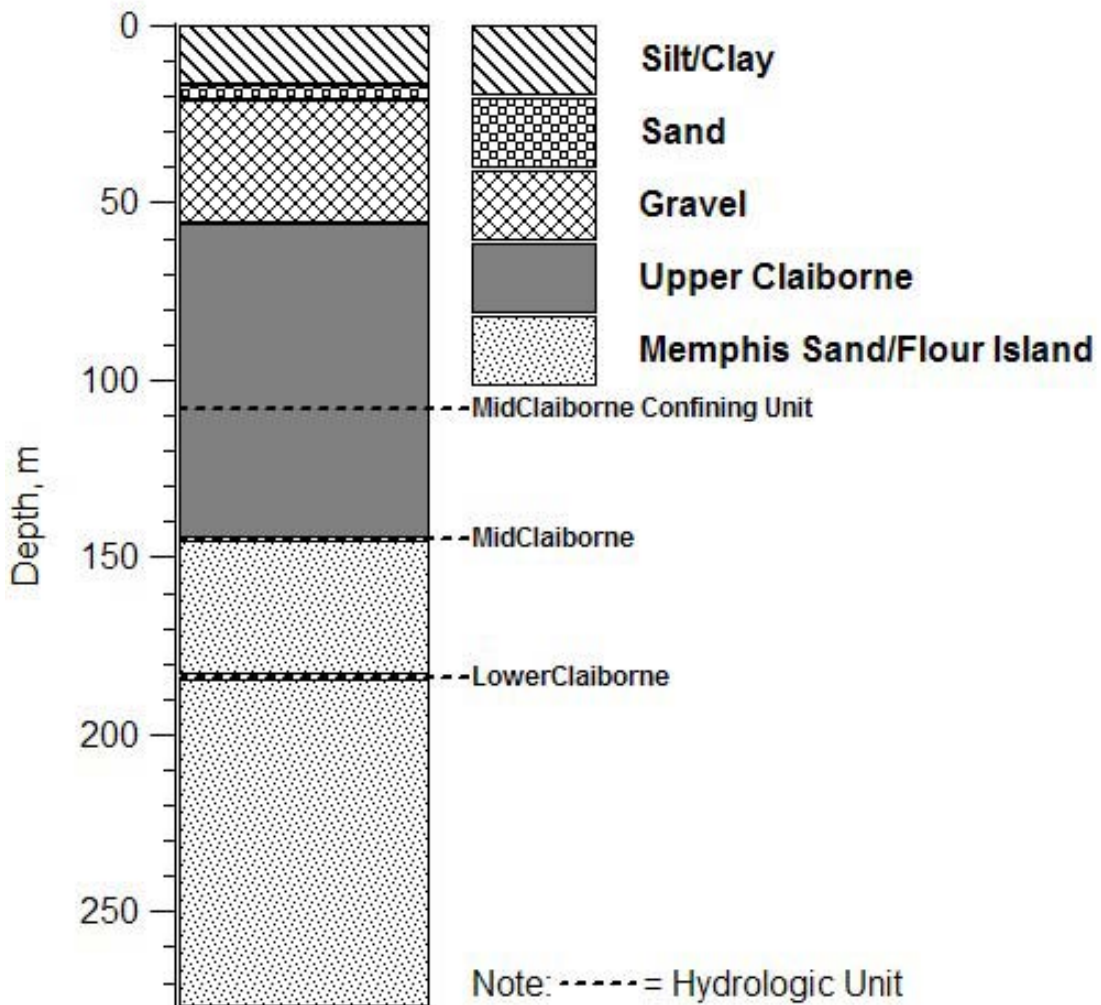


Figure 5.32 Estimated Soil Lithology at Site 9 (PENM).

5.11 SITE 10: EPRM

SASW and H/V measurements were performed on May 22, 2007 near the CERI seismic station named EPRM. Site 10 is located in Southeastern Missouri south of the town of East Prairie and west of Highway 102, approximately twenty-three miles northeast of Site 9. Site 10 is the northern-most site of this study. Figure 5.33 presents a Google Earth image of Site 10 with the extent and orientation of the SASW array shown with a black line. The surface wave measurements were performed as described in Section 4.3 of Chapter 4. The location of the source is indicated on the site map. The location of the CERI seismic station, EPRM, is also indicated in Figure 5.33. A maximum receiver spacing of 300 meters was used at Site 10 with a maximum total source-to-far-receiver distance of 600 meters. Figure 5.34 presents a view looking away from the source with Figure 5.35 showing a view looking towards the source.

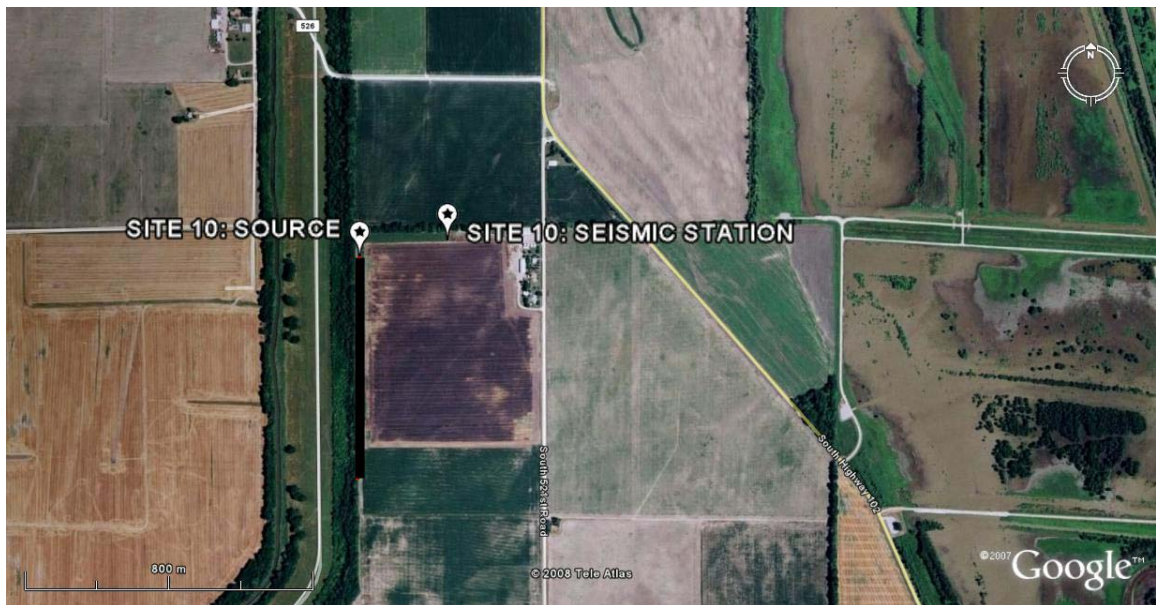


Figure 5.33 Google Earth Image of Site 10 (EPRM).



Figure 5.34 Photograph of Site Layout and Soil Conditions Looking Away from the Source.

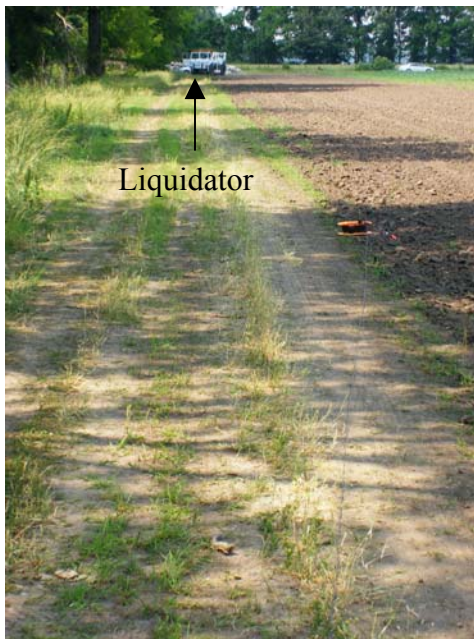


Figure 5.35 Photograph of Site Layout and Soil Conditions Looking Towards the Source.

Site 10 is located on Holocene-age, near-surface alluvial deposits. In Table 5.11 and Figure 5.36 the estimated site lithology down to the mid-Wilcox boundary (201 meters) is presented. Silt/clay, sand, and gravel compose the top three layers of the soil lithology followed by a relatively thin upper Claiborne layer overlying the Memphis Sand. The depth to bedrock at Site 10 is estimated to be approximately 450 meters.

Table 5.11 Estimated Profile at Site 10 (EPRM) Provided by Roy Van Arsdale from the University of Memphis.

Depth (meters)	Thickness (meters)	Deposit
0-12	12	Silt/Clay
12-26	14	Sand
26-48	22	Gravel
48-91	43	Upper Claiborne (Jackson, Cockfield and Cook Mountain Formations)
91-139	48	Mid Claiborne (Memphis Sand Formation)
139-201	62	Lower Claiborne/Upper Wilcox (Memphis Sand/Flour Island Formations)

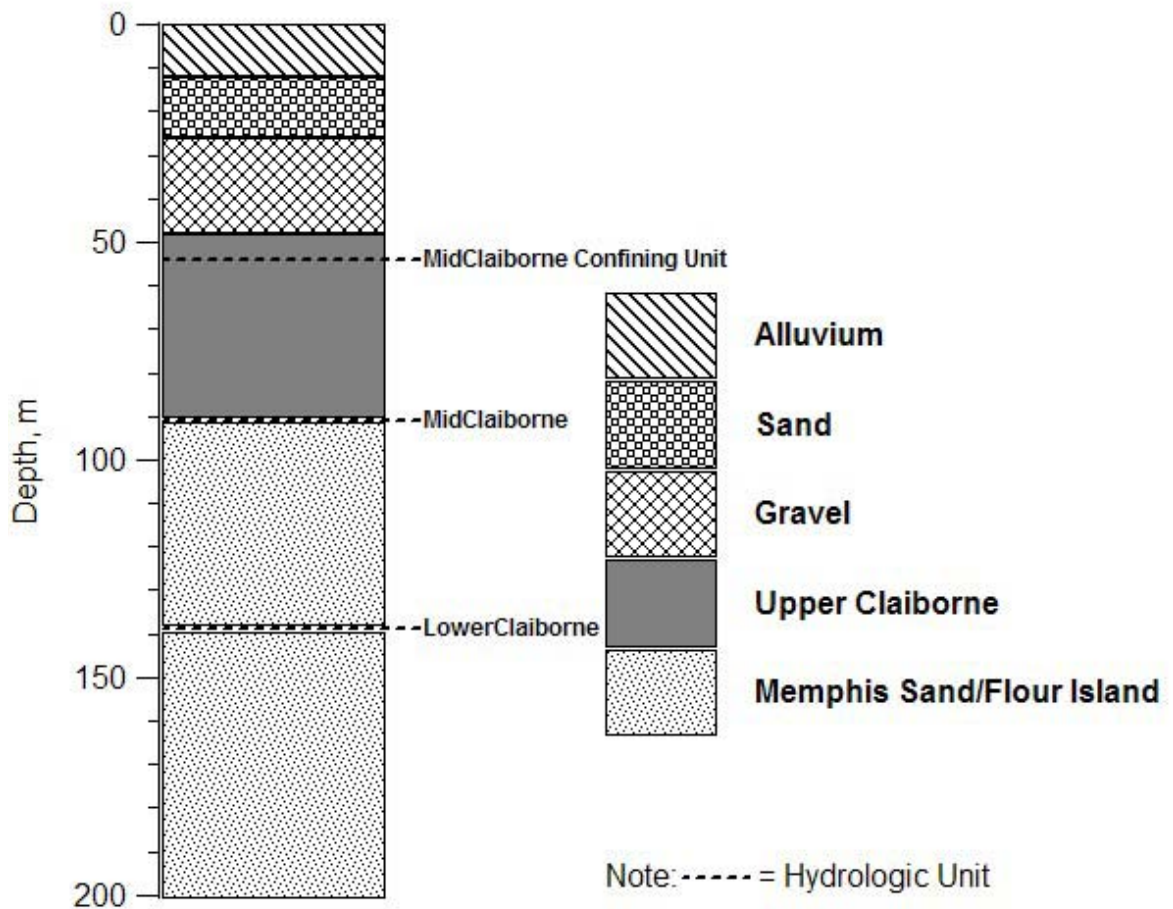


Figure 5.36 Estimated Soil Lithology at Site 10 (EPRM).

5.12 SITE 11: MSAR

SASW and H/V measurements were performed on May 23, 2007 at the CERI seismic station named MSAR. Site 11 is located in Arkansas west of Interstate 55 approximately fourteen miles southwest of Site 3. Figure 5.37 presents a Google Earth image of Site 11 with the extent and orientation of the SASW array shown with a black line. The surface wave measurements were performed as described in Section 4.3 of Chapter 4. The location of the source is indicated on the site map. The location of the CERI seismic station, MSAR, is also indicated in Figure 5.37. A maximum receiver spacing of 300 meters was used at Site 11 with a maximum total source-to-far-receiver distance of 600 meters. Figure 5.38 presents a view looking down the array towards the source.

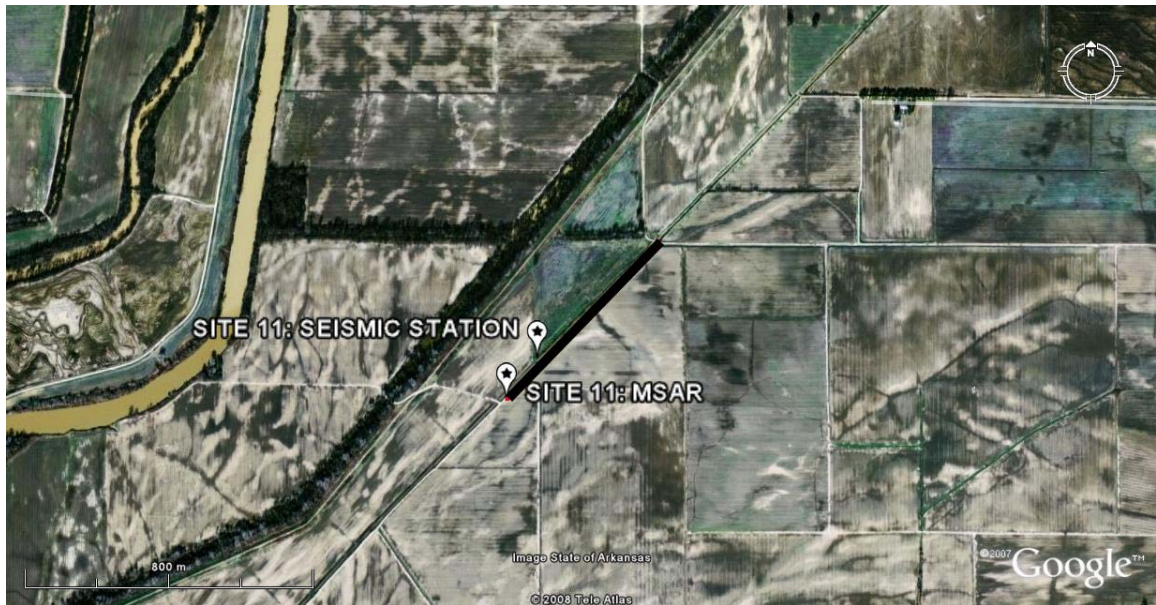


Figure 5.37 Google Earth Image of Site 11 (MSAR).



Figure 5.38 Photograph of Site Layout and Soil Conditions Looking Down the Array Towards the Source.

Site 11 is located on Holocene-age, near-surface alluvial deposits. In Table 5.12 and Figure 5.39 the estimated site lithology down to the mid-Wilcox boundary (294 meters) is presented. Silt/clay, sand, and gravel compose the top three layers of the soil lithology followed by a relatively thin upper Claiborne layer overlying the Memphis Sand. The depth to bedrock at Site 11 is estimated to be approximately 850 meters.

Table 5.12 Estimated Profile at Site 11 (MSAR) Provided by Roy Van Arsdale from the University of Memphis.

Depth (meters)	Thickness (meters)	Deposit
0-10	10	Silt/Clay
10-23	13	Sand
23-47	24	Gravel
47-88	41	Upper Claiborne (Jackson, Cockfield and Cook Mountain Formations)
88-164	76	Mid Claiborne (Memphis Sand Formation)
164-294	130	Lower Claiborne/Upper Wilcox (Memphis Sand/Flour Island Formations)

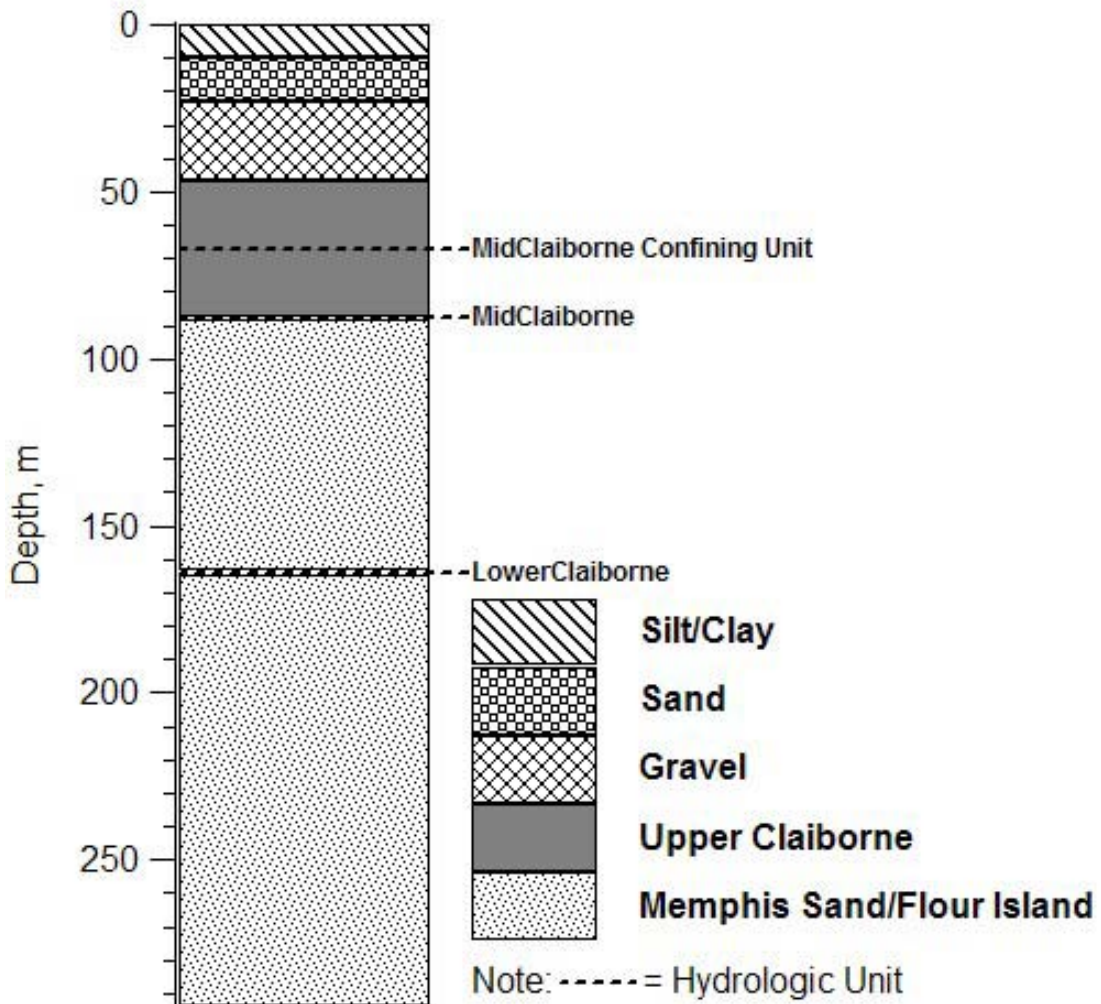


Figure 5.39 Estimated Soil Lithology at Site 11 (MSAR).

5.13 Summary

Eleven sites were evaluated in the upper Mississippi Embayment using both the SASW method as well as the H/V Spectral Ratio method. These locations were spread throughout the Upper Mississippi Embayment from north to south to sample a large portion of the embayment. The location, soil lithology, and site pictures were presented. Also, tables with estimated soil layer thickness as well as a visual representation of the soil profiles were provided for each site.

A trend that was exhibited in ten of the eleven sites was that the further south the site was located, the thicker the sediment depth to bedrock. At Site 4 this trend was not seen which is likely due to the bowl shaped nature of the Mississippi Embayment discussed in Chapter 2. Sites 1, 2, 6, and 9 showed thicker deposits of the upper Claiborne formation than the other seven sites. The depth of Memphis Sand varied from as shallow as 40 meters at Site 5 to as deep as 157 meters at Site 6.

CHAPTER 6

RESULTS AND ANALYSIS

6.1 Introduction

In this chapter the results from the SASW and H/V measurements performed at the eleven sites are presented. The V_s profiles determined from the SASW measurements are compared to existing V_s reference profiles that have been developed for the Mississippi Embayment and have been used in past site response studies. Average V_s values determined from the H/V measurements are compared with the results of past studies of the average V_s values for the Mississippi Embayment. Lastly, relationships between soil lithology and V_s determined from this work are presented and compared with the results of previous studies.

6.2 SASW Results

Presented within this section are the V_s profiles determined from SASW measurements at each of the eleven sites, along with the experimental and theoretical dispersion curves. The estimated soil lithology at each site, derived from nearby well information, is also presented.

6.2.1 V_s Profiles Using Generic Layering

For the eleven sites, V_s profiles were developed using a common generic profile layering. The generic layering was developed with no *a priori* knowledge of the soil profile at the site. The purpose of this was to see how well changes in V_s coming from the surface wave inversion procedure corresponded with the estimated depth of changes in lithology. Later, thicker layering with boundaries consistent with estimated formation depths was used to provide better estimates of the average V_s in different soil formations.

The data were processed and the inversion procedure was performed as discussed in Sections, 4.3.4 and 4.3.5 of Chapter 4, respectively. Figures 6.1a through 6.11a present the experimental dispersion curve at each site along with the matching theoretical dispersion curve used to develop the V_s profile. The final V_s profiles along with estimated soil lithology information are presented in these Figures 6.1b through 6.11b.

To provide a sense of the sensitivity of the solution to changes in the individual layer velocities, bounds were established based on the change in layer velocity needed to cause a 10% increase in the RMS error. The bounds are represented by the solid black lines shown for each layer of the profile from below the silt/clay layer to the bottom of the profile.

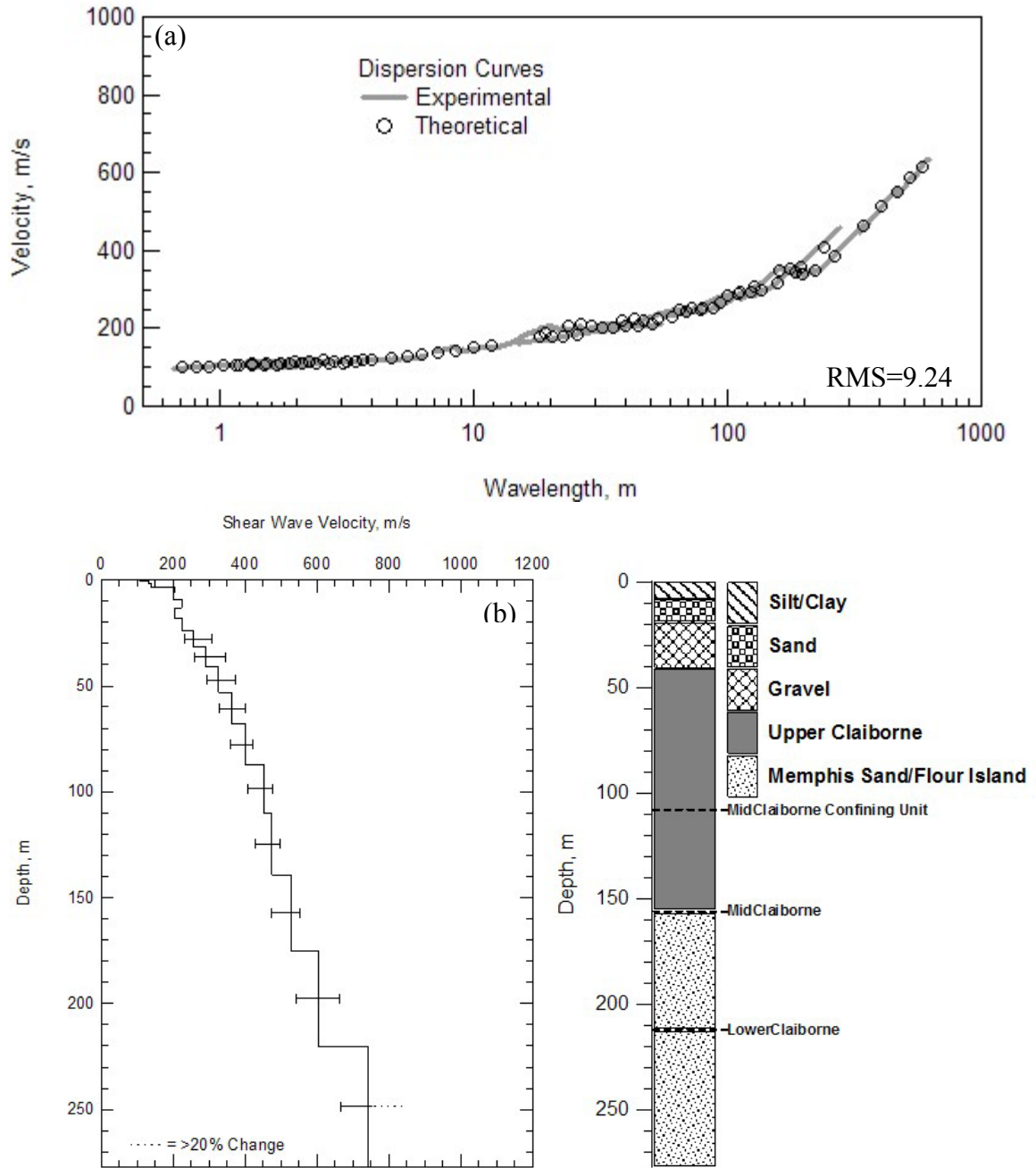


Figure 6.1 Results from SASW Measurements at Site 1 Showing (a) Experimental and Theoretical Dispersion Curves and (b) V_s Profile (with Sensitivity Bounds) and Estimated Soil Profile.

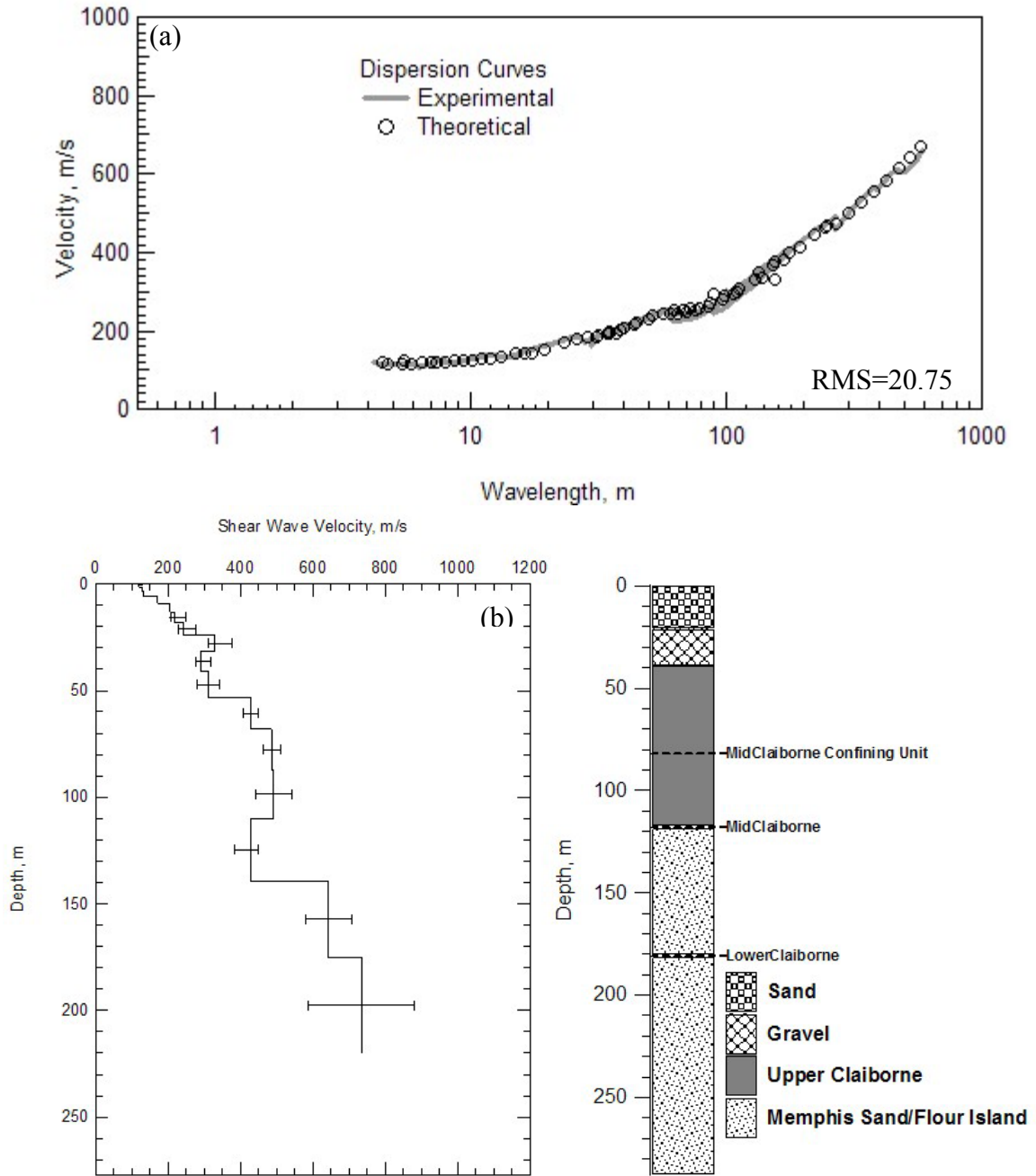


Figure 6.2 Results from SASW Measurements at Site 2 Showing (a) Experimental and Theoretical Dispersion Curves and (b) V_s Profile (with Sensitivity Bounds) and Estimated Soil Profile.

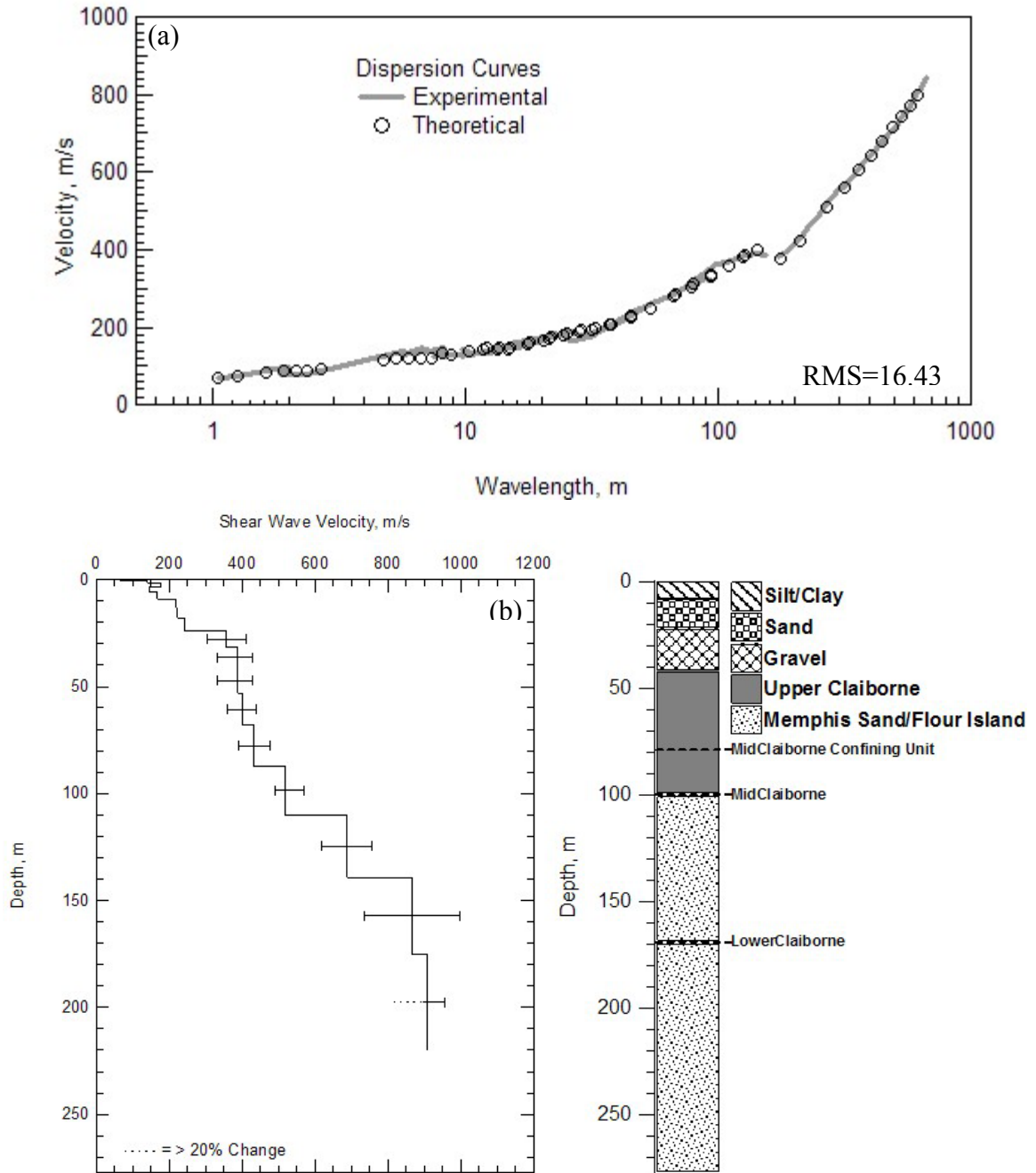


Figure 6.3 Results from SASW Measurements at Site 3 Showing (a) Experimental and Theoretical Dispersion Curves and (b) V_s Profile (with Sensitivity Bounds) and Estimated Soil Profile.

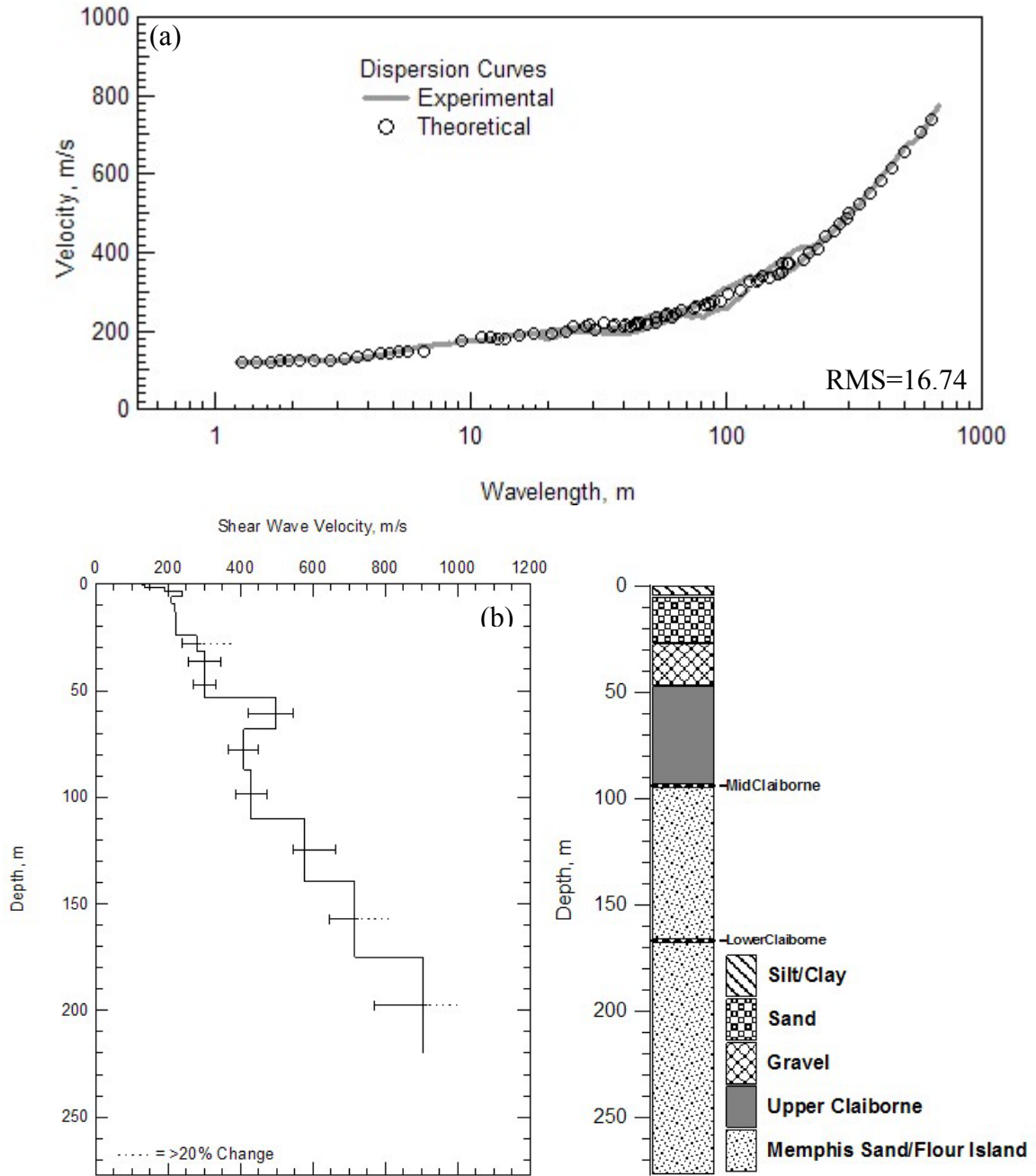


Figure 6.4 Results from SASW Measurements at Site 4 Showing (a) Experimental and Theoretical Dispersion Curves and (b) V_s Profile (with Sensitivity Bounds) and Estimated Soil Profile.

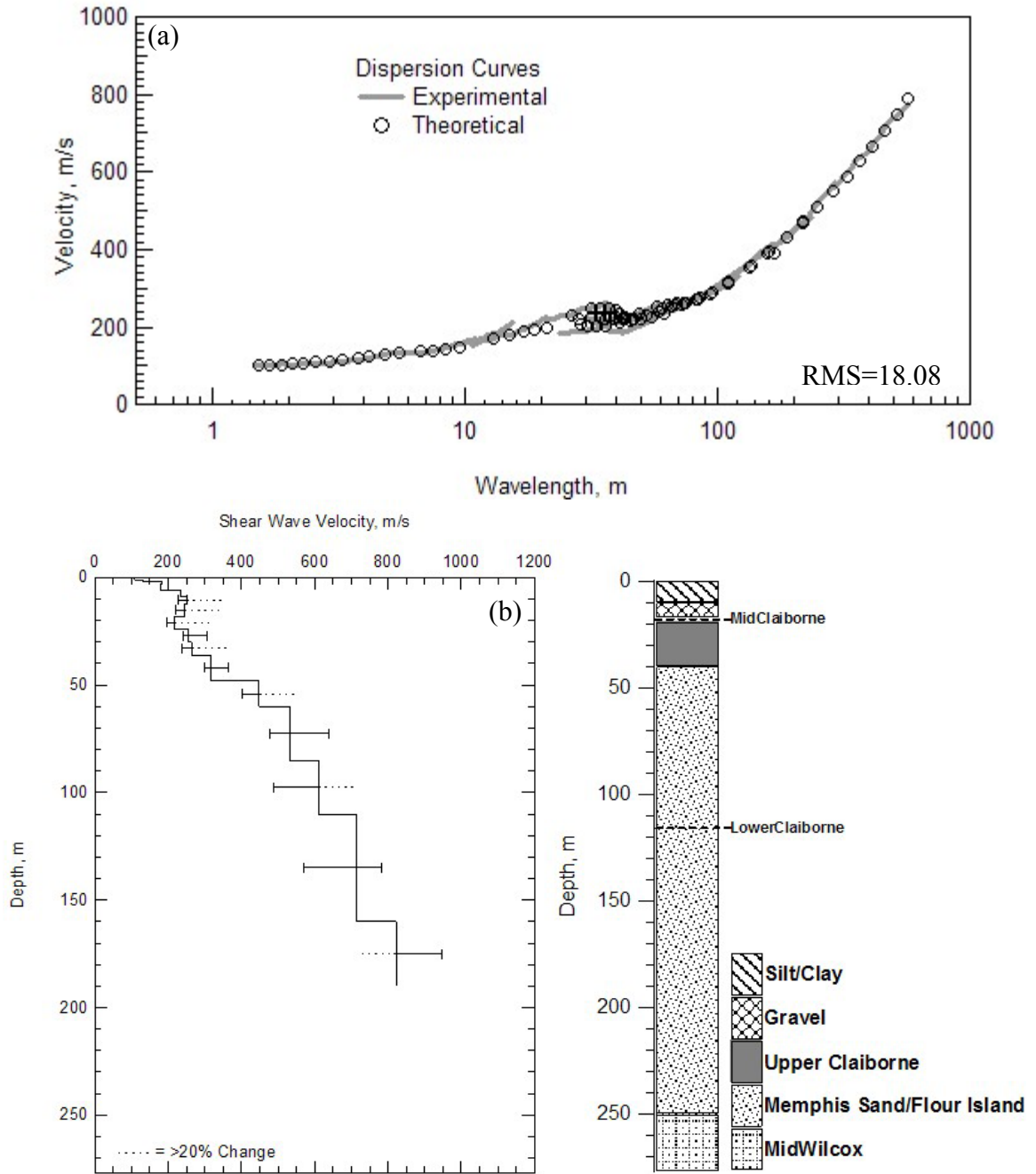


Figure 6.5 Results from SASW Measurements at Site 5 Showing (a) Experimental and Theoretical Dispersion Curves and (b) V_s Profile (with Sensitivity Bounds) and Estimated Soil Profile.

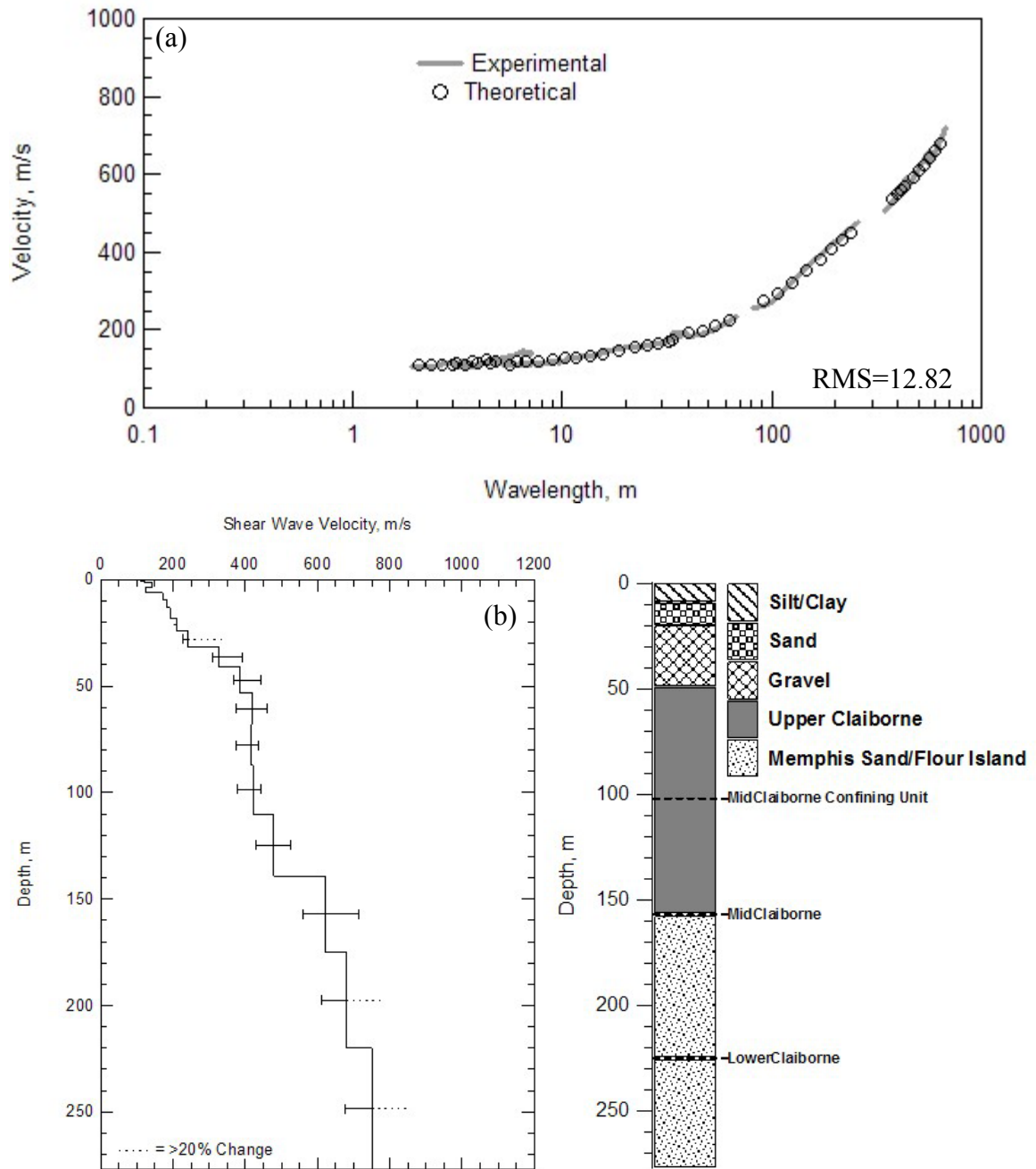


Figure 6.6 Results from SASW Measurements at Site 6 Showing (a) Experimental and Theoretical Dispersion Curves and (b) V_s Profile (with Sensitivity Bounds) and Estimated Soil Profile.

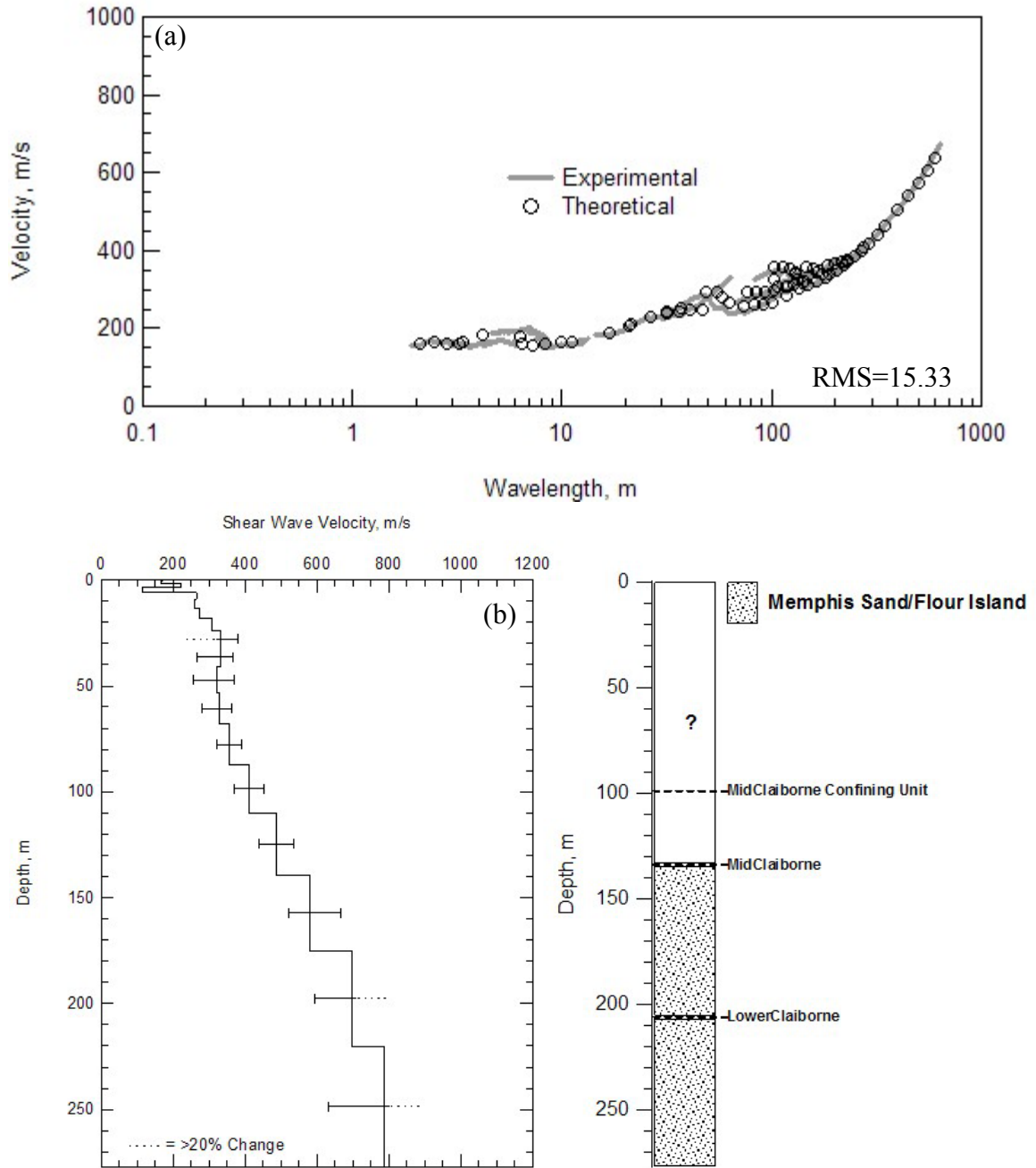


Figure 6.7 Results from SASW Measurements at Site 7 Showing (a) Experimental and Theoretical Dispersion Curves and (b) V_s Profile (with Sensitivity Bounds) and Estimated Soil Profile.

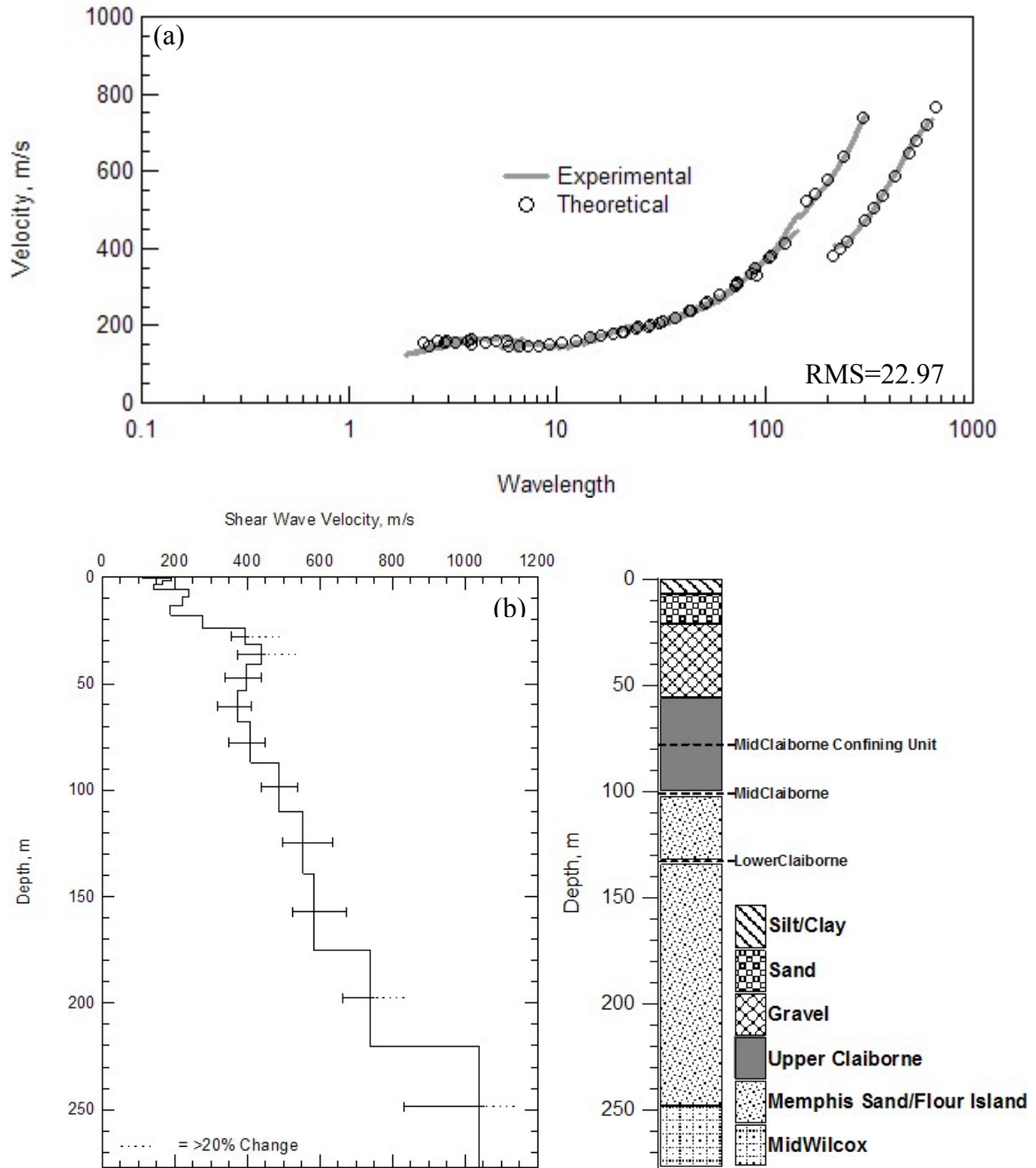


Figure 6.8 Results from SASW Measurements at Site 8 Showing (a) Experimental and Theoretical Dispersion Curves and (b) V_s Profile (with Sensitivity Bounds) and Estimated Soil Profile.

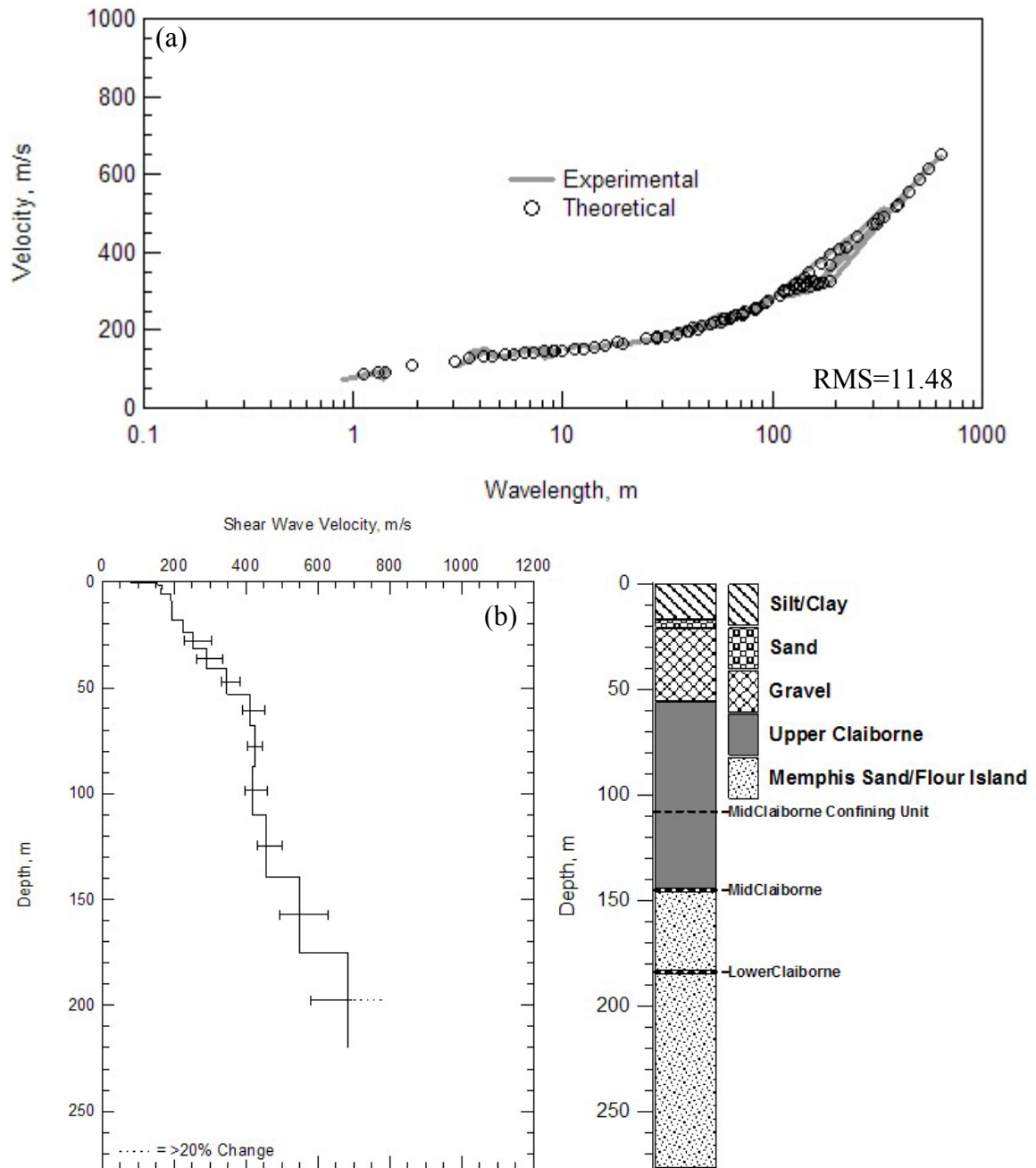


Figure 6.9 Results from SASW Measurements at Site 9 Showing (a) Experimental and Theoretical Dispersion Curves and (b) V_s Profile (with Sensitivity Bounds) and Estimated Soil Profile.

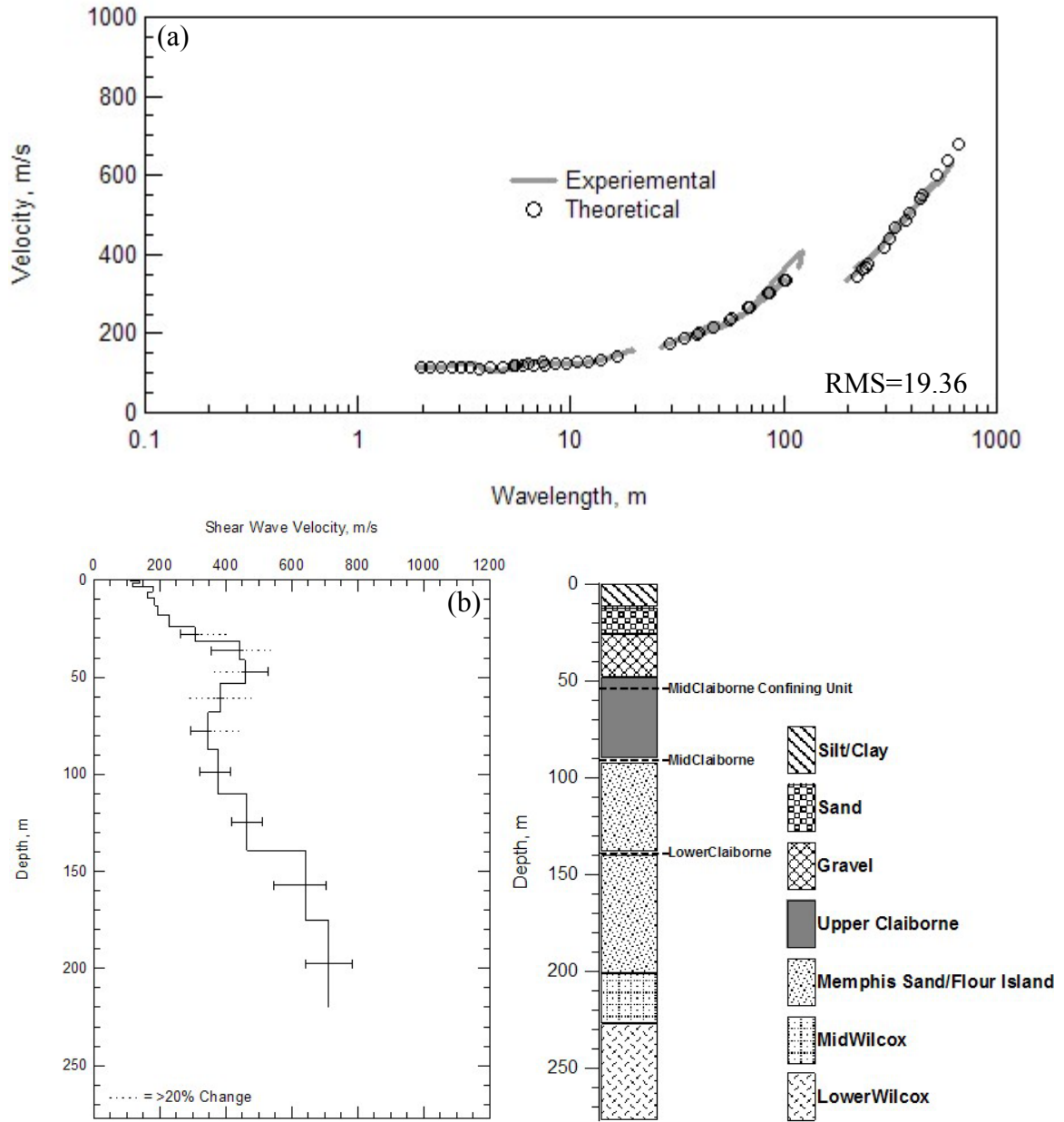


Figure 6.10 Results from SASW Measurements at Site 10 Showing (a) Experimental and Theoretical Dispersion Curves and (b) V_s Profile (with Sensitivity Bounds) and Estimated Soil Profile.

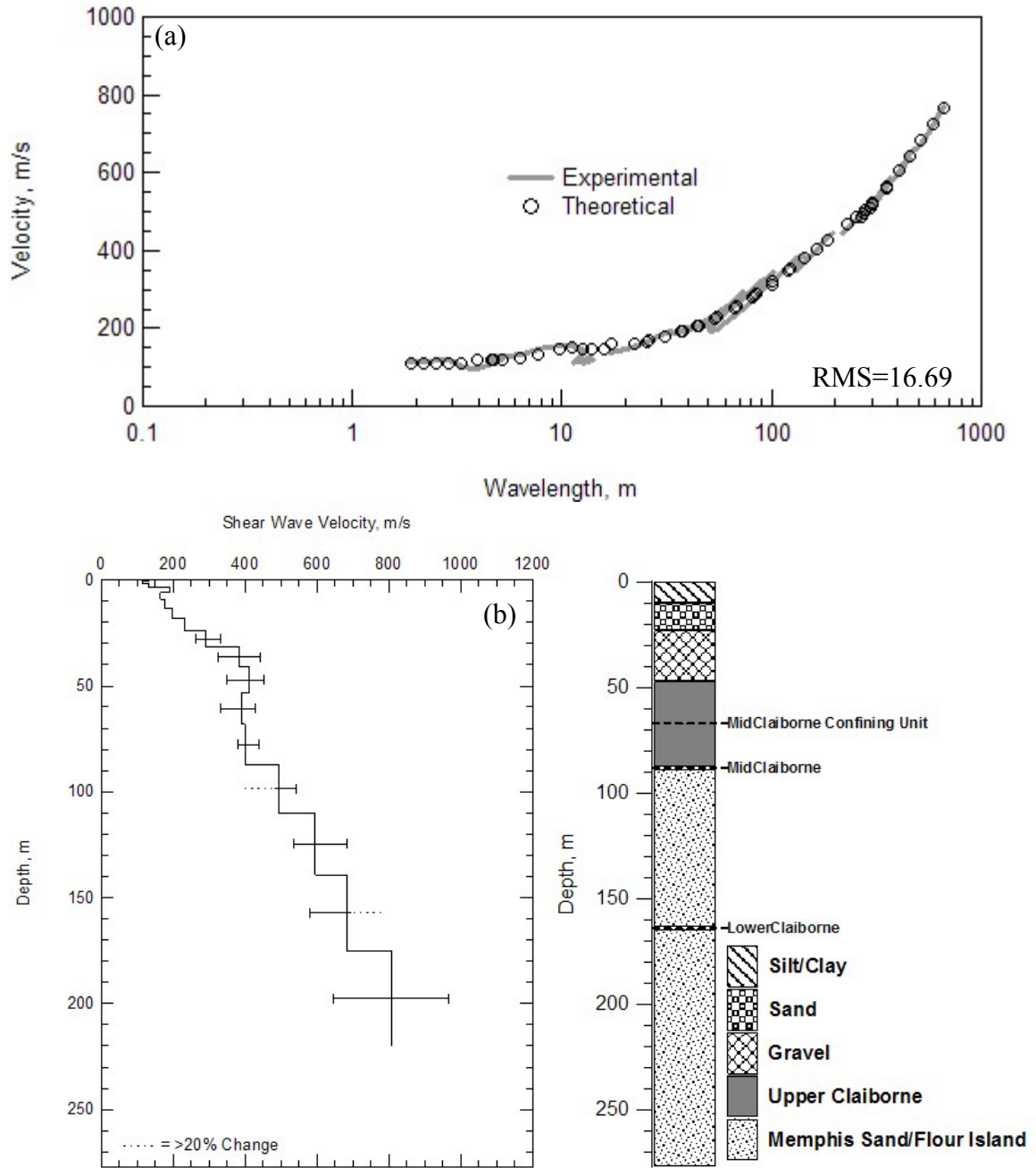


Figure 6.11 Results from SASW Measurements at Site 11 Showing (a) Experimental and Theoretical Dispersion Curves and (b) V_s Profile (with Sensitivity Bounds) and Estimated Soil Profile.

6.2.2 General Characteristics of V_s Profiles

The V_s profiles presented in Figures 6.1 through 6.11 exhibited similar characteristics within the depth of resolution for this study. All sites show low velocity near-surface soil deposits indicative of the soft alluvium present. The one upland site (Site 7) also showed similar, (though slightly higher velocities) near the surface. At many of the sites (Sites 2, 3, 4, 8, 10, 11), the V_s profile showed a distinct transition to velocities of 300-400 m/s at a depth that was consistent with the estimated depth of the top of the gravel layer. The velocity typically remained at approximately 400 m/s into the upper Claiborne deposit. The next transition occurred at a depth that was generally consistent with the estimated depth of the top of the Memphis Sand, where V_s transitioned from near 400 m/s up to 600 m/s and greater. The one exception to this trend was Site 10, which is discussed below. The apparent correlation between the top of the Memphis Sand and higher velocities is seen most clearly by comparing the Site 5 profile, where the Memphis Sand layer starts at approximately 40 meters below the ground surface with Sites 1, 6, 7, and 9 where the top of the Memphis Sand layer is estimated to be at 130 meters or greater below the ground surface. This velocity jump is also seen at depths corresponding to the estimated depth of the Memphis Sand at Sites 3, 4, 8, and 11. Based on these observations, it appears that the top of the Memphis Sand is associated with a distinct change in V_s from the overlying upper Claiborne deposits.

As mentioned above, Site 10 did not show a similar correlation between an increase in V_s and the estimated top of the Memphis Sand. To investigate the validity of the V_s profile developed at Site 10 the results are compared with a reflection study performed by Street and Woolery (2002) at a site within 1 kilometer of Site 10. Figure

6.12 presents the comparison of the two V_s profiles. It can be seen from this figure that the Site 10 profile is in good agreement with the reflection profile, especially at depths below 50 meters. Both profiles indicate that a large transition in V_s occurs at a depth of 140-160 meters, which is below the estimated depth of the Memphis Sand of 90 meters. This may indicate that the Memphis Sand is deeper at the site than was estimated from the well logs.

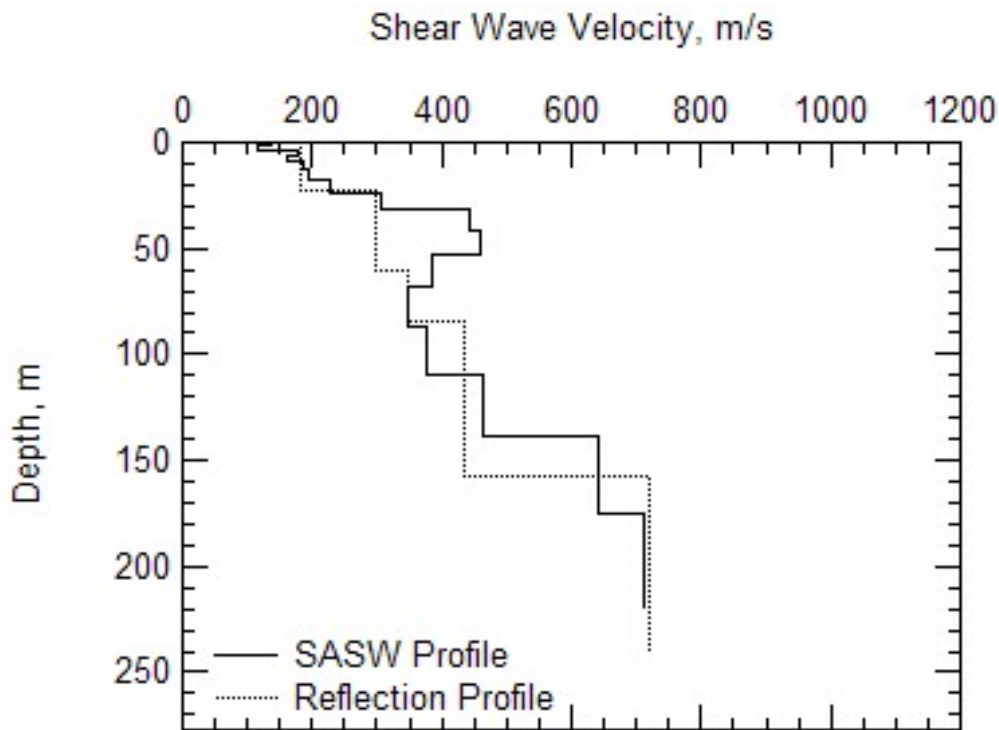


Figure 6.12 Comparison of V_s Profiles at Site 10 from SASW Measurements and Reflection Measurements Performed within 1 Kilometer of Site 10 (Woolery and Street, 2002).

6.2.3 Modified V_s Profiles

Based on the apparent correlation between soil formation and V_s observed at these sites, the inversion procedure was repeated using thicker layers with layer boundaries consistent with those provided from the well information. This procedure was performed to obtain better estimates of the average V_s for each soil formation. To perform this step,

the properties of alluvial layers (thickness and V_s) were held constant while the thicker lower layers representing, the gravel, upper Claiborne, and Memphis Sand were allowed to change. Dispersion fits with similar RMS errors (<10% change) to previous inversions were obtained with the thicker profiles. However, at Site 1 in order to obtain a good fit, it was necessary to represent the upper Claiborne formation with two layers, and at Site 5 it was necessary to represent the Memphis Sand formation with two layers. The revised profiles are presented in Figures 6.13 (a) through (k) for Sites 1-11, respectively with the original profiles shown in light gray. The sensitivity of each layer, calculated as previously described, is shown as the solid black lines. Average values and formation values are discussed below and compared to existing relationships that have been developed.

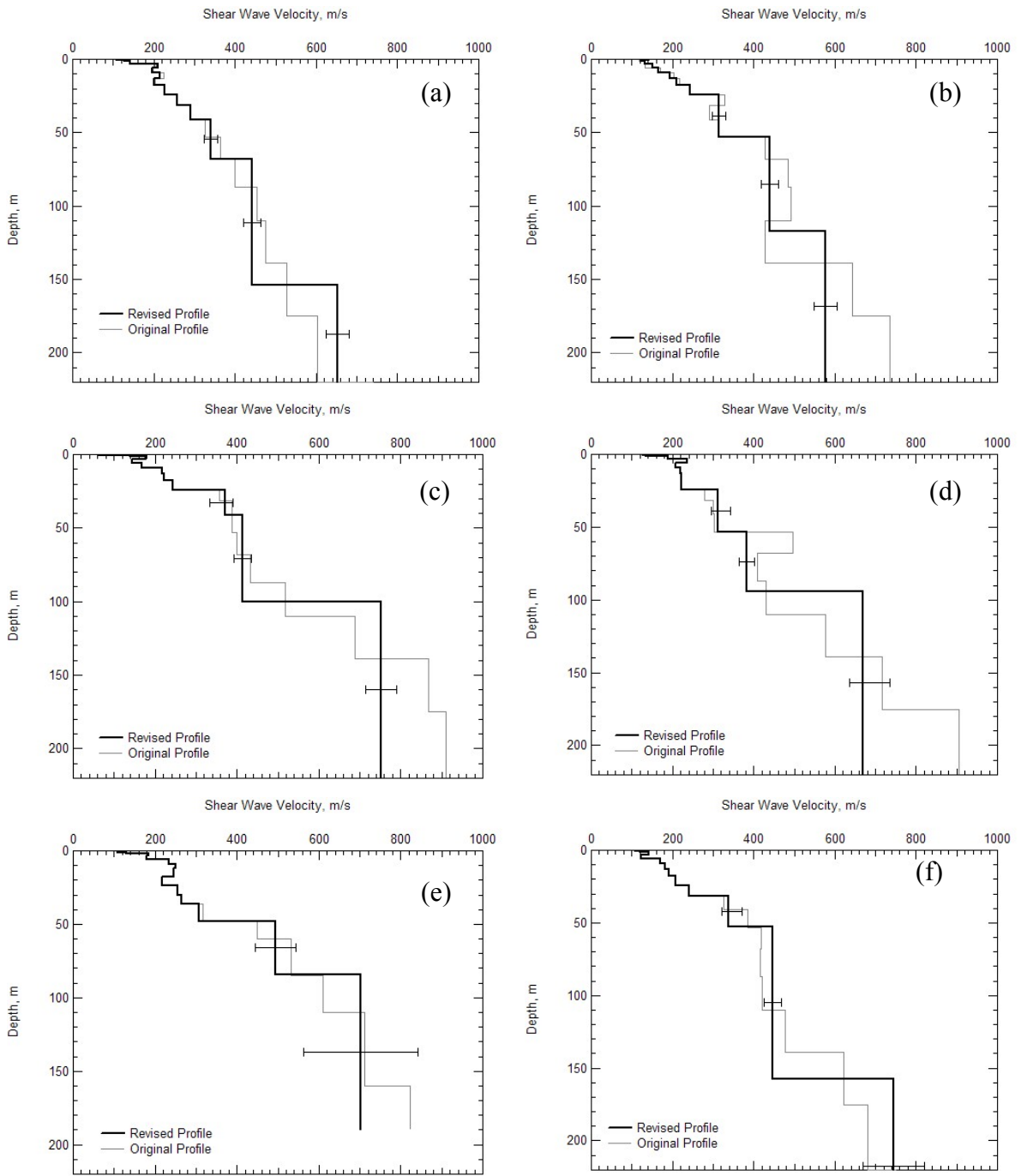


Figure 6.13 Modified V_s Profiles (Black) Overlaying the Original V_s Profiles (Gray) at Sites 1-11 as (a)-(k), Respectively Developed using Thicker Layers Consistent with Estimated Formation Boundaries.

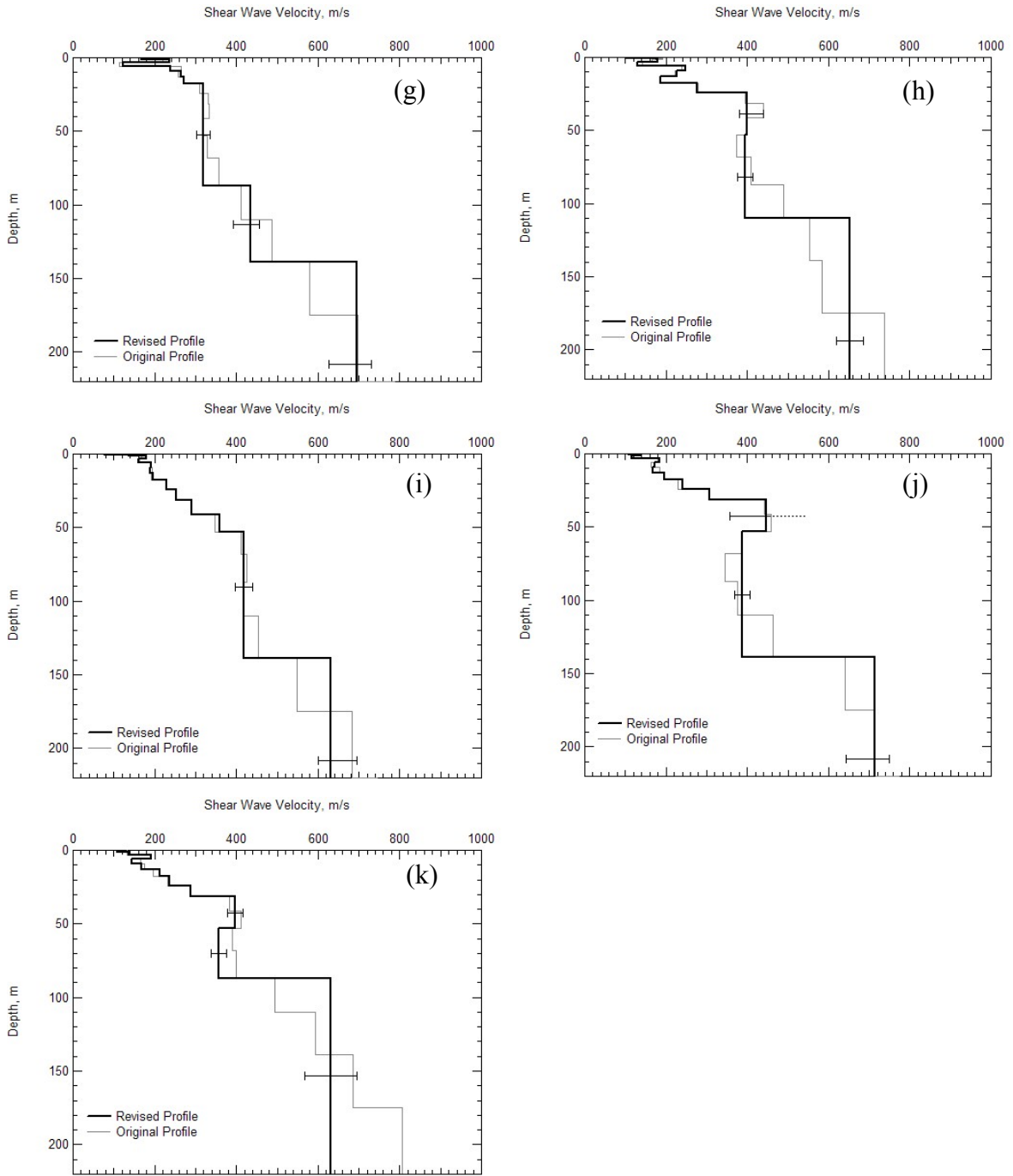


Figure 6.13 (Cont.) Modified V_s Profiles (Black) Overlaying the Original V_s Profiles (Gray) at Sites 1-11 as (a)-(k), Respectively Developed using Thicker Layers Consistent with Estimated Formation Boundaries Provided.

6.3 Discussion of SASW Results

In this section the V_s profiles developed for this study are compared to reference profiles developed for the Mississippi Embayment. Also a discussion of the soil lithology- V_s relationship is presented with comparisons to published findings. The variability of average V_s in the top 30 meters and 200 meters (V_{s30} and V_{s200}) are presented and discussed.

6.3.1 Comparison to Mississippi Embayment Reference Profiles

Three V_s reference profiles were used for comparison to this study. The first is the profile developed by Romero and Rix (2001), which was discussed in Section 3.2 and has been used for site response analysis studies of the Mississippi Embayment (Hashash and Park, 2001). Second was the reference V_s profile of Herrmann and Akinici (1999), which was developed assuming the following power law relation to estimate V_s (in m/s) throughout the sediments:

$$V_s = 250 \cdot h^{0.18}, \quad (6.1)$$

where h is the depth (in meters) of interest. Lastly, the Dorman and Smalley (1994) V_s reference profile is presented which was developed using sonic log data to estimate p-wave velocity (V_p), from which V_s was then derived.

Figure 6.14(a) presents a comparison of the reference profile to the average V_s values from this study to a depth of 70 meters. The average V_s profile from this study is shown as solid circles with plus and minus one standard deviation error bars. The average V_s profile was calculated from the arithmetic mean of the 10 lowland profiles presented in Figure 6.13 (excluding Site 7 which was an upland site) within the top 70 meters. As shown in Figure 6.14, the Herrmann and Akinici and Dorman and Smalley

reference profiles estimate much higher near-surface V_s values than measured in this study, while the comparison to the Romero and Rix profile is very good. Figure 6.14(b) presents the variability of the average V_s profile expressed using the coefficient of variation (COV), where

$$COV = \frac{\sigma}{\mu} \quad (6.2)$$

Romero and Rix assumed a log-normal distribution for V_s and expressed the variability as the standard deviation of the natural logarithm of V_s ($\sigma_{\ln(V_s)}$). For cases where $COV < 0.3$, $\sigma_{\ln(V_s)}$ is approximately equal to the coefficient of variability (Ang and Tang, 1975). Romero and Rix used a value for $\sigma_{\ln(V_s)}$ of 0.15 which is in good agreement with our measured values of COV for the 10 sites.

The same comparison is presented to a depth of 220 meters in Figure 6.15. In this case all eleven profiles were used to calculate the average profile. The average profile shows a gradual increase in V_s as is expected when averaging the profiles together. Below a depth of 70 meters the three reference profiles are in good agreement with our measured values, generally falling within one standard deviation.

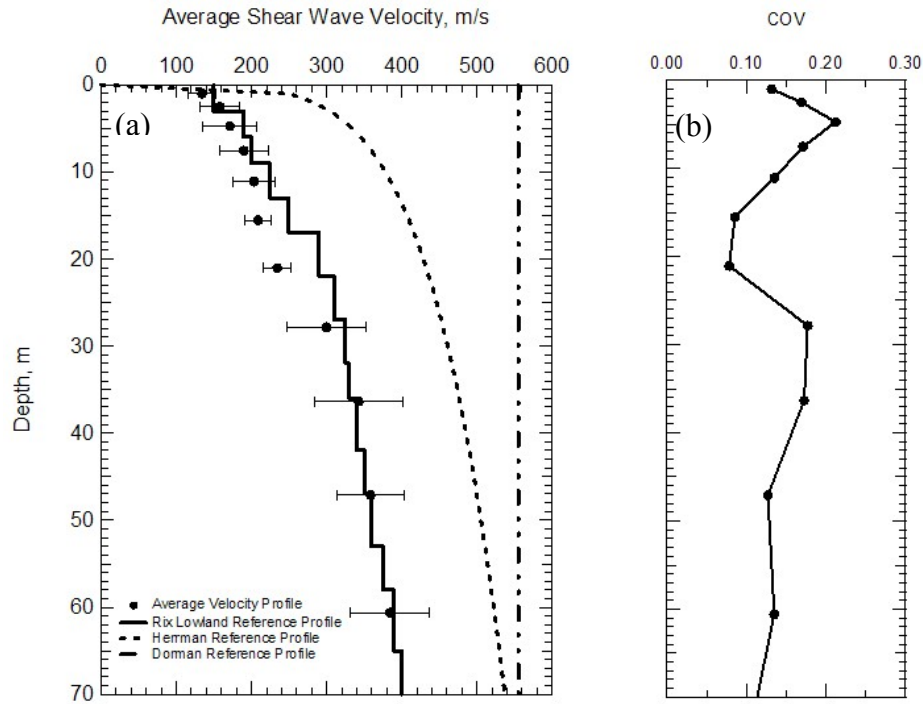


Figure 6.14 (a) Average V_s Profile (Using Arithmetic Mean of 10 Lowland Sites) in the Top 70 Meters Compared to Reference Profiles from Romero and Rix, Herrmann and Akinci, and Dorman and Smalley (b) Coefficient of Variation from 10 Lowland Sites.

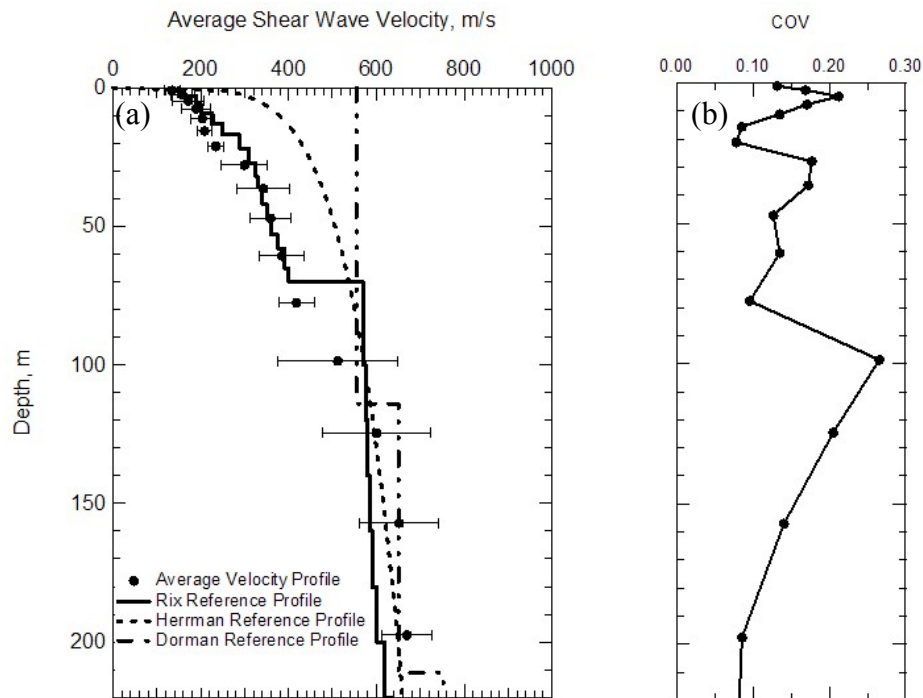


Figure 6.15 (a) Average V_s Profile (Using Arithmetic Mean of 11 Sites) in the Top 220 Meters Compared to Reference Profiles from Romero and Rix, Herrmann and Akinci, and Dorman and Smalley (b) Coefficient of Variation from 11 Sites.

6.3.2 V_s -Soil Lithology

In this section, the relationship between V_s and soil formations is examined. The V_s profiles presented in Figure 6.13 (a) through (k) are replotted in Figure 6.17 by grouping the V_s values into separate plots for: (a) alluvium (b) gravel (c) Jackson, Cockfield, and Cook Mountain (Upper Claiborne) and (d) Memphis Sand. The alluvium plot was developed by averaging the V_s in the layers above the top of the gravel. Also presented in Figure 6.16 (a) through (d) are values for these formations reported by Gomberg (2003) with the dotted black line representing the median V_s value and the gray box representing one standard deviation. The gravel formation is not compared with Gomberg (2003) due to the fact that the test sites for the Gomberg study are located within Pleistocene-age deposits where the gravel is of the Lafayette Formation, which is different from gravel within the Holocene age deposits. From Figure 6.16 it can be observed that the V_s values for the alluvium are slightly higher than the range reported by Gomberg (2003). The V_s values in the Jackson, Cockfield, and Cook Mountain (Upper Claiborne) formation, however, are consistent with Gomberg's values, while the Memphis Sand velocities from this study are higher. Comparisons to other values are presented below and possible reasons for the differences are discussed.

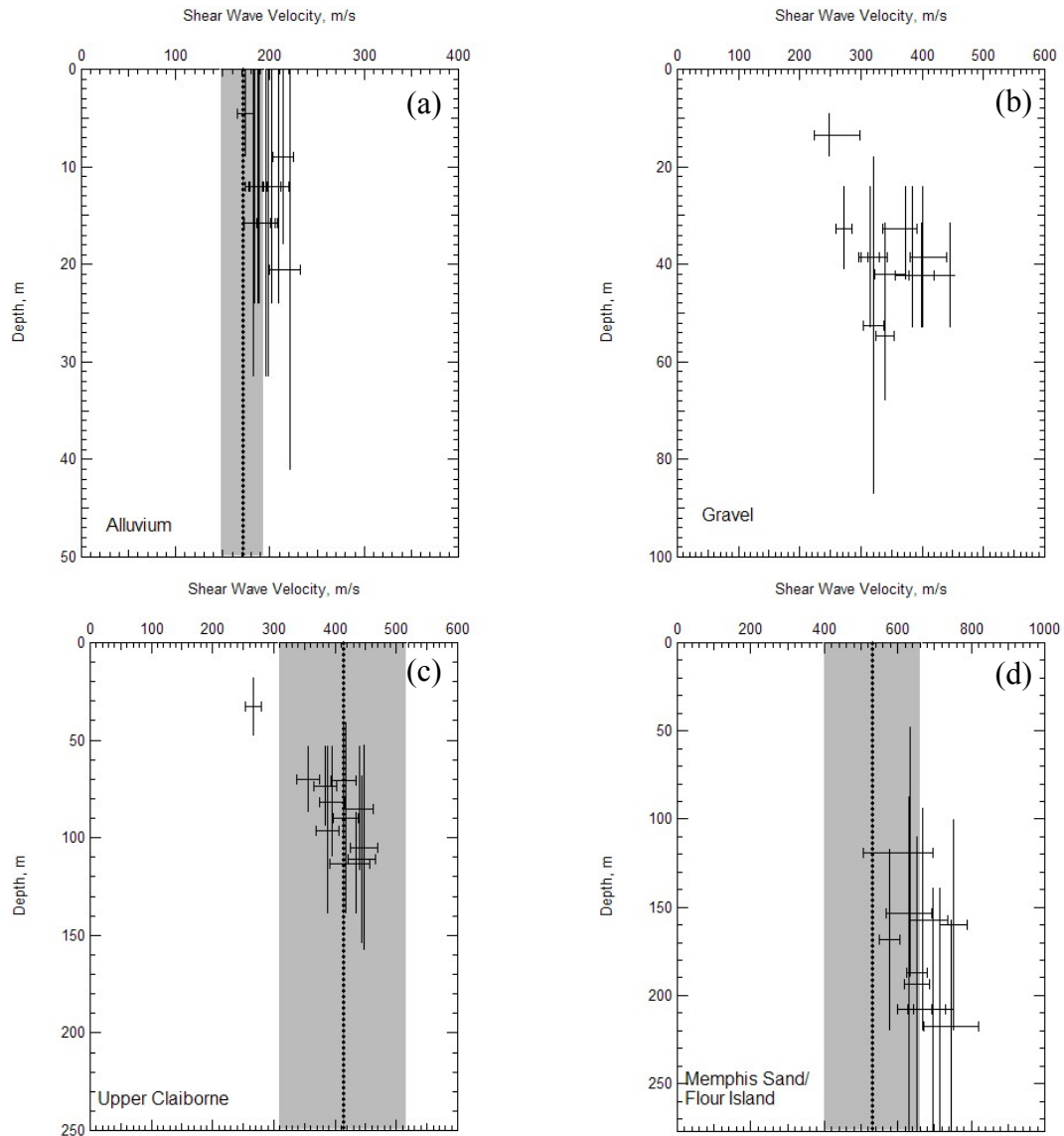


Figure 6.16 Shear Wave Velocity of the (a) Alluvium (b) Gravel (c) Jackson, Cockfield and Cook Mountain (Upper Claiborne) (d) Memphis Sand Soil Layer Compared with Median V_s Values \pm One Standard Deviation from Gomberg (2003).

The data from Figure 6.16 (a) through (d) are presented together in Figure 6.17.

From Figure 6.17 it can be observed how the V_s values compare at similar depths (hence, effective stress values). The alluvium has a distinctively lower V_s value than the upper Claiborne and gravel, which show similar V_s values. The Memphis Sand has distinctively higher V_s values than the upper Claiborne and gravel deposits.

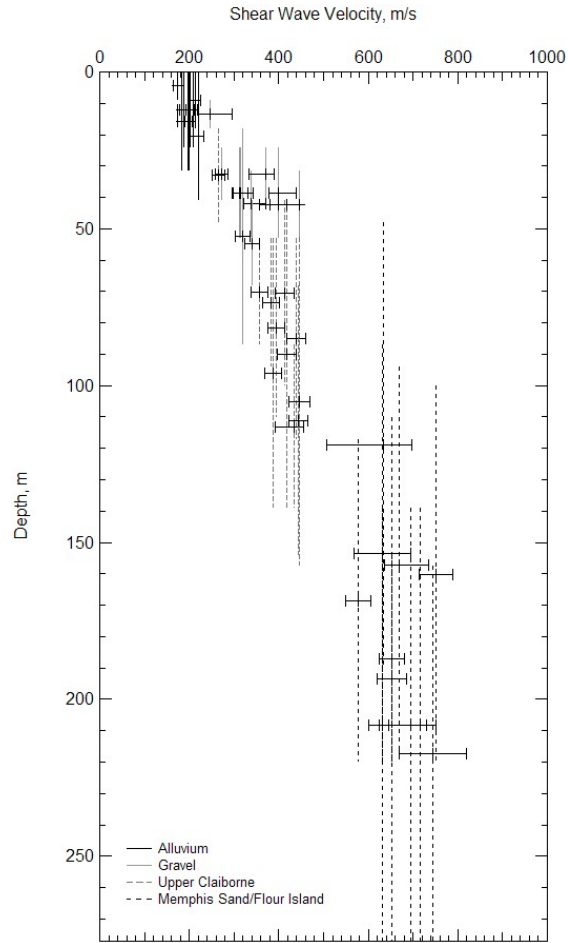


Figure 6.17 Comparison of V_s Values at Similar Depths of Four Soil Formations.

Table 6.1 presents the average values of V_s as a function of the soil lithology from this study as well as those determined by Gomberg et al (2003), William et al. (2003), and Romero and Rix (2001). In general, the average V_s values from this study fall within the ranges of those reported by the other studies with the exception of the Memphis Sand, which was clearly higher in this study. Two main differences between this study and those reported in Table 6.1 are the site locations and the depths of the formations. The eleven profiles developed in this study were spread throughout the upper Mississippi Embayment; whereas, the other studies are mostly developed from near Memphis, Tennessee where the Memphis Sand deposit is much closer to the surface. Also in the other studies there was limited data at depths beyond 70 meters; therefore, shallow

deposits dominate the velocity estimations where the velocity is expected to be lower for the Memphis Sand. It should be noted that the average V_s values for Memphis Sand from Gomberg (2003) were based on only 7 values no deeper than 80 meters, two of which were over 650 m/s. Although the average V_s value of Memphis Sand estimated from this study is higher than the other studies, it is consistent with the Memphis Sand V_s values measured using suspension logging in the MGLW 236 well, as shown in Figure 3.5.

Table 6.1 Average Values of Lithologic Units with Standard Deviation

FORMATION	Shear Wave Velocity (m/s)			
	Bailey, 2008	Gomberg, 2003	Williams, 2003	Rix, 2001
Silt/Clay (Mean, Std)	196 (+/-15)	171 (+/-24)	206	179 (+/-21)
Gravel (Mean, Std)	342 (+/-58)	-	-	-
Upper Claiborne (Mean, Std)	399 (+/-53)	413 (+/-105)	455*	-
Memphis Sand/Flour Island (Mean, Std)	669 (+/-53)	530 (+/-134)	530	554 (+/-15)

*Indicates Combination of Lafayette/Upper Claiborne Formations

6.3.3 Average Velocities

The average velocity within the top 30 meters at the eleven sites has been figured according to the procedure described in International Building Code (IBC) 2003 and are presented in Table 6.2. All eleven sites fall within the range of 180 m/s to 360 m/s, which represents Site Class D ($180 < V_s \leq 360$ m/s) according to the IBC. All sites fall on the low end of the site class with a maximum variability of approximately 20% (excluding upland Site 7 which is slightly higher).

The average velocity within the top 200 meters at the eleven sites was also calculated, as shown in Table 6.3. For the top 200 meters the highest V_s is approximately

17% above the lowest value. The lowest velocities were observed for sites with the thickest layer of upper Claiborne formation (Sites 1, 6, 9), while the highest was observed at Site 5 where the higher velocity Memphis Sand is at the shallowest depth.

The depth of this study was limited by the frequencies that could be excited by the source. In an attempt to extend the depth of the V_s profiles, H/V spectral ratio measurements were performed and are discussed below.

Table 6.2 Site Classifications Based on IBC Standards.

	SITE 1	SITE 2	SITE 3	SITE 4	SITE 5	SITE 6	SITE 7	SITE 8	SITE 9	SITE 10	SITE 11
V_{s30}	204 m/s	200 m/s	209 m/s	224 m/s	215 m/s	180 m/s	247 m/s	224 m/s	197 m/s	195 m/s	193 m/s
Site Class	D	D	D	D	D	D	D	D	D	D	D

Table 6.3 Average V_s Within the Top 200 Meters.

	SITE 1	SITE 2	SITE 3	SITE 4	SITE 5	SITE 6	SITE 7	SITE 8	SITE 9	SITE 10	SITE 11
V_{s200}	378 m/s	398 m/s	446 m/s	422 m/s	453 m/s	379 m/s	394 m/s	422 m/s	379 m/s	389 m/s	409 m/s

6.4 H/V Spectra Results

H/V measurements were performed at the eleven sites as described in Section 4.5 of Chapter 4. Professor Roy Van Arsdale for the University of Memphis provided the estimated depth to bedrock used to interpret the average V_s in the soil column over bedrock. Figures 6.18 through 6.28 show the results from the H/V measurements at Sites 1 through 11.

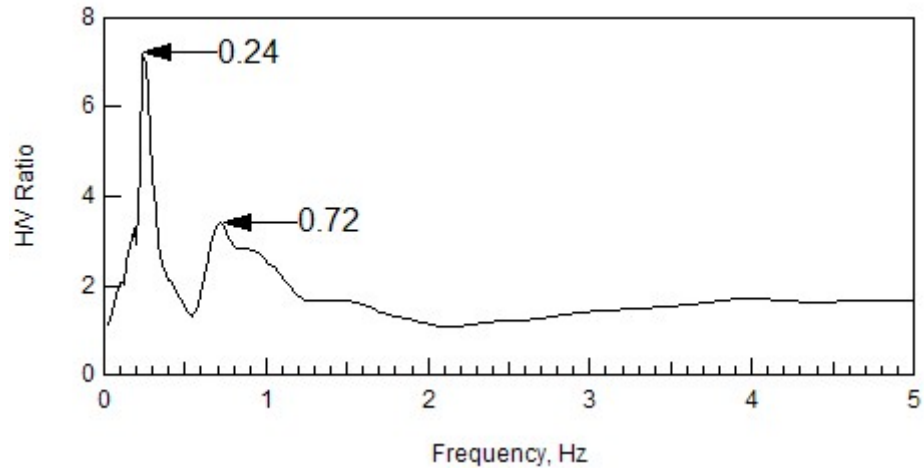


Figure 6.18 Peak Frequencies Obtained from H/V Measurements Performed at Site 1.

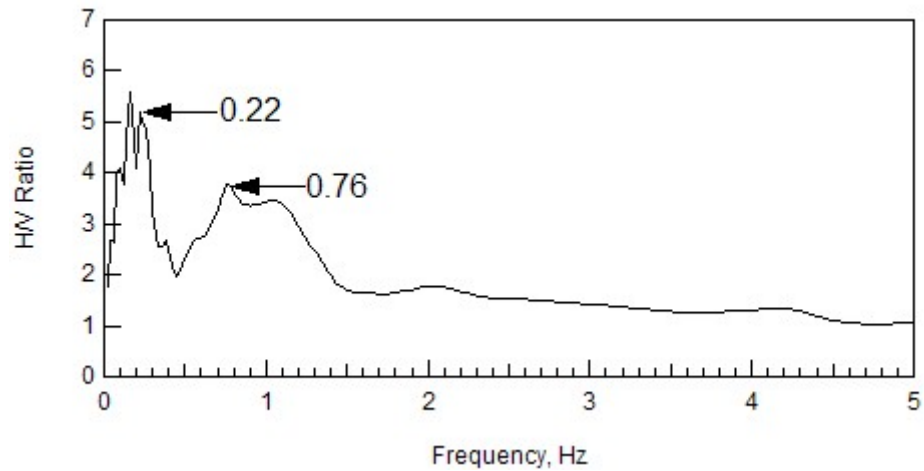


Figure 6.19 Peak Frequencies Obtained from H/V Measurements Performed at Site 2.

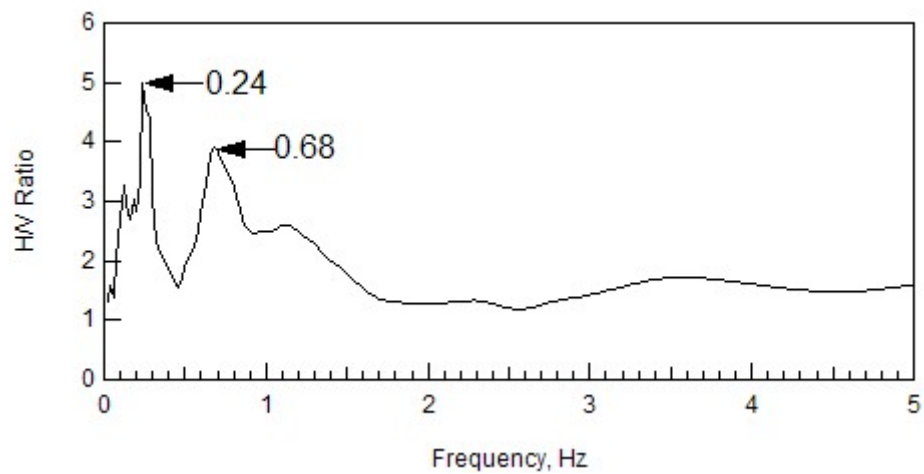


Figure 6.20 Peak Frequencies Obtained from H/V Measurements Performed at Site 3.

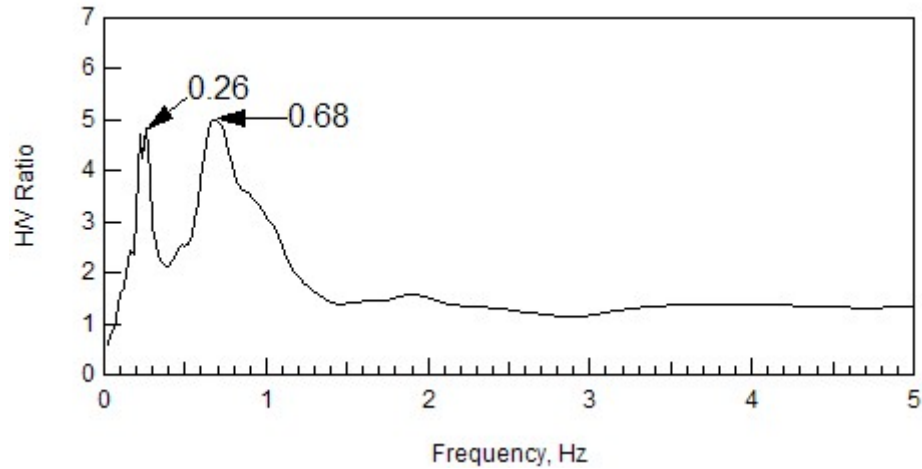


Figure 6.21 Peak Frequencies Obtained from H/V Measurements Performed at Site 4.

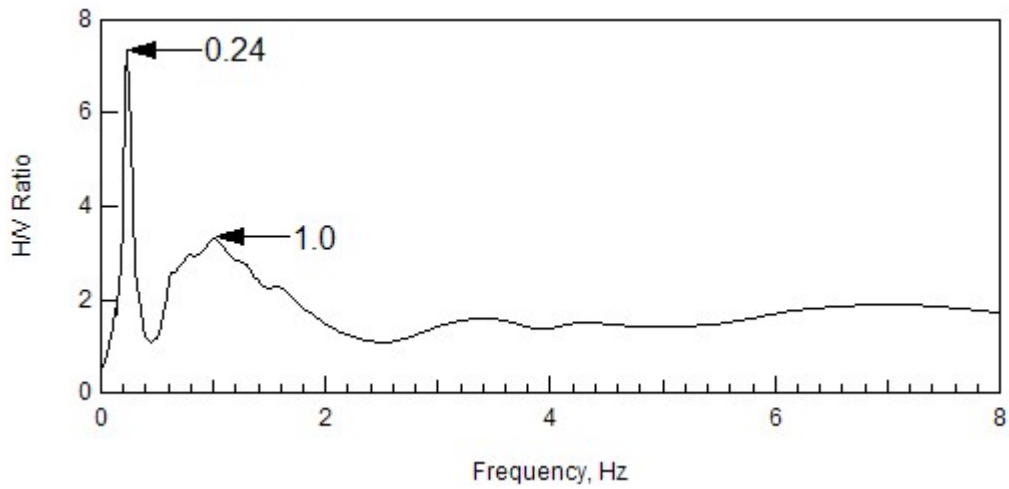


Figure 6.22 Peak Frequency Obtained from H/V Measurements Performed at Site 5.

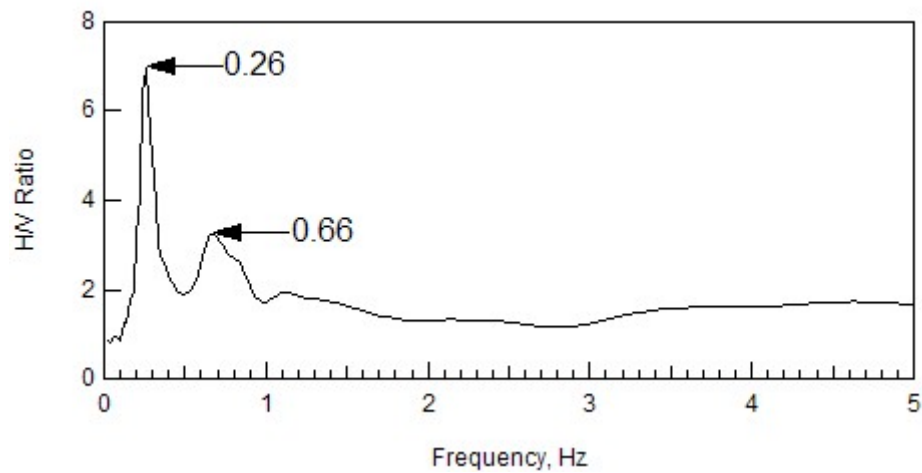


Figure 6.23 Peak Frequencies Obtained from H/V Measurements Performed at Site 6.

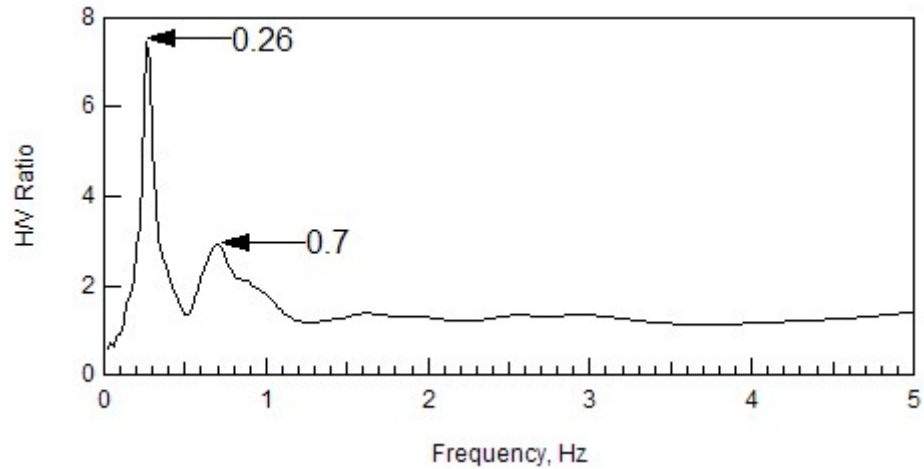


Figure 6.24 Peak Frequencies Obtained from H/V Measurements Performed at Site 7.

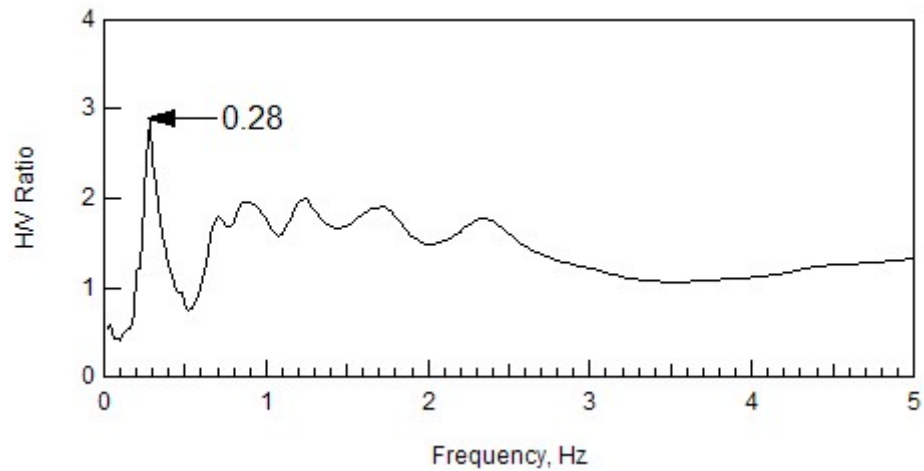


Figure 6.25 Peak Frequency Obtained from H/V Measurements Performed at Site 8.

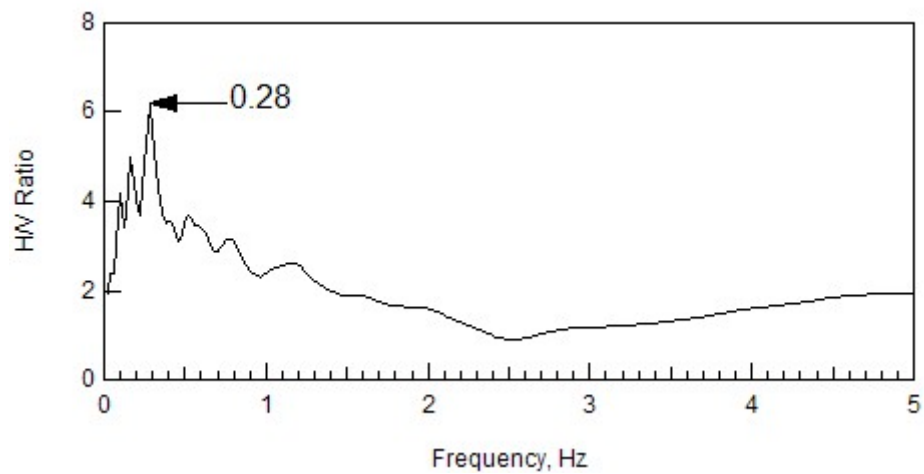


Figure 6.26 Peak Frequency Obtained from H/V Measurements Performed at Site 9.

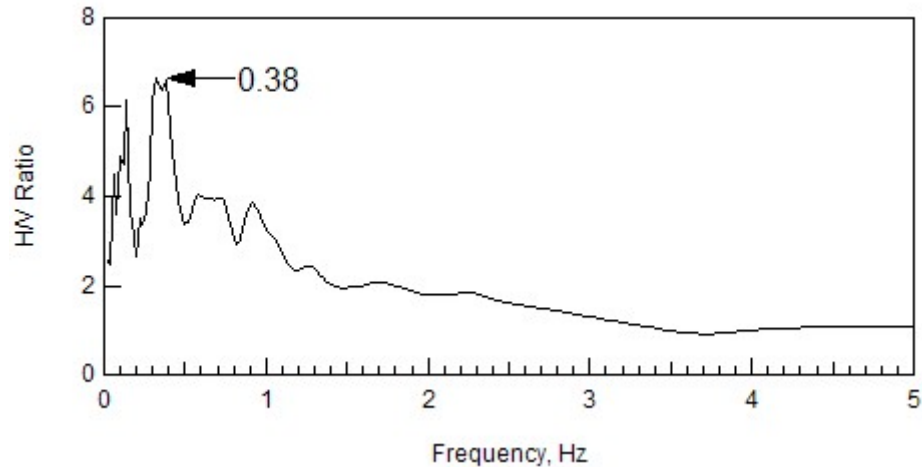


Figure 6.27 Peak Frequency Obtained from H/V Measurements Performed at Site 10.

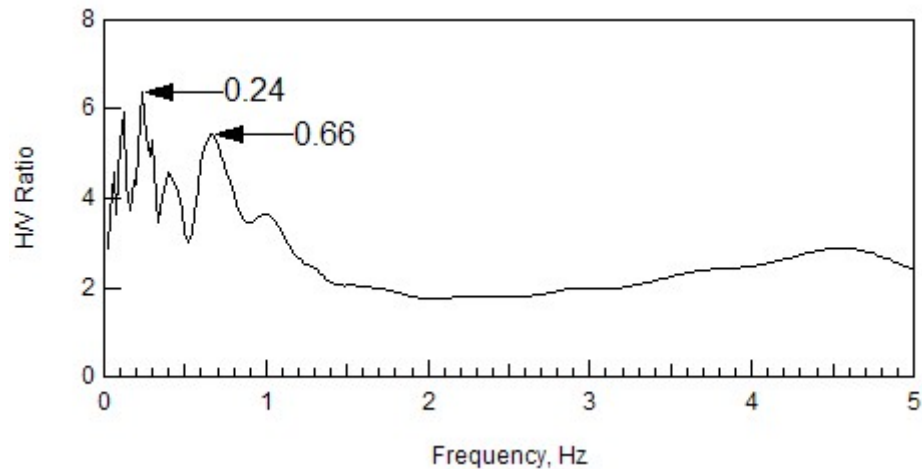


Figure 6.28 Peak Frequencies Obtained from H/V Measurements Performed at Site 11.

At most of the sites, a clear peak is observed at a frequency in the range of 0.22 to 0.38 Hz. At several of the sites a second clear peak is observed in the frequency range of approximately 0.66 to 0.76 Hz. The quality of the results is best for Sites 1-8 and is poorer in Sites 9-11. The lower frequency peak observed in this study has also been measured in past studies (Bodin, 2001) and has been interpreted as the fundamental resonance frequency of the full depth of sediments over bedrock. The source of the higher frequency peak, which was also observed in past studies, is not clear but could be interpreted as the first harmonic of site resonance or a resonance associated with a stiffer shallow layer (Bodin, 2001). This study is concerned with the lower frequency peak.

The average V_s to the full depth of the sediments can be calculated from the resonant frequency (low-frequency peak) and depth to bedrock using Equation 4.10. The average V_s values obtained at each site are presented in Table 6.4. Assuming a variability of ± 20 meters for the depth to bedrock along with using variability in frequency of ± 0.02 Hz, a range of average V_s values were estimated.

Table 6.4 Average V_s at each Site Estimated from H/V Measurements.

Site	Frequency	Depth To Bedrock (Meters)	Average Velocity (Meters/Second)
Site 1	0.24 +/- 0.02	703 +/- 20	601←675→752
Site 2	0.22 +/- 0.02	820 +/- 20	640←722→806
Site 3	0.24 +/- 0.02	783 +/- 20	671←752→835
Site 4	0.26 +/- 0.02	794 +/- 20	743←826→912
Site 5	0.24 +/- 0.02	840 +/- 20	722←806→894
Site 6	0.26 +/- 0.02	783 +/- 20	732←814→899
Site 7	0.26 +/- 0.02	751 +/- 20	702←781→863
Site 8	0.28 +/- 0.02	714 +/- 20	722←800→881
Site 9	0.28 +/- 0.02	586 +/- 20	588←656→727
Site 10	0.38 +/- 0.02	451 +/- 20	620←686→753
Site 11	0.27 +/- 0.02	847 +/- 20	728←813→902

6.5 Discussion of H/V Results

In this section a discussion of general characteristics of the H/V results is presented. Also, the results obtained are compared to the results of two previous studies performed to estimate the average V_s . Finally, a discussion of the validity of using H/V to extend the V_s profiles to bedrock is presented.

6.5.1 Comparison to Other Studies

Two previous studies were performed by Bodin et al. (2001) and Chen et al. (1996) to estimate the average V_s as a function of sediment depth in the Mississippi Embayment. As discussed in Section 3.4 of Chapter 3 these studies used different approaches to estimate the average V_s . Bodin used the H/V method and Chen used S-to-P

converted waves. The results of these studies, as well as the results obtained from the eleven test sites, are shown in Figure 6.29. It can be observed in Figure 6.29 that the results from the H/V measurements at the eleven sites are in general agreement with the relationship determined by Bodin using the same method. As in the case of Bodin's study, the H/V estimate of V_s is well above the estimate from Chen et al (1996).

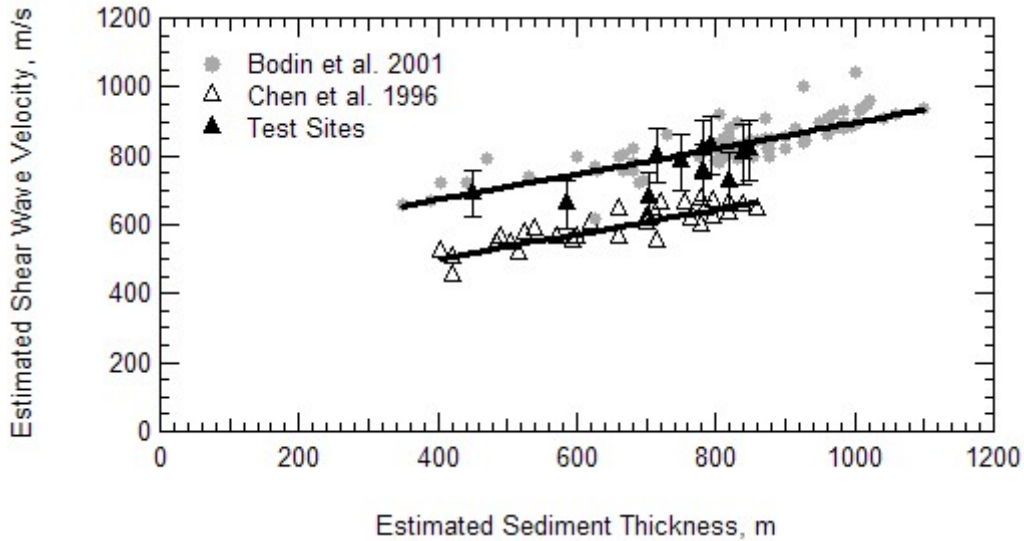


Figure 6.29 Results Obtained from H/V Measurements at Eleven Test Sites Plotted with Results from Bodin et al. 2001 and Chen et al. 1996 (Modified from Bodin et al. 2001).

The travel time through the sediments below the resolution depth of the SASW measurements was calculated from the difference between the travel time through the sediments within the depth of resolution of the SASW method, Δt_{SASW} and the total travel time estimated from the H/V measurements, Δt_{total} where:

$$\Delta t_{SASW} = \sum \frac{d_{iSASW}}{V_{siSASW}} \text{ (Depth of resolution of the SASW study),} \quad (6.1)$$

$$\Delta t_{total} = \sum \frac{d_t}{V_{st}} \text{ (Full depth).} \quad (6.2)$$

Using this difference along with the thickness of the sediments below the depth of the SASW results the average V_s below the depth of the SASW profile can be calculated from:

$$\bar{V}_{below} = \frac{d_t - d_{iSASW}}{\Delta t_{total} - \Delta t_{SASW}} \quad (6.3)$$

where, \bar{V}_{below} is the average shear velocity from the bottom of the SASW profile to bedrock, d_t is the total thickness of the sediments, and d_{iSASW} is the thickness of the sediments below the depth of resolution of the SASW method to bedrock. This procedure was applied to the results from Table 6.4 to calculate the average velocity of the sediments below the depth of the SASW resolution. The results are presented in Figure 6.30. This procedure was performed again using the variability estimates presented in Table 6.4 to produce sensitivity bounds. It should be noted that relatively small changes in frequency and depth produce large changes in V_s as represented by the horizontal black lines in Figure 6.30. The V_s calculation was then repeated using the average full-depth V_s value scaled from Chen's relationship. The results from these calculations are presented with the reference profiles in Figure 6.30.

The results show that using the H/V measurements to estimate full depth V_s values results in velocity estimates that are well above those of the three reference profiles. However, the average velocities of the lower sediments produced using Chen's estimate generally provide V_s values that are consistent with the reference profiles, although a little lower. From the findings it appears that the assumption of the H/V peak representing the fundamental frequency overestimates the average V_s of sediments. The validity of the H/V method is discussed in the following section.

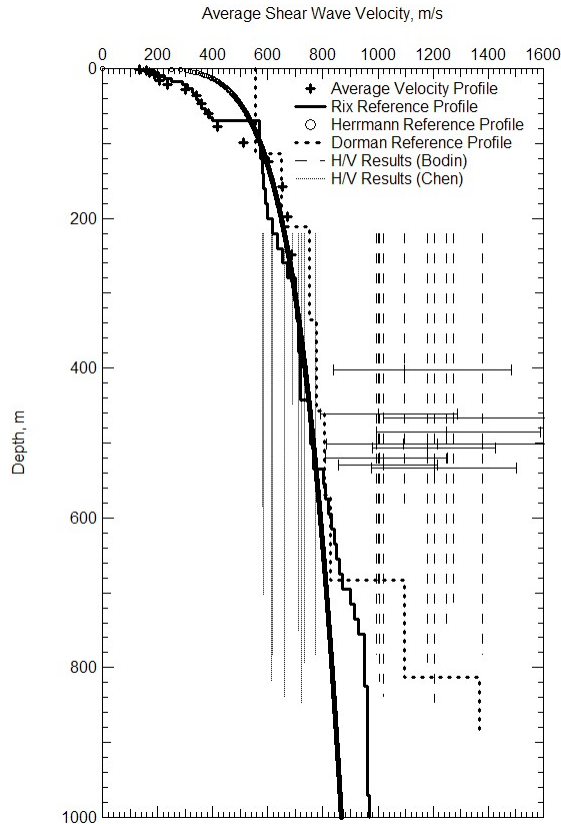


Figure 6.30 Average V_s Values Below the Depth of the SASW Profiles Determined from H/V Measurements Compared to Deep V_s Reference Profiles.

6.5.2 Validity of H/V Estimate of Average V_s

There are many published studies of H/V measurements showing general agreement between the H/V peak and the fundamental frequency of the site. However, the relationship is not always equal. Scherbaum et al, 2002, present results from simulations of H/V measurements using a randomized basin model where the depth to the base and the V_s values were varied. He compared the frequency peak from the H/V spectra to the frequency calculated using the quarter wavelength relationship

$$(fr = \frac{1}{4(t_t)} = \frac{V_s}{4H}, \text{ where } t_t \text{ is the travel time from the bedrock to the surface}). \text{ This}$$

relationship is presented in Figure 6.31 along with the ideal 1:1 relationship. These results show that for many of the profiles that were generated the fundamental frequency

estimated from the H/V peak was above the frequency calculated directly from the travel time. For example, at a frequency of 0.42 Hz from the travel time calculation, the H/V peak was at about 0.55, or about 30% higher. This may explain the generally higher estimates observed in Figure 6.30 for the H/V measurements. Given the average V_s is very sensitive to this value, the H/V approach may not provide a reliable estimate of the average V_s .

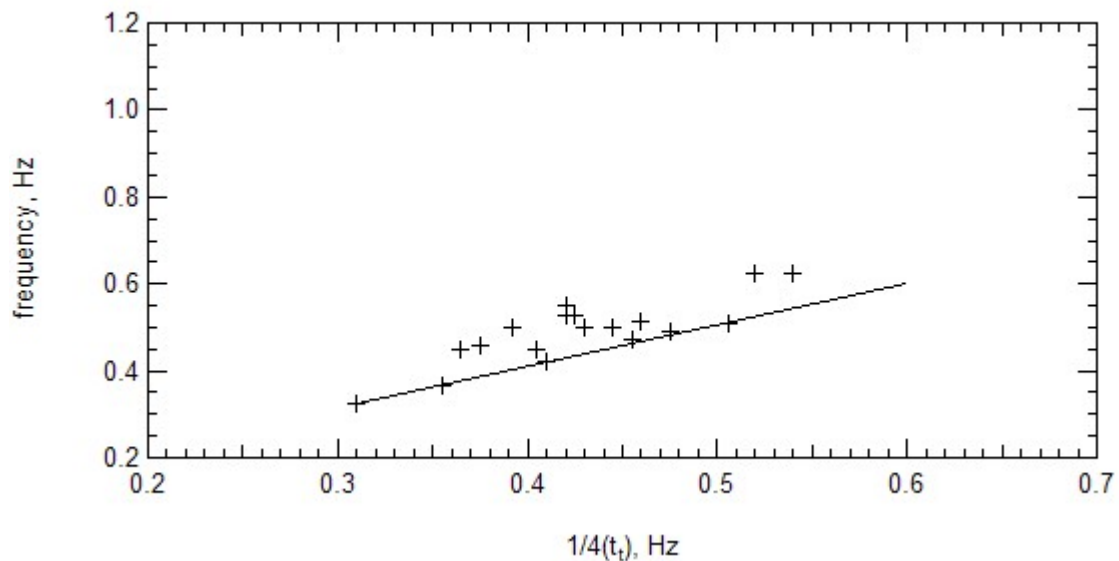


Figure 6.31 Travel Time Versus Frequency of Randomized Basin Models based on the V_s Profile Produced Within the Lower Rhine Embayment in the Cologne, Germany Area (Scherbaum, 2002).

6.6 Summary

To develop V_s profiles at the eleven test sites, the SASW and H/V methods were used. The SASW method allowed for non-intrusive characterization of sediments to depths of over 200 meters in most cases. These profiles were then compared to reference profiles from Romero and Rix (2001), Herrmann and Akinci (1999), and Dorman and Smalley (1994). The V_s values were then divided based on soil formation allowing for the examination of V_s as it relates to soil lithology. The values obtained for each soil unit were compared with values from Gomberg et al. (2003), Williams et al. (2003), and

Romero and Rix (2001). The H/V method was used to characterize the average V_s to bedrock, at the eleven sites. The H/V results were compared with previous studies performed by Bodin et al., 2001 and Chen et al., 1996. Finally the validity of the H/V method was discussed.

CHAPTER 7

CONCLUSIONS

7.1 Summary

The objective of this research was to provide much needed information on the V_s properties of the deep sediments of the Mississippi Embayment. Surface wave velocity measurements were performed at eleven sites in the upper Mississippi Embayment. The surface wave energy was excited using the low-frequency Network for Earthquake Engineering Simulation (NEES) vibrator. The data was processed using the SASW methodology and V_s profiles were developed to depths of approximately 220 m. A mean V_s profile and the associated variability were calculated and compared to reference V_s profiles that have been used in past studies. Estimates of soil lithology at the eleven sites provided by Professor Van Arsdale at the University of Memphis were used to relate observed changes in V_s to changes in soil formations. Relationships were developed between V_s and soil formation type and compared to past studies. Lastly, ambient noise measurements were performed at the eleven sites and the H/V spectral ratio method was used to estimate the fundamental frequency of the site and the average V_s of the full depth of the sediments.

7.2 Conclusions

The results from this study lead to several conclusions regarding the research and analysis methods.

1. The low-frequency NEES vibrator was effective at generating the low-frequency energy (less than 1 Hz) needed for developing deep V_s profiles. This was the first application of this unique equipment to surface wave

measurements at soil sites. The successful demonstration of the performance of this equipment for this application is an important contribution of this work.

2. The SASW method appears to be a viable approach to developing deep V_s profiles. This conclusion was drawn from the observed consistency of the theoretical dispersion curves to the experimental dispersion curves as well as the resulting V_s profiles that were consistent with the expected site conditions and V_s values from independent studies.
3. The V_s reference profile of Romero and Rix, 2001 was validated by the results of this study. The average V_s profile from the eleven sites of this study was in good agreement with the profile of Romero and Rix. This is an important contribution, as this profile has been used in past site response studies of the region, but was based on very limited data for the deep soils.
4. The variability in V_s profiles appears to be strongly related to changes in soil formation depths and thickness. The V_s profiles developed from this study showed very good agreement between the depth of changes in V_s and the estimated depths to formation tops. Relationships between V_s and soil formations from this study were in good agreement with data derived from past studies.
5. The H/V spectral ratio method appears to overestimate the average V_s for the full-depth of the sediments. The average V_s derived from this portion of the study were consistent with the measurements and results presented

by Bodin (2003). However, when combined with the results from the SASW method, the resulting V_s values in the deeper portion of the profile appear to be greatly overestimated.

7.3 Recommendations

From the findings reported in this thesis, several recommendations can be made for future work to further characterize the Mississippi Embayment as well as evaluate testing methods:

1. Future deep studies should be performed throughout the Mississippi Embayment in order to better characterize the subsurface variability. Measurements should be performed closer to sites with well-characterized subsurface conditions to provide better V_s -soil lithology relationships.
2. In this study the estimated depth to the top of the Memphis Sand was not varied in the SASW inversion. An investigation of the effect of changes in the depth to the top of the Memphis Sand layer on the estimated formation velocities derived from the SASW measurements should be performed.
3. An analytical study of the H/V spectral ratio method for different profile conditions should be performed in order to better understand the conditions that may impact the reliability of this method.
4. S-to-P converted wave measurements could be performed at each of the eight seismic station locations in order to better characterize the full-depth V_s of sediment at these sites.

APPENDIX

This appendix documents the results from Spectral-Analysis-Surface-Waves (SASW) tests as well as the H/V tests that were performed at 11 sites in the upper Mississippi Embayment. Each appendix contains the table of shear wave profile parameters, modified shear wave profile parameters, and “raw” H/V ratio data plots. All data used in this study will be publicly available at the NEES central data repository (central.NEES.org).

APPENDIX A

Table A.1 Profile Parameters Used to Develop Theoretical Dispersion Curve at Site 1

Thickness (m)	P-Wave Velocity (m/s)	S-Wave Velocity (m/s)	Density (g/cm³)	Poisson's Ratio	Damping Factor
0.5	186	107	1.9	0.25	0.02
1	227	131	1.9	0.25	0.02
2	242	140	1.9	0.25	0.02
2.5	1600	205	1.9	0.49	0.02
3.1	1600	199	1.9	0.49	0.02
4	1600	223	1.9	0.49	0.02
4.9	1600	204	1.9	0.49	0.02
6.1	1600	224	1.9	0.49	0.02
7.5	1600	257	1.9	0.49	0.02
9.5	1600	289	1.9	0.48	0.02
12	1600	326	1.9	0.48	0.02
15	1600	364	1.9	0.47	0.02
19	1600	400	1.9	0.47	0.02
23	1600	453	1.9	0.46	0.02
29	1600	475	1.9	0.45	0.02
36	1600	527	1.9	0.44	0.02
45	1600	603	1.9	0.42	0.02
∞	1800	742	1.9	0.40	0.02

Table A.2 Profile Parameters Used to Develop Modified Theoretical Dispersion Curve at Site 1

Thickness (m)	P-Wave Velocity (m/s)	S-Wave Velocity (m/s)	Density (g/cm³)	Poisson's Ratio	Damping Factor
0.5	188	109	1.9	0.25	0.02
1	223	128	1.9	0.25	0.02
2	245	142	1.9	0.25	0.02
2.5	1600	211	1.9	0.49	0.02
3.1	1600	197	1.9	0.49	0.02
4	1600	215	1.9	0.49	0.02
4.9	1600	201	1.9	0.49	0.02
6.1	1600	226	1.9	0.49	0.02
7.5	1600	257	1.9	0.49	0.02
9.5	1600	291	1.9	0.48	0.02
27	1600	340	1.9	0.48	0.02
86	1600	443	1.9	0.46	0.02
∞	1800	653	1.9	0.42	0.02

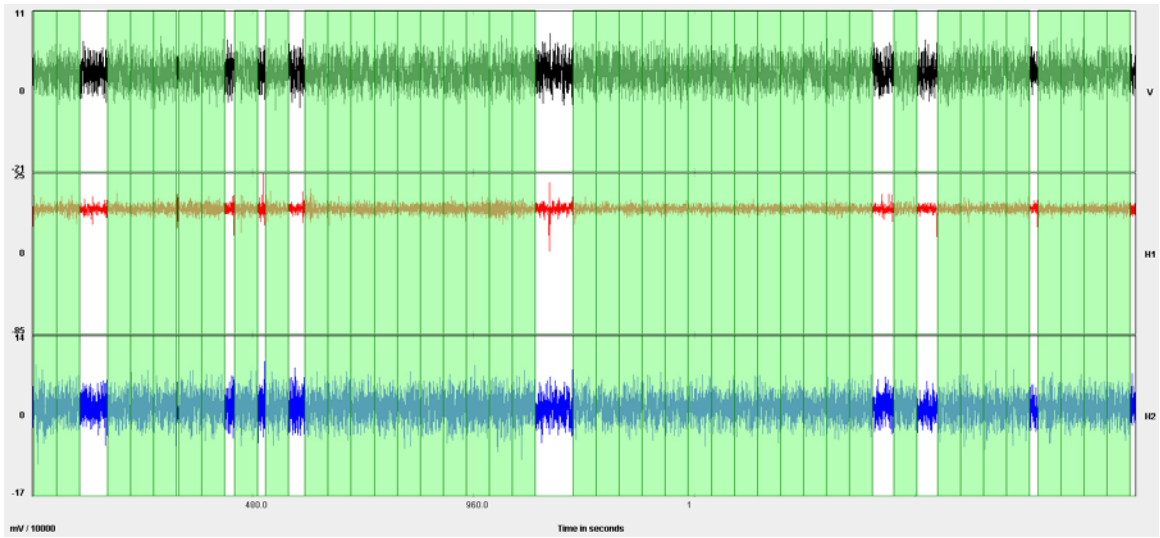


Figure A.1 H/V Showing Windows of Data Used (Shaded) in Analysis After Filter is Applied in the Program J-SESAME for Site 1.

APPENDIX B

Table B.1 Profile Parameters Used to Develop Theoretical Dispersion Curve at Site 2

Thickness (m)	P-Wave Velocity (m/s)	S-Wave Velocity (m/s)	Density (g/cm³)	Poisson's Ratio	Damping Factor
0.5	223	129	1.9	0.25	0.02
1	205	118	1.9	0.25	0.02
2	224	129	1.9	0.25	0.02
2.5	1600	133	1.9	0.50	0.02
3.1	1600	170	1.9	0.49	0.02
4	1600	204	1.9	0.49	0.02
4.9	1600	217	1.9	0.49	0.02
6.1	1600	241	1.9	0.49	0.02
7.5	1600	329	1.9	0.48	0.02
9.5	1600	290	1.9	0.48	0.02
12	1600	312	1.9	0.48	0.02
15	1600	429	1.9	0.46	0.02
19	1600	486	1.9	0.45	0.02
23	1600	491	1.9	0.45	0.02
29	1600	427	1.9	0.46	0.02
36	1600	643	1.9	0.40	0.02
∞	1800	735	1.9	0.40	0.02

Table B.2 Profile Parameters Used to Develop Modified Theoretical Dispersion Curve at Site 2

Thickness (m)	P-Wave Velocity (m/s)	S-Wave Velocity (m/s)	Density (g/cm³)	Poisson's Ratio	Damping Factor
0.5	245	141	1.9	0.25	0.02
1	215	124	1.9	0.25	0.02
2	231	133	1.9	0.25	0.02
2.5	1600	151	1.9	0.50	0.02
3.1	1600	166	1.9	0.49	0.02
4	1600	194	1.9	0.49	0.02
4.9	1600	211	1.9	0.49	0.02
6.1	1600	242	1.9	0.49	0.02
29	1600	314	1.9	0.48	0.02
64	1600	440	1.9	0.46	0.02
∞	1600	578	1.9	0.42	0.02

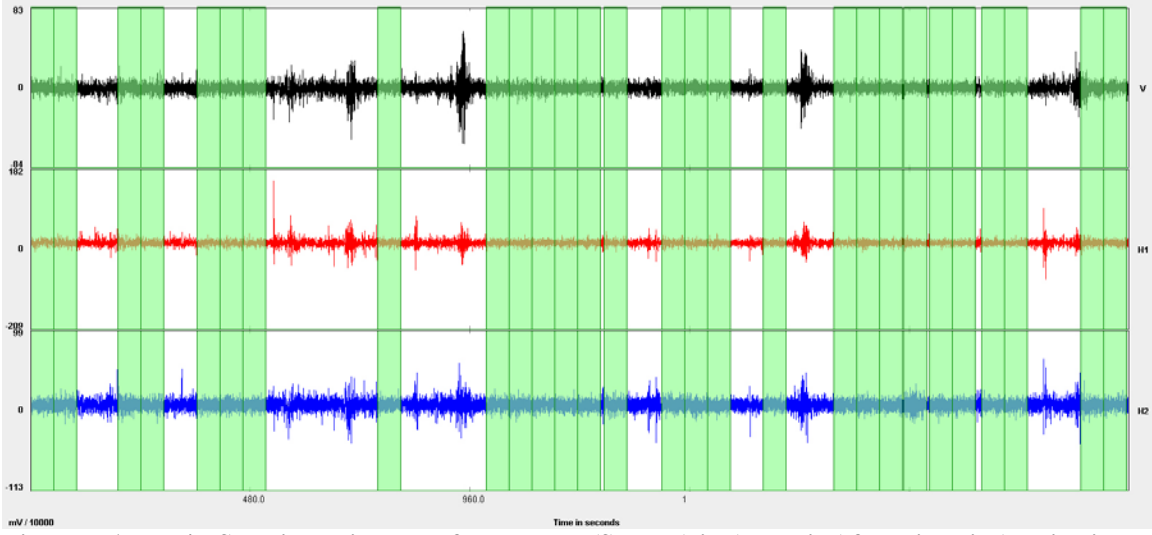


Figure B.1 H/V Showing Windows of Data Used (Shaded) in Analysis After Filter is Applied in the Program J-SESAME for Site 2.

APPENDIX C

Table C.1 Profile Parameters Used to Develop Theoretical Dispersion Curve at Site 3

Thickness (m)	P-Wave Velocity (m/s)	S-Wave Velocity (m/s)	Density (g/cm³)	Poisson's Ratio	Damping Factor
0.5	111	64	1.9	0.25	0.02
1	241	139	1.9	0.25	0.02
2	307	177	1.9	0.25	0.02
2.5	1600	144	1.9	0.50	0.02
3.1	1600	167	1.9	0.49	0.02
4	1600	218	1.9	0.49	0.02
4.9	1600	223	1.9	0.49	0.02
6.1	1600	243	1.9	0.49	0.02
7.5	1600	357	1.9	0.47	0.02
9.5	1600	388	1.9	0.47	0.02
12	1600	389	1.9	0.47	0.02
15	1600	399	1.9	0.47	0.02
19	1600	432	1.9	0.46	0.02
23	1600	517	1.9	0.44	0.02
29	1800	688	1.9	0.41	0.02
36	1800	866	1.9	0.35	0.02
∞	1800	910	1.9	0.33	0.02

Table C.2 Profile Parameters Used to Develop Modified Theoretical Dispersion Curve at Site 3

Thickness (m)	P-Wave Velocity (m/s)	S-Wave Velocity (m/s)	Density (g/cm³)	Poisson's Ratio	Damping Factor
0.5	175	101	1.9	0.25	0.02
1	305	176	1.9	0.25	0.02
2	310	179	1.9	0.25	0.02
2.5	1600	130	1.9	0.50	0.02
3.1	1600	247	1.9	0.49	0.02
4	1600	227	1.9	0.49	0.02
4.9	1600	188	1.9	0.49	0.02
6.1	1600	275	1.9	0.48	0.02
29	1600	400	1.9	0.47	0.02
57	1600	395	1.9	0.47	0.02
∞	1800	657	1.9	0.42	0.02

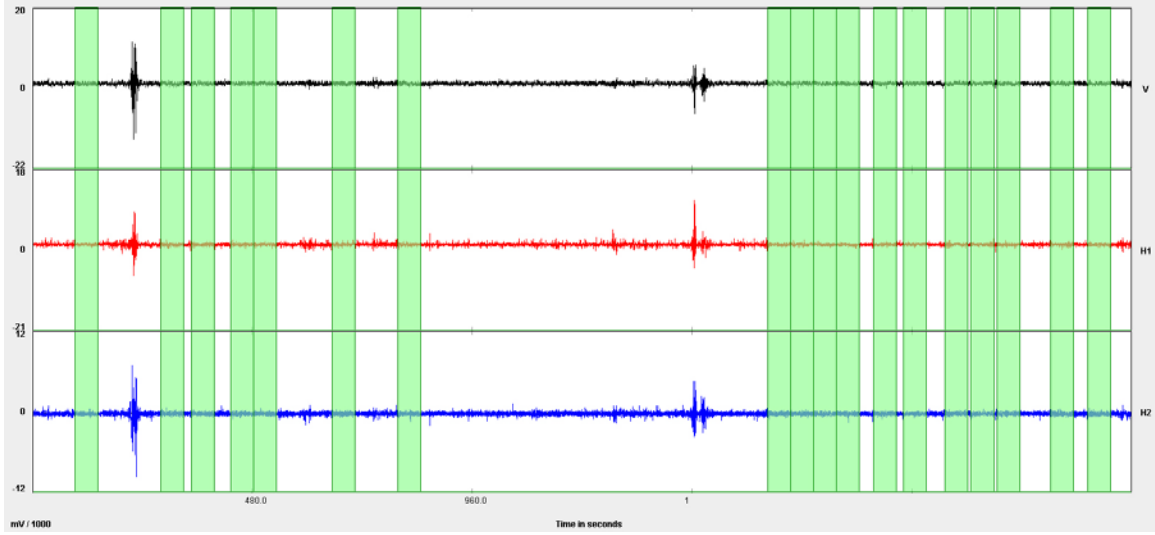


Figure C.1 H/V Showing Windows of Data Used (Shaded) in Analysis After Filter is Applied in the Program J-SESAME for Site 3.

APPENDIX D

Table D.1 Profile Parameters Used to Develop Theoretical Dispersion Curve at Site 4

Thickness (m)	P-Wave Velocity (m/s)	S-Wave Velocity (m/s)	Density (g/cm³)	Poisson's Ratio	Damping Factor
0.5	220	127	1.9	0.25	0.02
1	233	135	1.9	0.25	0.02
2	329	190	1.9	0.25	0.02
2.5	1600	237	1.9	0.49	0.02
3.1	1600	208	1.9	0.49	0.02
4	1600	219	1.9	0.49	0.02
4.9	1600	221	1.9	0.49	0.02
6.1	1600	222	1.9	0.49	0.02
7.5	1600	279	1.9	0.48	0.02
9.5	1600	301	1.9	0.48	0.02
12	1600	301	1.9	0.48	0.02
15	1600	496	1.9	0.45	0.02
19	1600	409	1.9	0.47	0.02
23	1600	429	1.9	0.46	0.02
29	1600	576	1.9	0.43	0.02
36	1800	716	1.9	0.41	0.02
∞	1800	905	1.9	0.33	0.02

Table D.2 Profile Parameters Used to Develop Modified Theoretical Dispersion Curve at Site 4

Thickness (m)	P-Wave Velocity (m/s)	S-Wave Velocity (m/s)	Density (g/cm³)	Poisson's Ratio	Damping Factor
0.5	220	127	1.9	0.25	0.02
1	233	135	1.9	0.25	0.02
2	329	190	1.9	0.25	0.02
2.5	1600	237	1.9	0.49	0.02
3.1	1600	208	1.9	0.49	0.02
4	1600	219	1.9	0.49	0.02
4.9	1600	221	1.9	0.49	0.02
6.1	1600	222	1.9	0.49	0.02
29	1600	312	1.9	0.48	0.02
41	1600	383	1.9	0.47	0.02
∞	1800	668	1.9	0.42	0.02

APPENDIX E

Table E.1 Profile Parameters Used to Develop Theoretical Dispersion Curve at Site 5

Thickness (m)	P-Wave Velocity (m/s)	S-Wave Velocity (m/s)	Density (g/cm³)	Poisson's Ratio	Damping Factor
1	188	108	1.9	0.25	0.02
1	227	131	1.9	0.25	0.02
1	320	185	1.9	0.25	0.02
3	1600	179	1.9	0.49	0.02
3	1600	234	1.9	0.49	0.02
3	1600	252	1.9	0.49	0.02
6	1600	246	1.9	0.49	0.02
6	1600	218	1.9	0.49	0.02
6	1600	255	1.9	0.49	0.02
6	1600	264	1.9	0.49	0.02
12	1600	316	1.9	0.48	0.02
12	1600	448	1.9	0.46	0.02
25	1600	531	1.9	0.44	0.02
25	1600	611	1.9	0.41	0.02
50	1800	713	1.9	0.41	0.02
∞	1800	822	1.9	0.37	0.02

Table E.2 Profile Parameters Used to Develop Modified Theoretical Dispersion Curve at Site 5

Thickness (m)	P-Wave Velocity (m/s)	S-Wave Velocity (m/s)	Density (g/cm³)	Poisson's Ratio	Damping Factor
1	188	108	1.9	0.25	0.02
1	227	131	1.9	0.25	0.02
1	320	185	1.9	0.25	0.02
3	1600	179	1.9	0.49	0.02
3	1600	234	1.9	0.49	0.02
3	1600	252	1.9	0.49	0.02
6	1600	246	1.9	0.49	0.02
6	1600	218	1.9	0.49	0.02
6	1600	255	1.9	0.49	0.02
6	1600	264	1.9	0.49	0.02
12	1600	307	1.9	0.48	0.02
36	1600	495	1.9	0.45	0.02
∞	1800	703	1.9	0.41	0.02

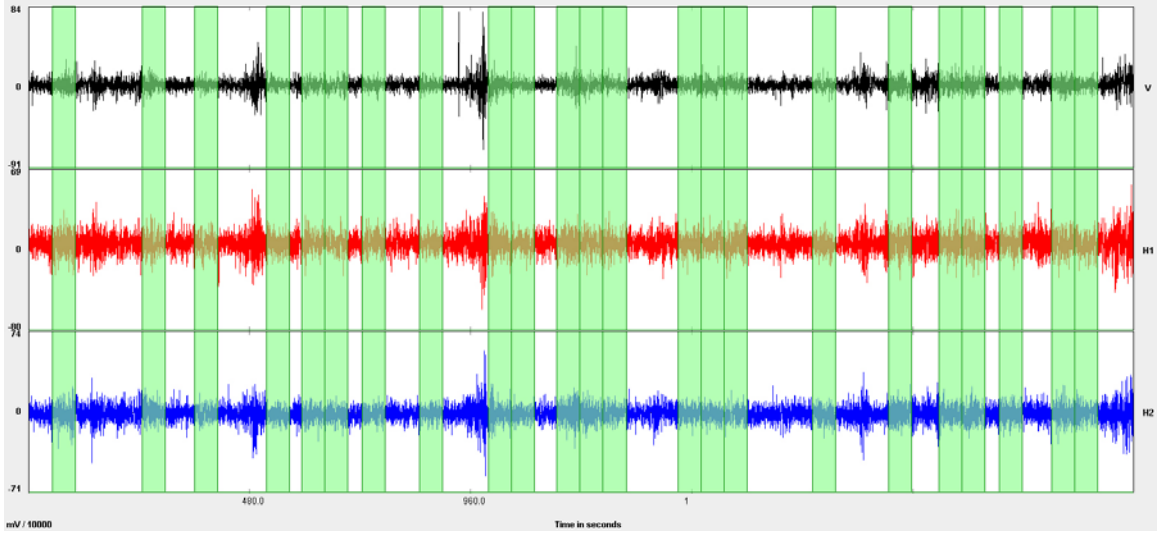


Figure E.1 H/V Showing Windows of Data Used (Shaded) in Analysis After Filter is Applied in the Program J-SESAME for Site 5.

APPENDIX F

Table F.1 Profile Parameters Used to Develop Theoretical Dispersion Curve at Site 6

Thickness (m)	P-Wave Velocity (m/s)	S-Wave Velocity (m/s)	Density (g/cm³)	Poisson's Ratio	Damping Factor
0.5	188	108	1.9	0.25	0.02
1	208	120	1.9	0.25	0.02
2	247	142	1.9	0.25	0.02
2.5	1600	123	1.9	0.50	0.02
3.1	1600	171	1.9	0.49	0.02
4	1600	182	1.9	0.49	0.02
4.9	1600	192	1.9	0.49	0.02
6.1	1600	209	1.9	0.49	0.02
7.5	1600	241	1.9	0.49	0.02
9.5	1600	327	1.9	0.48	0.02
12	1600	386	1.9	0.47	0.02
15	1600	418	1.9	0.46	0.02
19	1600	417	1.9	0.46	0.02
23	1600	421	1.9	0.46	0.02
29	1600	478	1.9	0.45	0.02
36	1600	621	1.9	0.41	0.02
45	1800	681	1.9	0.42	0.02
∞	1800	751	1.9	0.39	0.02

Table F.2 Profile Parameters Used to Develop Modified Theoretical Dispersion Curve at Site 6

Thickness (m)	P-Wave Velocity (m/s)	S-Wave Velocity (m/s)	Density (g/cm³)	Poisson's Ratio	Damping Factor
0.5	188	108	1.9	0.25	0.02
1	208	120	1.9	0.25	0.02
2	246	142	1.9	0.25	0.02
2.5	1600	123	1.9	0.50	0.02
3.1	1600	171	1.9	0.49	0.02
4	1600	182	1.9	0.49	0.02
4.9	1600	192	1.9	0.49	0.02
6.1	1600	209	1.9	0.49	0.02
7.5	1600	241	1.9	0.49	0.02
21	1600	339	1.9	0.48	0.02
105	1600	447	1.9	0.46	0.02
∞	1800	745	1.9	0.36	0.02

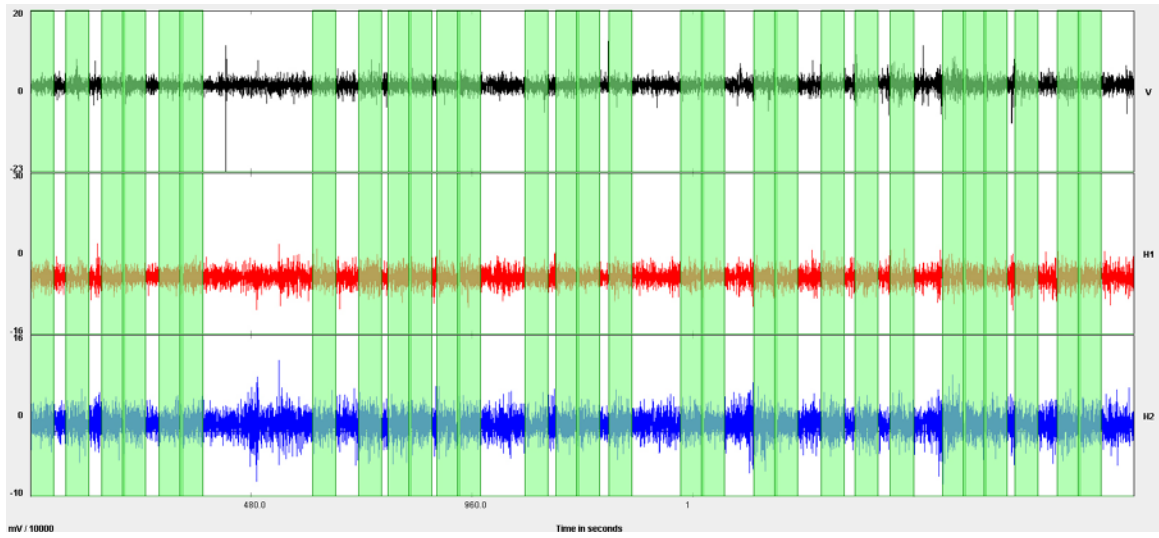


Figure F.1 H/V Showing Windows of Data Used (Shaded) in Analysis After Filter is Applied in the Program J-SESAME for Site 6.

APPENDIX G

Table G.1 Profile Parameters Used to Develop Theoretical Dispersion Curve at Site 7

Thickness (m)	P-Wave Velocity (m/s)	S-Wave Velocity (m/s)	Density (g/cm³)	Poisson's Ratio	Damping Factor
0.5	296	171	1.9	0.25	0.02
1	288	166	1.9	0.25	0.02
2	381	220	1.9	0.25	0.02
2.5	1600	114	1.9	0.50	0.02
3.1	1600	265	1.9	0.49	0.02
4	1600	258	1.9	0.49	0.02
4.9	1600	271	1.9	0.49	0.02
6.1	1600	309	1.9	0.48	0.02
7.5	1600	332	1.9	0.48	0.02
9.5	1600	333	1.9	0.48	0.02
12	1600	320	1.9	0.48	0.02
15	1600	329	1.9	0.48	0.02
19	1600	356	1.9	0.47	0.02
23	1600	412	1.9	0.46	0.02
29	1600	487	1.9	0.45	0.02
36	1600	579	1.9	0.42	0.02
45	1800	697	1.9	0.41	0.02
∞	1800	789	1.9	0.38	0.02

Table G.2 Profile Parameters Used to Develop Modified Theoretical Dispersion Curve at Site 7

Thickness (m)	P-Wave Velocity (m/s)	S-Wave Velocity (m/s)	Density (g/cm³)	Poisson's Ratio	Damping Factor
0.5	293	169	1.9	0.25	0.02
1	291	168	1.9	0.25	0.02
2	408	235	1.9	0.25	0.02
2.5	1600	123	1.9	0.50	0.02
3.1	1600	238	1.9	0.49	0.02
4	1600	265	1.9	0.49	0.02
4.9	1600	272	1.9	0.49	0.02
69.1	1600	320	1.9	0.48	0.02
52	1600	434	1.9	0.46	0.02
∞	1800	695	1.9	0.41	0.02

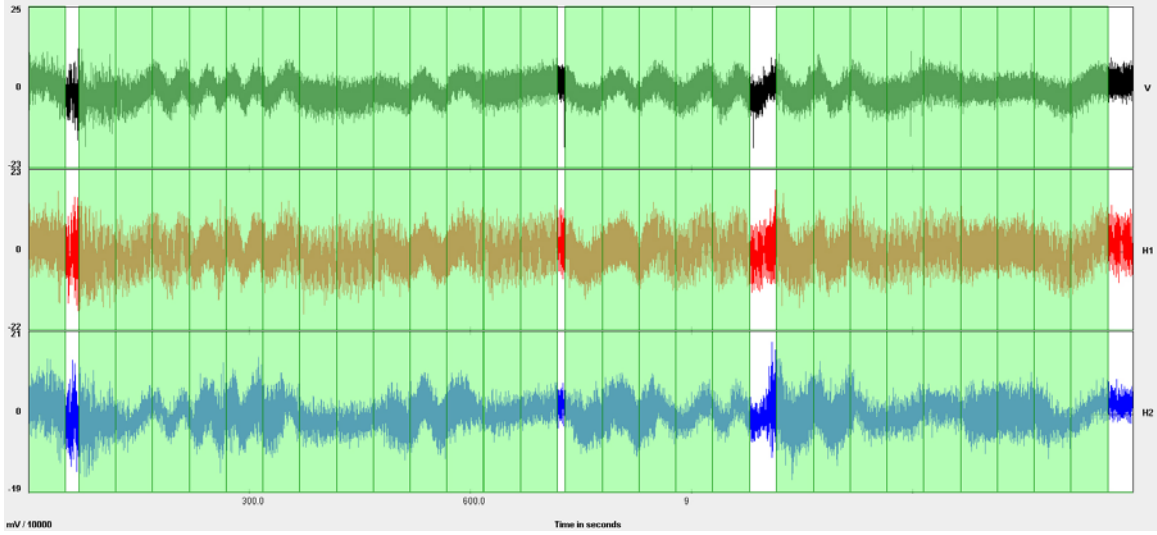


Figure G.1 H/V Showing Windows of Data Used (Shaded) in Analysis After Filter is Applied in the Program J-SESAME for Site 7.

APPENDIX H

Table H.1 Profile Parameters Used to Develop Theoretical Dispersion Curve at Site 8

Thickness (m)	P-Wave Velocity (m/s)	S-Wave Velocity (m/s)	Density (g/cm³)	Poisson's Ratio	Damping Factor
0.5	190	110	1.9	0.25	0.02
1	332	192	1.9	0.25	0.02
2	288	166	1.9	0.25	0.02
2.5	1600	142	1.9	0.50	0.02
3.1	1600	239	1.9	0.49	0.02
4	1600	222	1.9	0.49	0.02
4.9	1600	188	1.9	0.49	0.02
6.1	1600	278	1.9	0.48	0.02
7.5	1600	395	1.9	0.47	0.02
9.5	1600	439	1.9	0.46	0.02
12	1600	398	1.9	0.47	0.02
15	1600	374	1.9	0.47	0.02
19	1600	409	1.9	0.47	0.02
23	1600	489	1.9	0.45	0.02
29	1600	553	1.9	0.43	0.02
36	1600	584	1.9	0.42	0.02
45	1800	738	1.9	0.40	0.02
∞	1800	1041	1.9	0.25	0.02

Table H.2 Profile Parameters Used to Develop Modified Theoretical Dispersion Curve at Site 8

Thickness (m)	P-Wave Velocity (m/s)	S-Wave Velocity (m/s)	Density (g/cm³)	Poisson's Ratio	Damping Factor
0.5	175	101	1.9	0.25	0.02
1	305	176	1.9	0.25	0.02
2	310	179	1.9	0.25	0.02
2.5	1600	130	1.9	0.50	0.02
3.1	1600	247	1.9	0.49	0.02
4	1600	227	1.9	0.49	0.02
4.9	1600	188	1.9	0.49	0.02
6.1	1600	275	1.9	0.48	0.02
29	1600	400	1.9	0.47	0.02
57	1600	395	1.9	0.47	0.02
∞	1800	653	1.9	0.42	0.02

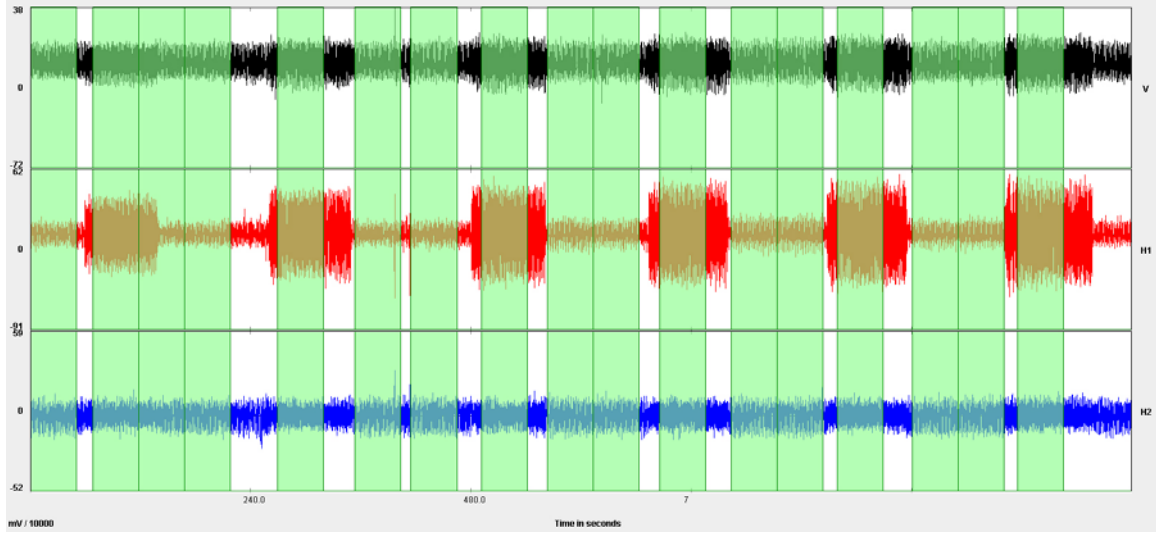


Figure H.1 H/V Showing Windows of Data Used (Shaded) in Analysis After Filter is Applied in the Program J-SESAME for Site 8.

APPENDIX I

Table I.1 Profile Parameters Used to Develop Theoretical Dispersion Curve at Site 9

Thickness (m)	P-Wave Velocity (m/s)	S-Wave Velocity (m/s)	Density (g/cm³)	Poisson's Ratio	Damping Factor
0.5	141	81	1.9	0.25	0.02
1	266	153	1.9	0.25	0.02
2	289	167	1.9	0.25	0.02
2.5	1600	163	1.9	0.49	0.02
3.1	1600	191	1.9	0.49	0.02
4	1600	194	1.9	0.49	0.02
4.9	1600	192	1.9	0.49	0.02
6.1	1600	226	1.9	0.49	0.02
7.5	1600	254	1.9	0.49	0.02
9.5	1600	290	1.9	0.48	0.02
12	1600	347	1.9	0.48	0.02
15	1600	411	1.9	0.46	0.02
19	1600	424	1.9	0.46	0.02
23	1600	419	1.9	0.46	0.02
29	1600	455	1.9	0.46	0.02
36	1600	548	1.9	0.45	0.02
∞	1800	683	1.9	0.42	0.02

Table I.2 Profile Parameters Used to Develop Modified Theoretical Dispersion Curve at Site 9

Thickness (m)	P-Wave Velocity (m/s)	S-Wave Velocity (m/s)	Density (g/cm³)	Poisson's Ratio	Damping Factor
0.5	145	84	1.9	0.25	0.02
1	251	145	1.9	0.25	0.02
2	296	171	1.9	0.25	0.02
2.5	1600	164	1.9	0.49	0.02
3.1	1600	192	1.9	0.49	0.02
4	1600	190	1.9	0.49	0.02
4.9	1600	200	1.9	0.49	0.02
6.1	1600	229	1.9	0.49	0.02
7.5	1600	246	1.9	0.49	0.02
9.5	1600	284	1.9	0.48	0.02
12	1600	359	1.9	0.47	0.02
86	1600	418	1.9	0.46	0.02
∞	1600	622	1.9	0.43	0.02

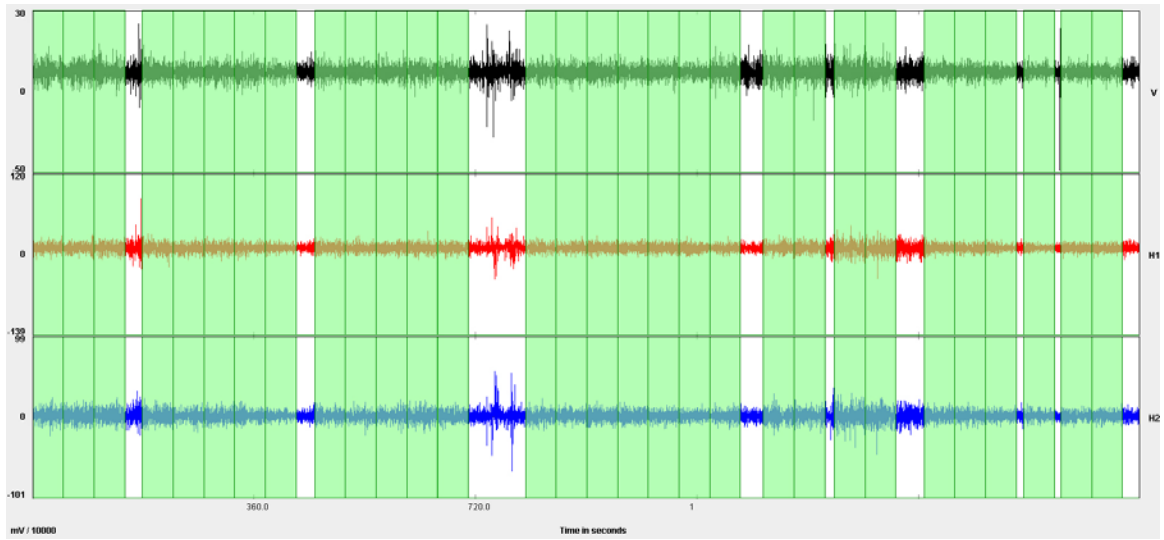


Figure I.1 H/V Showing Windows of Data Used (Shaded) in Analysis After Filter is Applied in the Program J-SESAME for Site 9.

APPENDIX J

Table J.1 Profile Parameters Used to Develop Theoretical Dispersion Curve at Site 10

Thickness (m)	P-Wave Velocity (m/s)	S-Wave Velocity (m/s)	Density (g/cm³)	Poisson's Ratio	Damping Factor
0.5	193	111	1.9	0.25	0.02
1	239	138	1.9	0.25	0.02
2	204	118	1.9	0.25	0.02
2.5	1600	179	1.9	0.49	0.02
3.1	1600	162	1.9	0.49	0.02
4	1600	184	1.9	0.49	0.02
4.9	1600	194	1.9	0.49	0.02
6.1	1600	229	1.9	0.49	0.02
7.5	1600	307	1.9	0.48	0.02
9.5	1600	443	1.9	0.46	0.02
12	1600	459	1.9	0.46	0.02
15	1600	385	1.9	0.47	0.02
19	1600	346	1.9	0.48	0.02
23	1600	376	1.9	0.47	0.02
29	1600	463	1.9	0.45	0.02
36	1600	640	1.9	0.40	0.02
∞	1800	712	1.9	0.41	0.02

Table J.2 Profile Parameters Used to Develop Modified Theoretical Dispersion Curve at Site 10

Thickness (m)	P-Wave Velocity (m/s)	S-Wave Velocity (m/s)	Density (g/cm³)	Poisson's Ratio	Damping Factor
0.5	187	108	1.9	0.25	0.02
1	242	139	1.9	0.25	0.02
2	200	115	1.9	0.25	0.02
2.5	1600	185	1.9	0.49	0.02
3.1	1600	172	1.9	0.49	0.02
4	1600	169	1.9	0.49	0.02
4.9	1600	196	1.9	0.49	0.02
6.1	1600	240	1.9	0.49	0.02
7.5	1600	307	1.9	0.48	0.02
21.5	1600	446	1.9	0.46	0.02
86	1600	388	1.9	0.47	0.02
∞	1800	715	1.9	0.41	0.02

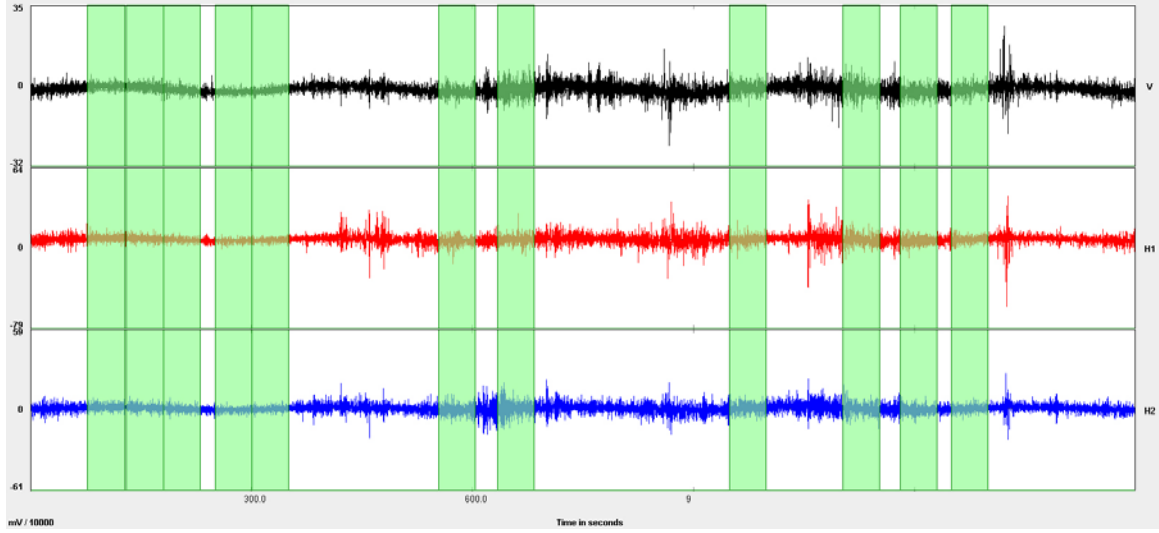


Figure J.1 H/V Showing Windows of Data Used (Shaded) in Analysis After Filter is Applied in the Program J-SESAME for Site 10.

APPENDIX K

Table K.1 Profile Parameters Used to Develop Theoretical Dispersion Curve at Site 11

Thickness (m)	P-Wave Velocity (m/s)	S-Wave Velocity (m/s)	Density (g/cm³)	Poisson's Ratio	Damping Factor
0.5	227	131	1.9	0.25	0.02
1	196	113	1.9	0.25	0.02
2	230	133	1.9	0.25	0.02
2.5	1600	190	1.9	0.49	0.02
3.1	1600	164	1.9	0.49	0.02
4	1600	175	1.9	0.49	0.02
4.9	1600	197	1.9	0.49	0.02
6.1	1600	231	1.9	0.49	0.02
7.5	1600	290	1.9	0.48	0.02
9.5	1600	384	1.9	0.47	0.02
12	1600	412	1.9	0.46	0.02
15	1600	390	1.9	0.47	0.02
19	1600	399	1.9	0.47	0.02
23	1600	494	1.9	0.45	0.02
29	1600	594	1.9	0.42	0.02
36	1800	685	1.9	0.42	0.02
∞	1800	807	1.9	0.37	0.02

Table K.2 Profile Parameters Used to Develop Modified Theoretical Dispersion Curve at Site 11

Thickness (m)	P-Wave Velocity (m/s)	S-Wave Velocity (m/s)	Density (g/cm³)	Poisson's Ratio	Damping Factor
0.5	224	129	1.9	0.25	0.02
1	190	110	1.9	0.25	0.02
2	236	136	1.9	0.25	0.02
2.5	1600	191	1.9	0.49	0.02
3.1	1600	144	1.9	0.50	0.02
4	1600	167	1.9	0.49	0.02
4.9	1600	212	1.9	0.49	0.02
6.1	1600	236	1.9	0.49	0.02
7.5	1600	289	1.9	0.48	0.02
21.5	1600	398	1.9	0.47	0.02
34	1600	356	1.9	0.47	0.02
∞	1600	631	1.9	0.43	0.02

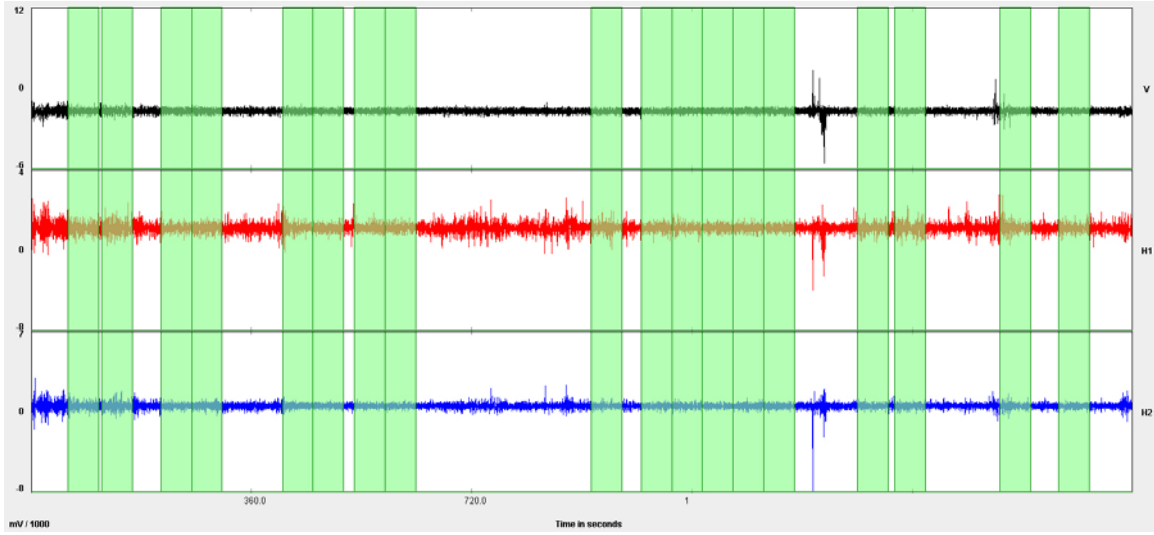


Figure K.1 H/V Showing Windows of Data Used (Shaded) in Analysis After Filter is Applied in the Program J-SESAME for Site 11.

REFERENCES

- Ang, A., Tang, W., 1975. Probability Concepts in Engineering Planning and Design: Basic Principles, vol. 1, Wiley, New York.
- Asten, M.W., 2003. Comment on “Microtremor observations of deep seiment resonance in metropolitan Memphis, Tennessee” by Paul Bodin, Kevin Smith, Steve Horton and Howard Hwang. *Engineering Geology* 72, 343–349.
- Bay, J., 2003. Shallow Shear Wave Velocity Profiling of Poorly Characterized Earthquake Site-Response Units in Urban Salt Lake Valley. NEHRP Program, USGS Award #03HQGR0049.
- Bodin, P., Smith, K., Horton, S., Hwang, H., 2001. Microtremor observations of deep sediment resonance in metropolitan Memphis, Tennessee. *Engineering Geology* 62, 159–168.
- Brown, L.T., Boore, D.M., Stokoe II, K.H., 2000. Comparison of shear-wave velocity profiles from SASW and downhole seismic tests at a strong-motion site, in Proc. 12th World Conference on Earthquake Engineering, Auckland, New Zealand, 30 January–4 February, 2000 (in press).
- Brown, L.T., Boore, D.M., Stokoe II, K.H., 2002. Comparison of shear-wave slowness profiles at 10 strong-motion sites from noninvasive SASW measurements and measurements made in boreholes. *Bulletin of the Seismological Society of America* 92, 3116–3133.
- Casey, T., McGillvray, A., Mayne, P.W., 1999. Results of Seismic Piezocone Penetration Tests Performed in Memphis, Tennessee. GTRC Project E-20-E87.
- Chen, K., Chiu, J., Yang, Y., 1996. Shear-wave velocity of the sedimentary basin in the upper Mississippi embayment using *S*-to-*P* converted waves. *Bulletin of the Seismological Society of America* 86 (3), 848–856.
- Cramer, C.H., Gomberg, J.S., Schweig, E.S., Waldron, B.A., Tucker, K., 2004. The Memphis, Shelby County, Tennessee, Seismic Hazard Maps. U.S. Geological Survey Open File Report 2004-1294., 41 pp.
- Cramer, C., 2006. Quantifying the uncertainty in site amplification modeling and its effects on site specific seismic hazard estimation in the upper Mississippi Embayment and adjacent areas. *Bulletin of Seismological Society of America* 96, 2008-2020.
- Crone, A.J. Russ, D.P., 1979. Preliminary report on an exploratory drill hole New Madrid test well 1-X in southeast Missouri. US Geological Survey Open-File Report 79-1216: 14 pp.

Cushing, E.M., Boswell, E.H., Hosman, R.L., 1964, General Geology of the Mississippi Embayment. Water Resources of the Mississippi Embayment, U.S. Geological Survey Professional Paper 448-B.

Dorman, J., Smalley, R., 1994. Low-frequency seismic surface waves in the upper Mississippi embayment. *Seismological Research Letters* 65 (2), 137-148.

Ge, J., Pujol, J., Pezeshk, S., Stovall, S., 2007. Determination of shallow shear-wave velocity at Mississippi Embayment sites using vertical seismic profiling data. *Bulletin of the Seismological Society of America* 97, 614–623.

Gomberg, J., Waldron, B., Schweig, E., Hwang, H., Webbers, A., Van Arsdale, R., Tucker, K., Williams, R., Street, R., Mayne, P., Stephenson, W., Odum, J., Cramer, C., Updike, R., Hutson, S., Bradley, M., 2003. Lithology and shear velocity in Memphis, Tennessee. *Bulletin of the Seismological Society of America* 93, 986–997.

Hashash, M.A., Park, D., 2001. Non-linear one-dimensional seismic ground motion propagation in the Mississippi Embayment. *Engineering Geology* 62, 185-206

Herrmann, R.B., Akinci, A., 1999. Mid-America Ground Motion Models. Department of Earth and Atmospheric Sciences, Saint Louis University, St. Louis, MO, 63103, 8pp. See <http://www.eas.slu.edu/People/RBHerrmann/MAE/maecgnd.html>

International Code Council, 2003. International Building Code (IBC) 2003, p. 324.

Joh, S.H., 1996. Advances in Interpretation and Analysis techniques for Spectral-Analysis-of-Surface-Waves (SASW) Measurements. Ph.D. Dissertation, Department of Civil Engineering, University of Texas at Austin.

Johnston, A., Nava, S., 1985. Recurrence rates and probability estimates for the New Madrid seismic zone. *Journal of Geophysical Research* 90, 6737-6753.

Kausel, E., and Roesset, J.M., 1981. Stiffness matrices for layered soils. *Bulletion of the Seismological Society of America* 71, 1743-1761.

Liu, H.P., Hu, Y., Dorman, J., Chang, T.S., Chiu, J.M., 1997. Upper Mississippi embayment shallow seismic velocities measured in situ. *Engineering Geology* 46, 313–330.

Luzietti, E.A., Kanter, L.R., Schweig, E.S., Shedlock, K.M., VanArsdale, R.B., 1992. Shallow deformation along the Crittenden County Fault Zone near the southeastern boundary of the Reelfoot Rift, northeast Arkansas. *Seismological Research Letters* 63, 263-295.

Mento, D.J., Ervin, C.P., McGinnis, L.D., 1986. Periodic energy release in the New Madrid seismic zone. *Bulletin of the Seismological Society of America* 76, 1001-1009.

- Nakamura, Y., 1989. A method for dynamic characteristic estimation of subsurface using microtremor on the ground surface. QR Railway Technical Research Institute, 30.
- Parks, W.S., Carmichael, J.K., 1990. Geology and Ground-Water Resources of the Memphis Sand in Western Tennessee. U.S. Geological Survey Water Resources Investigation Report 88-4182, 30 pp.
- Park, D., Hashash, M.A., (2005). Evaluation of seismic site factors in the Mississippi Embayment. II. Probabilistic seismic hazard analysis with nonlinear site effects. *Soil Dynamic Earthquake Engineering* 25, 145-156.
- Rix, G., K.H. Stokoe II., 1989. Stiffness Profiling of Pavement Subgrades. In *Transportation Research Record 1235*, TRB, National Research Council, Washington, D.C., pp. 1-9
- Rix, G., 2004. Vertical arrays and deep wells in the central and eastern United States. International Workshop for Site Selection, Installation, and Operation of Geotechnical Strong-Motion Arrays
- Romero, S., Rix, G., 2000. Regional variations in near surface shear wave velocities in the greater Memphis area. *Engineering Geology* 61 (2) 137-158.
- Romero, S.M., Rix, G.J., 2001. Ground Motion Amplification of Soil in the Upper Mississippi Embayment. GIT-CEE/GEO-01-1, National Science Foundation Mid America Center, Atlanta.
- Saucier, R.T., 1994. Geomorphology and Quaternary geologic history of the lower Mississippi Valley. U.S. Army Corps of Engineers Waterways Experiment Station, 364
- Scherbaum, F., Hinzen, K.G., Ohrnberger, M., 2003. Determination of shallow shear wave velocity profiles in the Cologne Germany area using ambient vibration. *Geophysical Journal International* 152, 597-612.
- Schneider, J.A., Mayne, P.W., 1998. Results of Seismic Piezocone Penetration Tests Performed in Memphis, TN and West Memphis, AR. Interim Report MAEC Project No. GT-3, p. 67.
- Seht, M.I., Wohlenberg, J., 1999. Microtremor measurements used to map thickness of soft sediments. *Bulletin of the Seismological Society of America* 89, 250–259.
- Steinwachs, M., 1974. Systematische Untersuchungen der kurzperiodischen seismischen Bodenunruhe in der Bundesrepublik Deutschland, *Geologisches Jahrbuch* E3.

Stokoe II, K.H., Rix, G.J., and Nazarian, S., 1989. In situ seismic testing with surface wave: XII International Conference on Soil Mechanics and Foundation Engineering Proceedings, 331–334.

Stokoe II, K.H., Wright, G.W., Bay, J.A., Roesset, J.M., 1994. Characterization of geotechnical sites by SASW method, *in* Geophysical characterization of sites, ISSMFE Technical Committee #10, edited by R.D. Woods, Oxford Publishers, New Delhi.

Stokoe II, K.H., Nazarian, S., Rix, G.J., Sanchez-Salinero, I., Sheu, J.C., and Mok, Y.J., 1988. In-situ seismic testing of hard-to-sample soils by surface wave method. *In* Earthquake engineering and soil dynamics. II: Recent advances in ground-motion evaluation. Edited by J.L. Von Thun. American Society of Civil Engineers, Geotechnical Special Publication 20. pp. 264–279.

Tuttle, M.P., Schweig, E.S., Sims, J.D., Lafferty, R.H., Wolf, L.W., Haynes, M.L., 2002. The earthquake potential of the New Madrid seismic zone. *Bulletin of the Seismological Society of America* 92, 6, 2080–2089.

Van Arsdale, R.B., TenBrink, R.K., 2000. Late Cretaceous and Cenozoic Geology of the New Madrid Seismic Zone. *Bulletin of the Seismological Society of America* 90, 345–356.

Williams, R.A., Odum, J.K., Stephenson, W.J., Worley, D.M., 2000. Surface seismic reflection/refraction measurements of P-andS-wave velocities in the Memphis, TN, region. *Seismological Research Letters* 71(1), 113.

Williams, R.A., Stephenson, W.J., Odum, J.K., 2003. Comparison of P- and S- wave velocity profiles obtained from surface seismic refraction/reflection and downhole data. *Tectonophysics* 368, 71–88.

Woolery, E.W., Street, R., 2002. Quaternary fault reactivation in the Fluorspar Area Fault Complex of western Kentucky: evidence from shallow SH-wave reflection profiles. *Seismological Research Letters* 73 (5), 628-639.